Technical Report Documentation Page

1. Report No.	2. Government Accession No.	3. Recipient's Catalog No.
FAA-RD-74-22		

4. Title and Subtitle	5. Report Date
Large Gradient VOR Handbook	August 1974
	6. Performing Organization Code
	8. Performing Organization Report No.
7. Author(s) DIPAK L. SENGUPTA,	011218-5-T
9. Performing Organization Name and Address The University of Michigan Radiation Laboratory Department of Electrical and Computer Engineering Ann Arbor, Michigan 48105	10. Work Unit No. (TRAIS) 11. Contract or Grant No. FA-72WA-2832
12. Sponsoring Agency Name and Address U.S. Department of Transportation Federal Aviation Administration Systems Research and Development Service Washington, D.C. 20590	13. Type of Report and Period Covered Final Report for Period 30 May 1972 - 15 August 1974 14. Sponsoring Agency Code

15. Supplementary Notes

16. Abstract

The merits of using a large gradient antenna in the ground station of a conventional VOR system are theoretically investigated. A theory has been developed for the course amplitude scalloping errors in the bearing indications of a conventional VOR system. The theory takes into account the vertical plane pattern of the transmitting antenna and the scattering properties of the multipath sources.

The vertical plane patterns of conventional VOR and large gradient antennas located above ground are studied in detail. Observed scalloping amplitudes for antennas located at variable height and with isolated isotropic multipath sources located at various distances from the antennas and at variable height above ground are calculated and compared with each other. It has been found that in certain difficult siting conditions the large gradient antennas reduce considerably the scalloping errors. Extensive curves are plotted so that problems associated with siting problems in conventional VOR may be studied.

17. Key Words	18. Distribution Statement
Scalloping errors in conventional VOR, Conventional VOR antenna patterns, Large gradient VOR antennas, VOR siting problems.	Document is available to the public through the National Technical Information Service, Springfield, Virginia 22151.

19. Security Classif. (of this report)	20. Security Classif. (of this page)	21. No. of Pages	22. Price
UNCLASSIFIED	UNCLASSIFIED	132	

Form DOT F 1700.7 (8-72) Reproduction of completed page authorized

TABLE OF CONTENTS

Table of contents, continued

I

BACKGROUND INFORMATION

1.1 Introduction

The ability of a standard VOR system to provide accurate bearing information to a flying aircraft depends on many factors, e.g., the terrain surrounding the transmitting antenna, the transmitting antenna radiation characteristics, the aircraft receiving antenna, the aircraft receiver characteristics, etc. At the present time FAA requires extensive site preparation for a standard VOR system to be installed (FAA Handbook, 1968). Even with such a system and assuming ideal VOR receiving characteristics, the existence of multipath sources between the ground station and the aircraft degrades the VOR indications at the aircraft. It has been known that in such cases the VOR performance may be improved by appropriately shaping the vertical plane pattern of the VOR transmitting antenna. The present Handbook provides detailed information about the effects of the standard VOR and large gradient antenna radiation characteristics on the accuracy of the VOR indications. It is hoped that the information provided may be found useful: (i) in determining the improvement in VOR siting errors that may be expected with a given large gradient antenna system under a specified set of conditions and (ii) in evaluating the VOR siting errors in the existing systems under specified set of conditions.

1.2 Discussion on Standard VOR System Performance

It is appropriate here to give a short discussion on the performance of a standard VOR system. This will put into proper perspective the need for the use of parasitic loop counterpoise or other large gradient antennas to improve VOR systems.

The operation of standard VHF omnirange systems is described in detail by Hurley, et al (1951). In this section we discuss certain aspects of the standard VOR system performance and its antenna system which are appropriate for our purpose. A detailed description of standard VOR antenna systems was given by Anderson, et al (1953) and Anderson (1965) and will not be repeated here. The antenna system of a standard VOR system consists of four Alford loops located at the same height above a 52' diameter circular and conducting ground plane or counterpoise. These four loops are mounted at the corners of a square symmetrically around the axis of the system and they lie in a plane parallel to the counterpoise. The antenna is oriented with the ground plane lying in a horizontal plane. The entire antenna assembly is usually mounted such that the counterpoise is at a height approximately 15' above ground. Depending on the local terrain conditions, the entire antenna assembly may be located at different heights. Henceforth this antenna will be referred to as the standard VOR or 4-Alford loop counterpoise antenna. The standard VOR system operates at a frequency within the band 108-118 MHz.

The requirements of the VOR system are such that the antenna operates in two distinct modes. In the first mode, called the carrier mode, all four loops are simultaneously driven in phase with carrier frequency currents. The carrier mode pattern of the antenna is omnidirectional in azimuth. In the second mode, called the side band mode, at any instant of time each diagonal pair of loops is excited such that the horizontal plane pattern of each pair of loops above the counterpoise is a figure-of-eight. The relative phase between the pairs of loops is such that the combined effects of these in space is to produce a single figure-of-eight azimuthal pattern rotating at 30 revolutions per second. The free space elevation plane patterns of the antenna in both modes

are symmetrical about the vertical axis and have principal maxima at 30^{o} - 35^{o} above the horizon and have minima in the axial direction (Sengupta et al, 1968; Sengupta, 1971). Thus when the carrier field is combined with the total side band field at each instant of time throughout the goniometer cycle, a rotating limacon field pattern results. The free space patterns of such antennas show considerable response in directions below the plane of the counterpoise. It is known that the field gradient at the horizon (defined to be the rate of decrease of field just below the horizon) is about $3dB/6^{o}$ in both modes of operation. The field gradient value has significant influence on the accuracy obtainable from a conventional VOR system.

In the ideal situation the standard VHF omnirange produces two 30 Hz signals for reception by a flying aircraft: one is constant in phase and independent of the aircraft position, and the other varies in relative phase directly in accordance with the magnetic bearing of the aircraft from the VOR station. The former is referred to as the reference phase signal and the latter as the variable phase signal. The reference phase signal is obtained by frequency modulating at 30 Hz a 9.960 KHz subcarrier signal which in turn amplitude modulates the rf carrier signal. The reference phase signal is radiated by the antenna in the carrier mode of operation having an omnidirectional pattern discussed earlier. The variable phase signal is produced by space amplitude modulating the rf carrier signal with 30 Hz sideband radiated energy. This signal is radiated in the form of a figure-of-eight pattern in azimuth, by effectively rotating it at 30 revolutions per second thereby providing the desired variable signal under this condition. In this case the antenna operates in the side band mode. A phase measuring device in the receiver enables the pilot to obtain his bearing with respect to the station by determining the phase difference between these signals. In the ideal situation when there exists no disturbing object between the VOR station and the flying aircraft the bearing indications obtained by the aircraft in the above manner are found to be quite accurate.

1.3 Standard VOR Performance in Non-Ideal Location

In an actual situation whenever there exists a multipath between the VOR ground station and the flying aircraft, the multipath signals combine with the desired signals at the aircraft. The source of these multipath signals may be trees, buildings, etc., or any other scattering object. The strengths of the multipath signals at the aircraft are directly proportional to the free space response of the antenna in directions below the plane of the counterpoise, if it is assumed that the scattering objects are located below the counterpoise plane. The overall effects of the multipath signals combine to produce siting errors and scalloping in the bearing indications of a conventional VOR (Anderson, 1965).

To avoid the errors in the bearing indications of the standard VOR systems the ideal requirements on the free space antenna radiation pattern are such that in the upper half plane of the counterpoise the elevation field pattern should resemble the Alford loop counterpoise pattern and in directions below the counterpoise plane should be zero or negligible. In other words, the field gradient at the horizon should be infinite or very large. Such a pattern is possible only with an infinitely large counterpoise. However, to increase the counterpoise diameters well beyond the values used in the existing systems is impractical and expensive.

From the discussion given above it is evident that any antenna system having overall free space radiation pattern characteristics mentioned above but which produces little field in directions below the horizontal plane is potentially capable of reducing the VOR siting errors. Such antennas will be called large gradient antennas.

1.4 Limitations of Standard VOR Systems

The performance of a conventional VOR system located in ideal terrain has been discussed in section 1.2. In an actual situation the scattered and/or specular reflections from the ground and other nearby objects (in fact whenever there exists

a multipath between the VOR station and the flying aircraft) combine with the desired signals at the aircraft. The overall effect of this is to disturb the direct relationship between the previously mentioned phase difference and the bearing of the aircraft and thereby produce omni-range course scalloping. This causes siting errors and scalloping in the bearing indications of a VOR. Detailed discussions on the scalloping amplitude and frequency under various situations are given by Anderson and Kearey (1952).

In general it can be said that the phenomenon of scalloping and associated effects depend mainly on two factors: (i) the free space vertical plane pattern characteristics in the directions near and below the plane of the counterpoise, and (ii) the nature of the scattering properties of the disturbing objects and of the multipath sources. The second factor is more or less beyond the control of the designer. There are a number of locations where the antenna must be installed at a considerable height above the ground in order to avoid interference from surrounding objects such as heavily wooded or built-up areas (Winick and Brandewie, 1970). In such cases, the first factor, i.e., the vertical plane antenna pattern characteristics near the horizon become quite important in determining the accuracy of the existing conventional VOR bearing indications.

From the viewpoint of scalloping effects, the ideal requirement on the free space vertical plane pattern of a VOR antenna would be such that the response of the antenna goes abruptly to zero in all directions below the horizon, i.e., the field gradient at the horizon would be infinite. As mentioned before, the field gradient obtainable from existing conventional VOR antennas using 52' diameter counterpoises is about $3dB/6^{o}$ which may be considered to be rather low. This is the fundamental reason why an elevated conventional VOR station located in non-ideal terrain tend to produce inaccurate results in the presence of multipath signals. One of the objectives of the present Handbook is to prove whether or not an improvement in siting error can be brought about by properly shaping the vertical plane pattern of the VOR transmitting antenna.

Another undesirable phenomenon that is encountered in a standard VOR is the appearance of nulls in the vertical plane patterns of such antennas elevated above ground. Assuming a perfectly conducting infinite ground plane, it is easy to show that for the horizontal polarization due to reflection from the ground, there will appear some minima and maxima in the vertical plane patterns. The number of these minima (or maxima) will depend on the height of the antenna above the ground. Depending on the free space elevation pattern of the antenna, some of these minima in the pattern may in some cases actually become nulls. It is quite straightforward to show that the radiation from the antenna in directions below the horizon are mainly responsible for such minima or nulls in the pattern. Usually the minimum in the pattern nearest the horizon is deepest. Siting errors and scalloping effects become most intense in these null directions. It is again obvious that such undesirable effects are produced by the standard VOR system because of the unfavorable vertical plane characteristics of the antenna near the horizon.

1.5 Application of Large Gradient Antennas

It is evident from the discussions given in the previous sections that an antenna having a large field gradient, if incorporated into the present-day standard VOR system, would produce at least two-fold improvement in the overall system performance: (i) it would reduce the multipath signals caused by scalloping objects in the vicinity of and below the counterpoise plane of the elevated VOR antenna, and (ii) it would reduce the depths of the minima that appear in the vertical plane patterns of a VOR antenna due to the ground reflections encountered at typical sites and thereby improve the accuracy of the system.

II

FREE SPACE RADIATION PATTERNS

2.1 Introduction

The theoretical free space radiation patterns of various VOR antennas are discussed in the present chapter. Appropriate theoretical expressions for the radiation patterns are given here without derivations; these may be found in the references cited. The antennas considered are standard 4-loop arrays above the counterpoise (or standard VOR antennas), optimum double parasitic loop counterpoise antenna (or DPLC antenna) and the stacked arrays of 4-loop VOR arrays (or stacked array antennas).

2.2 Standard VOR Antenna

The standard VOR antenna consists of four Alford loop antennas located 4' above a 52' diameter counterpoise (Anderson et al 1953; Anderson, 1965). The horizontal plane pattern of the antenna is omnidirectional in the carrier mode and is a figure-of-eight in the side-band mode of operation. The free-space vertical plane patterns produced by standard VOR antennas operating in the carrier and side-band modes have been discussed elsewhere both theoretically and experimentally (Sengupta and Weston, 1969; Sengupta and Ferris, 1972; Sengupta, 1971).

For the purpose of theoretical analysis, the standard VOR antenna is assumed to consist of a point source with appropriate far field variation and located above the counterpoise as shown in Figure 2-1. The free space radiation field of the point source, in the absence of the counterpoise, is represented by:

$$E_{\phi}^{i} = \eta_o I_o \left(\frac{ka}{2}\right)^2 f(\theta, \phi) \sin\theta \frac{e^{ikr}}{r} , \qquad (2.1)$$

where,

r, θ and ϕ = usual spherical coordinates of the far field point with origin located at the point source,

η_o = intrinsic impedance of free space,

$k = \frac{2\pi}{\lambda}$ = free space propagation constant,

I_o = amplitude of current in the equivalent circular loop,

a = equivalent radius of each Alford loop,

$f(\theta, \phi)$ = source pattern function which is determined by the method of excitation and orientation of the Alford loops.

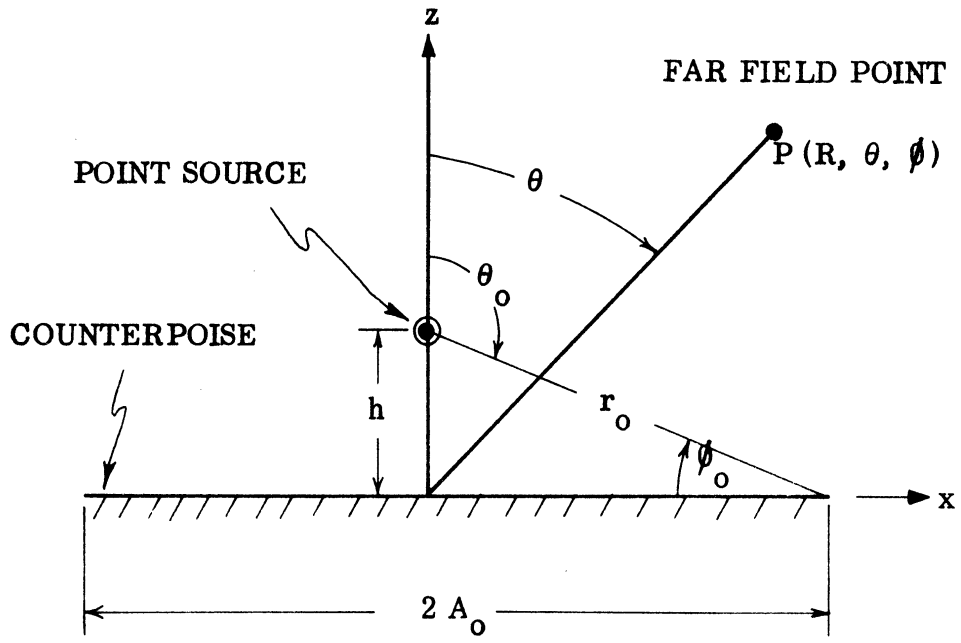

Figure 2-1: Theoretical model for the standard VOR antenna.

The assumed time dependence is $e^{-i\omega t}$ and will be suppressed. If the diagonally opposite Alford loops are separated by a distance 2d (typically $d \simeq 0.15\lambda$) and are excited with signals having equal amplitude but opposite phase (as in the side-band mode operation) then $f(\theta, \phi)$ can be explicitly written as:

$$f(\theta, \phi) = 2i \sin(kd \sin\theta \cos\phi) \quad . \tag{2.2}$$

In the carrier mode of operation $f(\theta, \phi) = 1$. Following the method discussed in [Sengupta 1971], it can be shown that the pattern of the antenna valid in the region $0 < \theta < \pi$, $\theta \leq \phi \leq 2\pi$ is given by

$$E_\phi \sim \eta_o I_o \left(\frac{ka}{2}\right)^2 \frac{e^{i(kR - \pi/4)}}{R} S^A(\theta, \phi) \ , \tag{2.3}$$

where,

$$S^A(\theta, \phi) = \left\{ \frac{F^o(\theta) f(\theta, \phi) \sin\theta}{\sqrt{2}} e^{-ikA_o \sin\theta} + \frac{|\cos\theta| \sin\left(\frac{\phi_o}{2}\right)}{\sqrt{\pi kr_o \sin\theta}} e^{-ikr_o} L^o(\theta, \phi) \right\} \ , \tag{2.4}$$

$$F^o(\theta) = e^{ikr_o \sin(\theta - \phi_o)} \int_{-\infty}^{p_1} e^{i\pi t^2/2} dt - e^{ikr_o \sin(\theta + \phi_o)} \int_{-\infty}^{p_2} e^{i\pi t^2/2} dt \ , \tag{2.5}$$

$$L^{o}(\theta, \phi) = \frac{e^{i\left(\frac{\pi}{2} - kA_o \sin\theta\right)}}{\sqrt{1 - \sin\theta}} \frac{f(\theta_o, \phi)\cos^{3/2}\phi_o - f(\theta, \phi)\sin^{3/2}\theta}{\cos\phi_o - \sin\theta}$$

$$- \frac{e^{ikA_o \sin\theta}}{\sqrt{1 + \sin\theta}} \frac{f(\theta_o, \phi)\cos^{3/2}\phi_o}{\cos\phi_o + \sin\theta} \quad , \tag{2.6}$$

$$p_1 = 2\left(\frac{k r_o}{\pi}\right)^{1/2} \cos\left(\frac{\phi_o - \theta - \pi/2}{2}\right) \quad , \tag{2.7}$$

$$p_2 = 2\left(\frac{k r_o}{\pi}\right)^{1/2} \cos\left(\frac{\phi_o + \theta + \pi/2}{2}\right) \quad , \tag{2.8}$$

$$\tan\phi_o = \frac{h}{A_o}, \quad r_o^2 = h^2 + A_o^2 \tag{2.9}$$

With appropriate choice of $f(\theta,\phi)$, given by Eq. (2.2), $S^{A}(\theta,\phi)$ in Eq. (2.3) may be identified with the carrier and side-band pattern of the antenna.

It should be noted that, in obtaining the above expressions the basic assumptions of geometrical theory of diffraction have been used. In the present case, it mainly implies that Eq. (2.3) is valid for $kA_o >> 1$. Detailed discussion of the pattern expressions and the computer program for the evaluation of the vertical plane patterns of the standard VOR antennas may be found in (Sengupta and Ferris, 1972; Sengupta and Weston 1969; Sengupta, 1971).

The theoretical carrier and side-band mode patterns in the $\phi = 0^{o}$ plane for the standard VOR antenna, as computed from the above expressions, are shown in Figure 2-2. The important free space pattern characteristics of the standard VOR antenna are noted below:

Property	Carrier Mode	Side-band Mode
θ_{max}	58^{o}	60^{o}
α_f	10.44dB	9.47dB
α_g	3.11dB	3.05dB

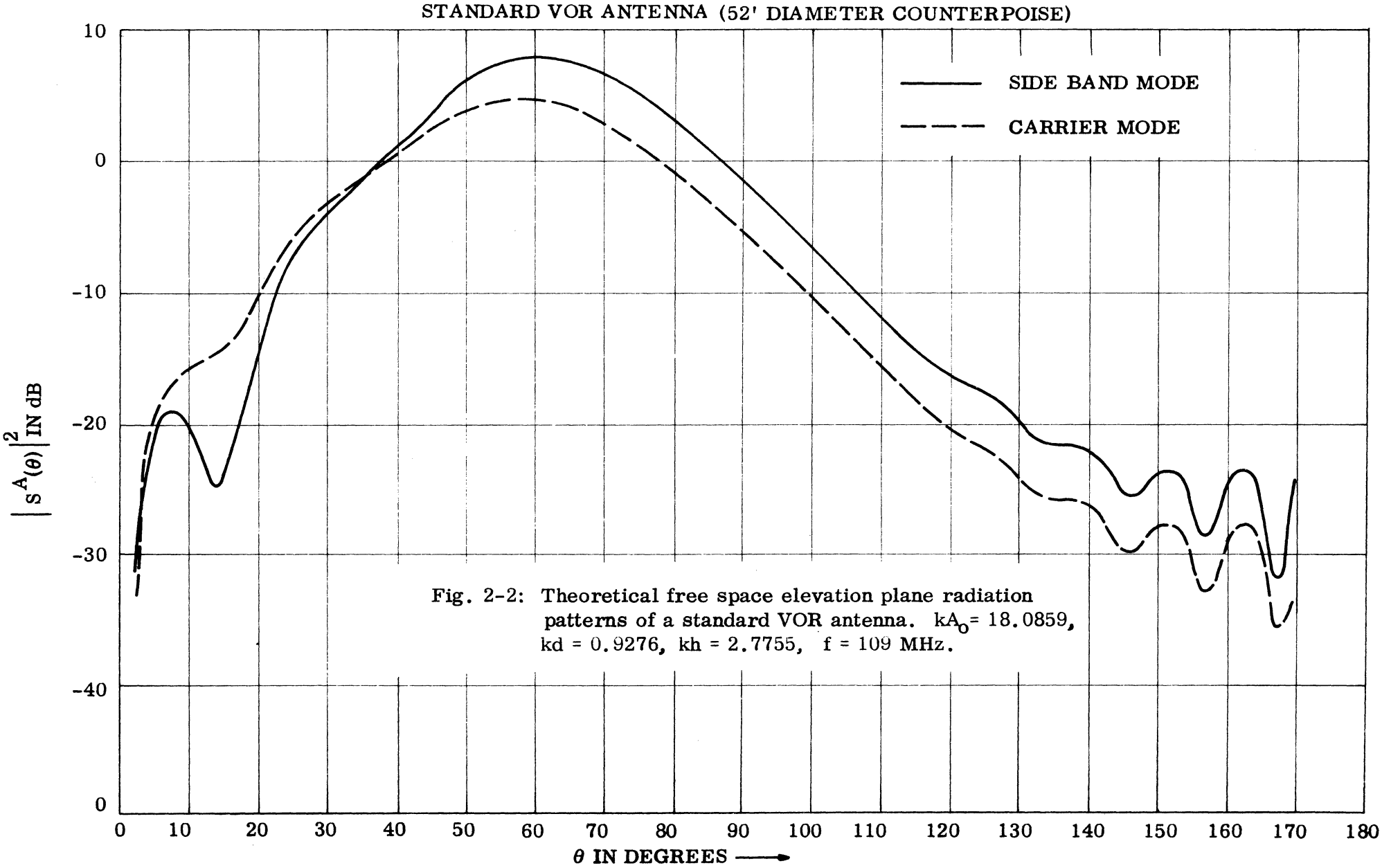

Fig. 2-2: Theoretical free space elevation plane radiation patterns of a standard VOR antenna. $kA_0 = 18.0859$, $kd = 0.9276$, $kh = 2.7755$, $f = 109$ MHz.

where the various parameters in the first column are as follows:

$\theta = \theta_{max}$ is the position of the principal maximum

α_f = field reduction in the direction $\theta = \pi/2$

$$= -20 \log_{10} \frac{\text{field strength at } \pi = \pi/2}{\text{field strength at } \theta = \theta_{max}}$$

α_g = field gradient at the horizon

$$= -20 \log_{10} \frac{\text{field strength at } \pi = 96^{o}}{\text{field strength at } \pi = \pi/2} \quad .$$

As discussed in the references, the agreement between the theoretical and measured patterns has been found to be very good.

2.3 Optimum Double Parasitic Loop Counterpoise (DPLC) Antenna

The large gradient VOR antenna considered here is an optimized double parasitic loop counterpoise antenna whose theory has been discussed in (Sengupta and Ferris, 1970; 1972; Sengupta 1973). The standard VOR antenna shown in Figure 2-1 may be converted into a large gradient antenna by introducing two large (diameter >> wavelength) parasitically excited perfectly conducting loops at appropriate heights above and parallel to the counterpoise. A schematic diagram of the DPLC antenna is shown in Figure 2-3. The optimum DPLC antenna is obtained by choosing the two parasitic loop parameters H_1, H_2, B_1, B_2 and b such that the side-band mode elevation plane pattern of the antenna exhibits maximum rate of decay of fields (or the field gradient) in directions just below the plane of the counterpoise. Typically the normalized dimensions of an optimum DPLC antenna at f = 109 MHz (λ = 9.02') are:

$kA_0 = 18.09$ $\qquad$ $kB_1 = 16.9$

$kh = 2.78$ $\qquad$ $kH_2 = 10.9$

$kd = 0.93$ $\qquad$ $kB_2 = 12.1$

$kH_1 = 3.6$ $\qquad$ $k = 2\pi/\lambda$.

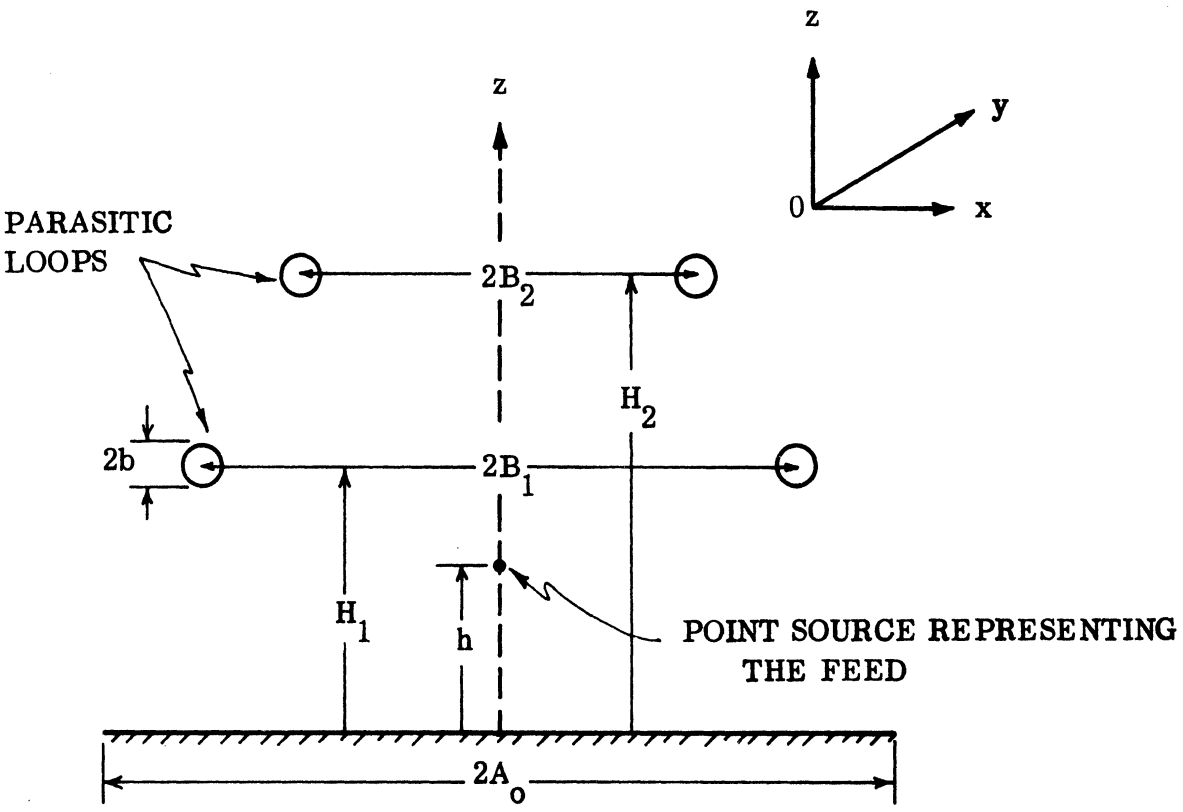

Fig. 2-3: Theoretical model for the DPLC antenna.

The dimensions will be different for different values of the counterpoise diameter.

The complete expression for the side-band mode radiation field pattern in the $\phi = 0^o$ plane for the double parasitic loop counterpoise antenna is given by:

$$E_\phi \sim \eta_o I_o \left(\frac{ka}{2}\right)^2 \frac{e^{i(kR - \pi/4)}}{R} S(\theta), \quad 0 < \theta < \pi \ , \tag{2.10}$$

where

$$S(\theta) = S^A(\theta, 0) + S_1^P(\theta) + S_2^P(\theta) \ .$$

It should be noted that the figure-of-eight pattern in the azimuthal plane has its maximum at $\phi = 0^o$. The three terms on the right hand side of Eq. (2.9) are respectively the complex far fields produced by the feed, the first and the second parasitic loop in the presence of the counterpoise. $S^A(\theta, 0)$ is obtained from Eq. (2.9) with $\phi = 0^o$. Explicit expressions for $S_1^P(\theta)$ are given by the following:

$$S_1^P(\theta) = P_1(\theta) + Q_1(\theta) \ , \tag{2.12}$$

$$P_1(\theta) = \frac{\pi (kB_1)^2}{M} \left[f_1(\theta_1) \frac{e^{ikr_1}}{(kr_1)^2} - f_1(\theta_2) \frac{e^{ikr_2}}{(kr_2)^2} \right] F_1(\theta) \ , \tag{2.13}$$

$$Q_1(\theta) = \frac{i\pi^2 (kB_1)^2}{2M^2} \frac{e^{ikr_1}}{(kr_1)^2} f_1(\theta_1) \times$$

$$\times \left[\frac{1}{(\pi kB_1)^{1/2}} e^{i(2kB_1 + \pi/4)} - \frac{1}{(\pi kH_1)^{1/2}} e^{i(2kH_1 - \pi/4)} \right] F_1(\theta) \ , \tag{2.14}$$

$$\left.\begin{aligned} r_1^2 &= B_1^2 + (H_1-h)^2;\ r_2^2 = B_1^2 + (H_1+h)^2 \\ \sin\theta_1 &= B_1/r_1;\ \sin\theta_2 = B_1/r_2 \end{aligned}\right\}, \tag{2.15}$$

$$M = 0.577 + \ell n\,(kb/2) - i\,\pi/2 \quad , \tag{2.16}$$

$$\begin{aligned} f(\theta, \phi) &= 2i \sin(kd \sin\theta \cos\phi) \\ &\simeq 2ikd \sin\theta \cos\phi = f_1(\theta)\cos\phi \quad , \end{aligned} \tag{2.17}$$

B_1 = radius of the first parasitic loop,

H_1 = height of the first parasitic loop above the counterpoise,

b = radius of the conducting wire used in the parasitic element,

$$\begin{aligned} F_1(\theta) = {} & \frac{J_1'(kB_1 \sin\theta)}{\sqrt{2}}\, F_1^{\,p}(\theta)\, e^{-ikA_o \sin\theta} \\ & + \frac{|\cos\theta|\, \sin\left(\frac{\phi_{p_1}}{2}\right)}{\sqrt{\pi kr_{p_1} \sin\theta}}\, e^{ikr_p}\, L_1^{\,p}(\theta) \quad , \end{aligned} \tag{2.18}$$

J_1 is the Bessel function of the first kind and first order,

$$\begin{aligned} L_1^{\,p}(\theta) = {} & \frac{e^{i(\pi/2 - kA_o \sin\theta)}}{\sqrt{1-\sin\theta}} \left[\frac{\cos^{1/2}(\phi_{p_1})\, J_1'(kB_1 \cos\phi_{p_1}) - \sin^{1/2}(\theta)\, J_1(kB_1 \sin\theta)}{\cos\phi_{p_1} - \sin\theta} \right] \\ & - \frac{e^{ikA_o \sin\theta}}{\sqrt{1+\sin\theta}}\, \frac{\cos^{1/2}(\phi_{p_1})\, J_1'(kB_1 \cos\phi_{p_1})}{\cos\phi_{p_1} + \sin\theta} \end{aligned} \tag{2.19}$$

$$F_1^{p}(\theta) = e^{ikr_{p_1}\sin(\theta-\phi_{p_1})} \int_{-\infty}^{p_5} e^{i\pi t^2/2}\,dt$$

$$-e^{ikr_{p_2}\sin(\theta+\phi_{p_1})} \int_{-\infty}^{p_6} e^{i\pi t^2/2}\,dt \quad , \tag{2.20}$$

$$p_5 = 2\left(\frac{kr_{p_1}}{\pi}\right)^{1/2} \cos\left(\frac{\phi_{p_1} - \theta - \pi/2}{2}\right) \quad , \tag{2.21}$$

$$p_6 = 2\left(\frac{kr_{p_1}}{\pi}\right)^{1/2} \cos\left(\frac{\phi_{p_2} + \theta + \pi/2}{2}\right) \quad , \tag{2.22}$$

$$r_{p_1}^2 = A^2 + H_1^2 \; ; \; \tan\phi_{p_1} = \frac{H_1}{A_o} \quad . \tag{2.23}$$

$S_2^{P}(\theta)$ may be obtained from Eqs. (2.12 - 2.23) by interchanging the subscripts corresponding to the parasitic loop 1 to those corresponding to the parasitic loop 2. The expressions given above have been obtained by neglecting the effect of mutual interaction between the parasitic currents. If $(H_2 - H_1) \geq \lambda$ this is a fairly accurate approximation (Sengupta, 1973). The carrier mode pattern of the same antenna may be obtained from the above set of equations with $f_1(\theta) = 1$, i.e. $f_1(\theta_1) = f_1(\theta_2) = 1$ in eqs. (2.13), (2.14) and (2.17) and $\phi = 0^{o}$ in eq. (2.17).

Figure 2-4 shows the theoretical free space carrier and side-band mode patterns in the $\phi = 0^{o}$ plane for an optimized double parasitic loop counterpoise antenna. The important free space pattern characteristics of a large gradient VOR antenna are noted below.

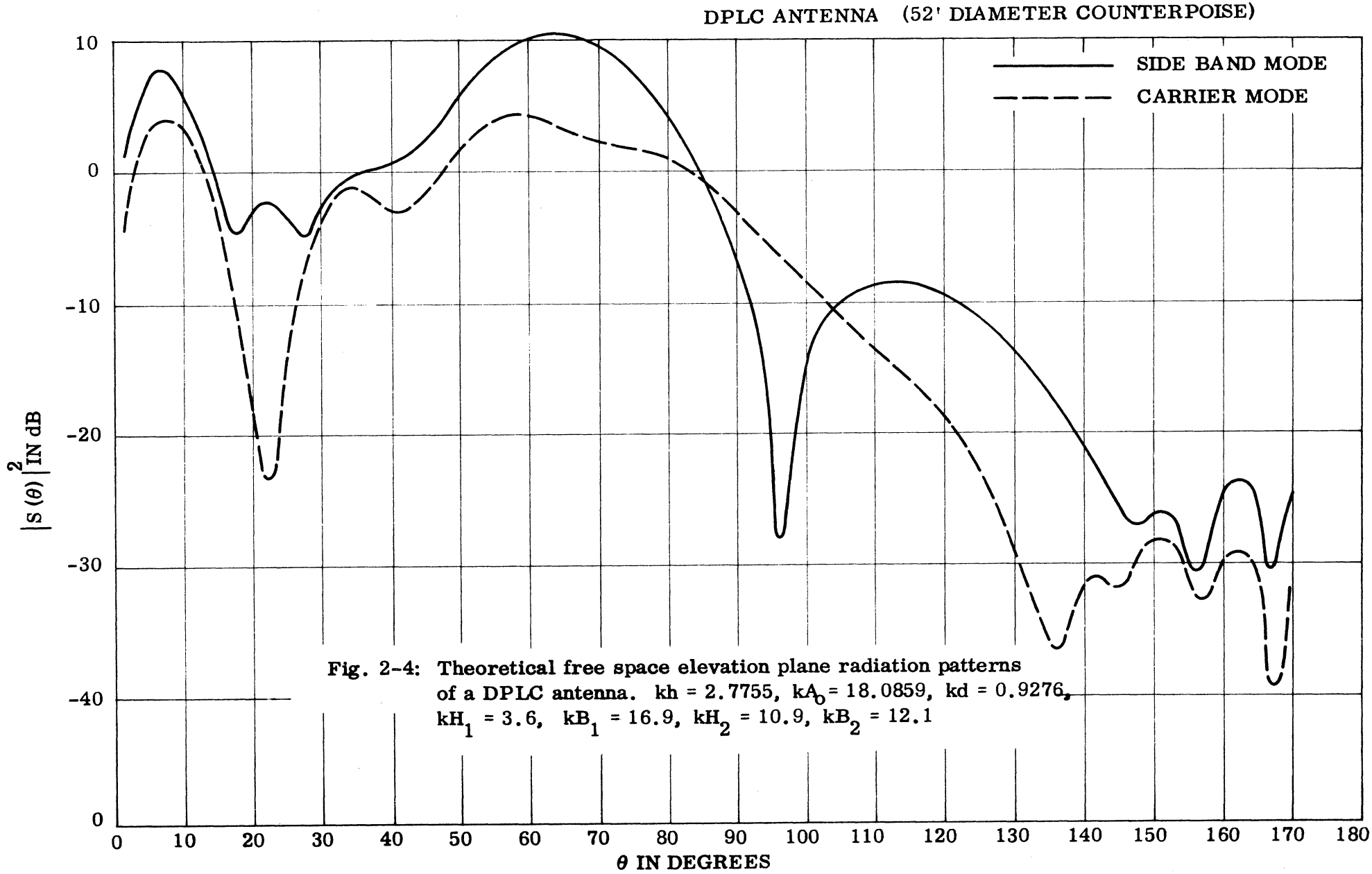

Fig. 2-4: Theoretical free space elevation plane radiation patterns of a DPLC antenna. kh = 2.7755, kA_0 = 18.0859, kd = 0.9276, kH_1 = 3.6, kB_1 = 16.9, kH_2 = 10.9, kB_2 = 12.1

Property	Carrier Mode	Side-band Mode
θ_{max}	58^{o}	60^{o}
α_f	7.40 dB	16.50 dB
α_g	3.11dB	21.22dB

The agreement between the theoretical and measured patterns has been found to be satisfactory (Sengupta and Ferris, 1970; Sengupta, 1973).

2.4 Stacked Array Antenna

It consists of a linear array of five elements or bays. Each bay consists of a standard 4-loop VOR array. Figure 2-5 shows schematically the array geometry. The direction of the z-axis will be referred to as the vertical direction. The numbering of the array elements is as shown in Figure 2-5. The position of the nth element with respect to the origin is denoted by d_n. Note that d_n is positive for elements above the x-axis and negative for elements below the x-axis. As can be seen from Figure 2-5, the array is non-uniformly spaced and excited. However, the spacing of the antenna elements are symmetrical with respect to the x-axis.

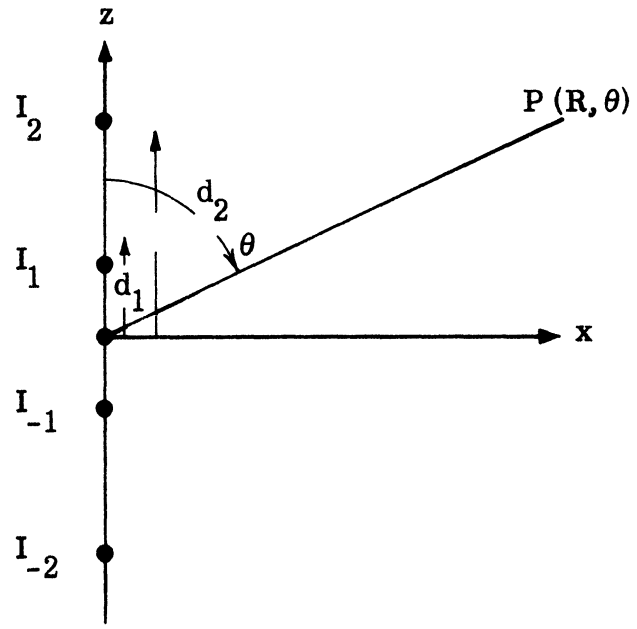

Figure 2-5: Schematic representation of the stacked array.

The Scanwell laboratories optimized the antenna parameters I_n (= $|I_n| e^{i\alpha n}$), d_n such that the free space pattern of the antenna in the x-z plane produces maximum field gradient (α_g) at the horizon. The optimum parameters of the antenna under such conditions are such that the following conditions hold:

$$\left.\begin{aligned} |I_n| &= |I_{-n}| \\ \alpha_n &= -\alpha_{-n}, \text{ where } \alpha_n \text{ is the angle of } I_n, \\ d_n &= |d_{-n}| \quad . \end{aligned}\right\} \tag{2.24}$$

It is assumed that each element or bay has a $\sin\theta$ - type pattern in the z-x plane. Thus, the free space vertical plane complex pattern of the antenna may be written as follows:

$$S(\theta) = \sin\theta \left[|I_0| + 2 \sum_{n=1}^{2} |I_n| \cos(kd_n \cos\theta - \alpha_n) \right] \tag{2.25}$$

The fundamental approximation made in Eq. (2.25) is that the element pattern, i.e., the pattern of the 4-loop VOR array is $\sin\theta$ - type in the x - z plane and that it is the same in both carrier and side-band modes. Because of this Eq. (2.25) indicates that the antenna has the same pattern in the carrier and side band mode of operation. Figure 2-6 shows the free space pattern of the optimum stacked array antenna. The excitation coefficients of the optimum antenna, as obtained by the Scanwell Laboratories, are as follows:

$$|I_o| = 1, \quad \alpha_0 = 0$$
$$|I_1| = 0.62, \quad \alpha_1 = 96.3^o$$
$$|I_2| = 0.19, \quad \alpha_2 = 108.9^o \quad .$$

The element spacings in the optimum antenna are $d_1 = \lambda/2$, $d_2 = 3\lambda/2$ where λ is the operating wavelength. (The field gradient obtained for the optimum antenna is $a_g \simeq 16\text{dB}/6^o$.) This antenna will be referred to as the optimum stacked array antenna or the stacked array antenna number 1.

It is of interest to study the free space patterns of the antenna for slightly different excitations but with the same element spacings. The following table gives the non-optimum excitations and the corresponding field gradients obtained:

$\|I_0\|$	$\|I_1\|$	$\|I_2\|$	α_0	α_1	α_2	α_g
1	0.55	0.15	0	96.3^o	$108^o.9$	$10.20\text{dB}/6^o$
1	0.50	0.10	0	$96^o.3$	$108^o.9$	$6.74\text{dB}/6^o$
1	0.4	0.10	0	$96^o.3$	$108^o.9$	$4.98\text{dB}/6^o$

The above three antennas will be referred to as stacked array antennas number 2, 3 and 4 respectively. Figure 2-7 shows the complete patterns of the antenna for different excitations. It can be seen from Figure 2-7 that for the variation of the excitation used here, the main beam of the pattern is not affected appreciably. However, the field gradient as well as the minor lobe details are affected considerably by the change in the excitations.

2.5 Summary of Results

The important free space side-band mode elevation plane pattern characteristics of the above antennas operating at 109 MHz are shown in the following table:

TABLE I

FREE SPACE SIDE-BAND MODE ELEVATION PLANE PATTERN CHARACTERISTICS OF VOR ANTENNAS AT 109 MHz

			Stacked Arrays			
Property	Standard VOR	DPLC	1	2	3	4
θ_{max}	60^o	60^o	74^o	74^o	73^o	74^o
α_f	9.47dB	16.50dB	8.88dB	7.75dB	6.64dB	5.72dB
$\alpha_g/6^o$	3.05dB	21.22dB	16.93dB	10.20dB	6.74dB	4.98dB

Observe that the antennas listed in the above table have different field gradients. The four stacked arrays are obtained by using four different excitations appropriate for the indicated field gradients. Stacked array 1 is the optimum configuration.

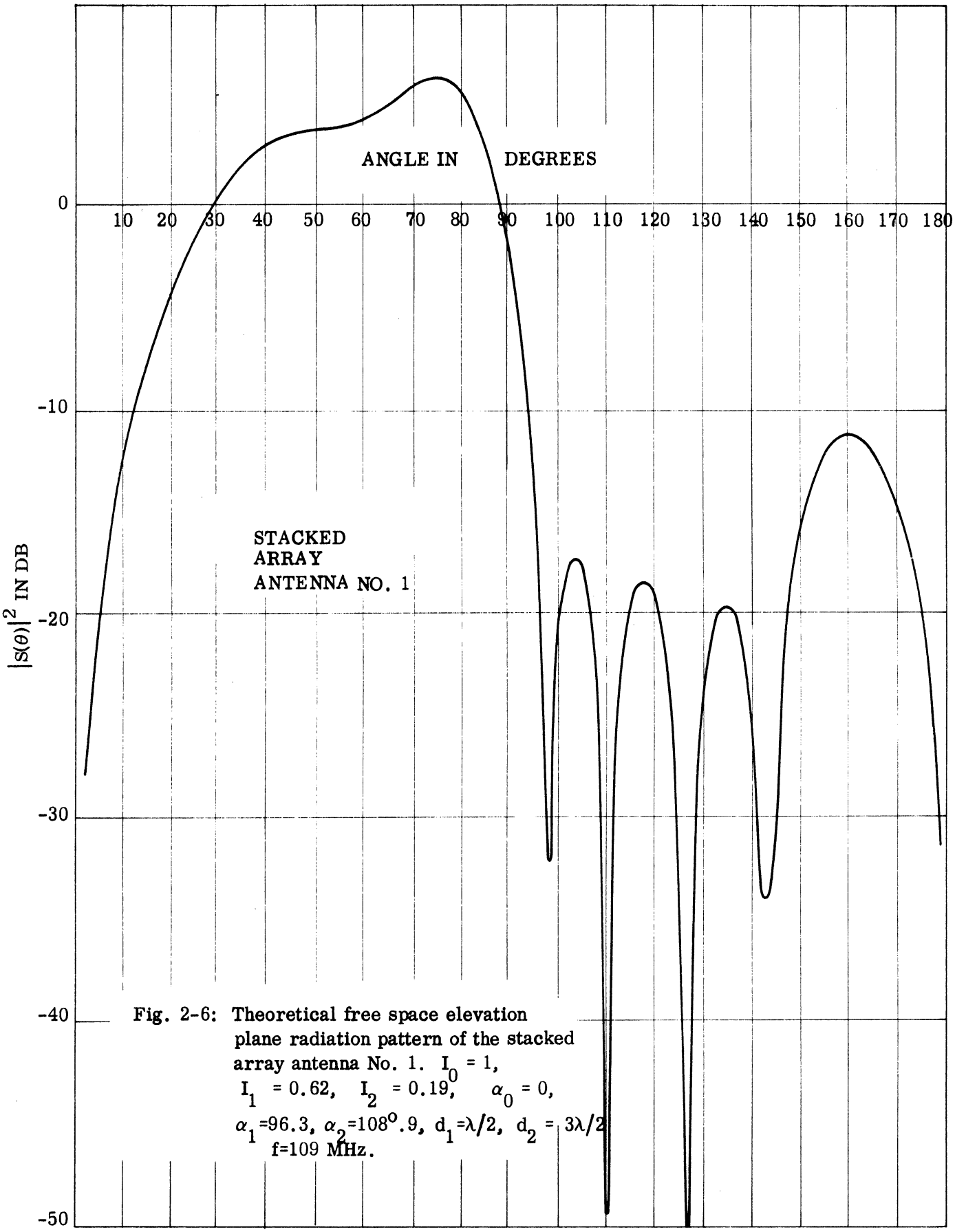

Fig. 2-6: Theoretical free space elevation plane radiation pattern of the stacked array antenna No. 1. $I_0 = 1$, $I_1 = 0.62$, $I_2 = 0.19$, $\alpha_0 = 0$, $\alpha_1 = 96.3$, $\alpha_2 = 108^{o}.9$, $d_1 = \lambda/2$, $d_2 = 3\lambda/2$ f=109 MHz.

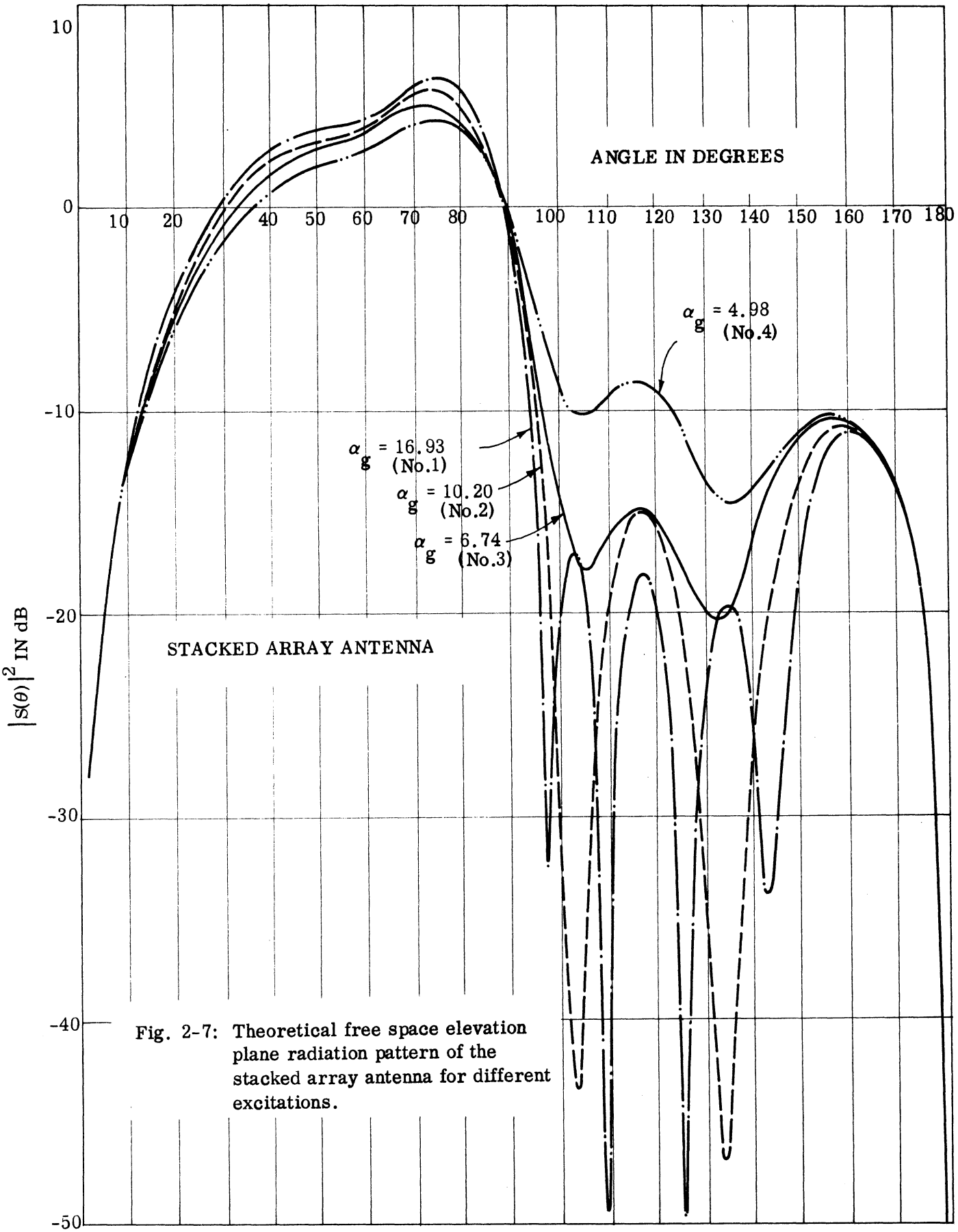

Fig. 2-7: Theoretical free space elevation plane radiation pattern of the stacked array antenna for different excitations.

III

RADIATION PATTERNS OF VARIOUS VOR ANTENNAS LOCATED ABOVE GROUND

3.1 Introduction

In this chapter we discuss the elevation plane radiation patterns produced by standard VOR, DPLC and stacked array antennas located above a perfectly conducting infinite planar ground. Assuming that the counterpoise is located at a height Z_0 above ground, it can be shown that the elevation plane complex pattern of the antenna in the presence of ground is given by:

$$S_T(\theta) = e^{-ikZ_0 \cos\theta} S(\theta) - e^{ikZ_0 \cos\theta} S(\pi-\theta) \quad , \qquad (3.1)$$

where $S(\theta)$ is the free space pattern of the antenna as discussed in chapter II. After substituting the appropriate expressions for $S(\theta)$ into Eq. (3.1), the effects of ground on the antenna radiation pattern can be studied.

3.2 Complete Elevation Plane Patterns

Complete side-band mode patterns for standard VOR, DPLC and stacked array antennas have been computed by using Eq. (3.1), for selected values of Z_0 in the range $0 \leq Z_0 \leq 500'$. During this part of computation the patterns have been calculated in the range $0 \leq \theta \leq \pi/2$ at 1^o intervals. Some of the computed patterns are shown in Figures 3-1 through 3-3 for the standard VOR, DPLC and the optimum stacked array antennas. Observe that as the height Z_0 of the antenna above ground is increased, the number of minima in the pattern increases. Notice that the geometry of the stacked array antenna restricts the minimum height Z_0 to 15'. It can also be seen from the figures that with the increase of Z_0, the depth of the

null nearest to $\theta=\pi/2$ increases. The depth of a minimum (or null) in the pattern is defined locally to be given by $\frac{|S_T(\theta)|_{\text{at B}}}{|S_T(\theta)|_{\text{at A}}}$ or expressed in dB it is given by $|S_T(\theta)|_{\text{at B}} - |S_T(\theta)|_{\text{at A}}$ (see Figure 3-1b). For example, the depth of the minimum nearest to $\theta = \pi/2$ is about 2dB.

3.3 Position of the Pattern Minima

The results shown in Figs. 3-1 - 3-3 indicate that the predominant effect of the ground on the elevation plane pattern is the generation of a number of minima and maxima in the patterns. Figure 3-4 shows the positions of the first few minima above the horizon ($\theta=\pi/2$) as functions of the antenna height. Notice that the positions of the minima are expressed in angles above the horizon (i.e., above 90^{o}). The curves shown are self-explanatory. It is interesting to observe that for $Z_0 > 200'$ the position of the nth minimum above the horizon may be obtained with sufficient accuracy for the formula;

$$\theta_n^1 = \sin^{-1}\left(\frac{n\lambda}{2Z_0}\right)$$

which corresponds to the case of a horizontally polarized isotropic antenna located at a height Z_1 above ground.

The locations of the corresponding pattern minima for the DPLC and stacked array antennas may be found approximately by using Figure 3-4. For $Z_0 > 100'$ the results are good. However, for $Z_0 < 100'$ for more accuracy, the minima obtained from individual pattern calculations should be used (Sengupta and Chan, 1973).

3.4 Depth of the Nulls

The depth of a minimum (or null) in the pattern in a certain direction has been defined in Section 3.2. Figures 3-5 through 3-10 show the depths of the first few minima

above the horizon as a function of the antenna height for the three antennas. In general it is found that the depth of the minima increases continuously with Z_0; for a given Z_0, the minimum nearest the horizon is deepest and the depth decreases with the order of the minimum. It is also found that the depth of the minimum decreases with increase of the field gradient.

3.5 Patterns Near the Horizon

The minima in the elevation plane patterns near the horizon are of considerable importance in studying the performance of a VOR system. Figures 3-11 through 3-14 show the behavior of the pattern near the horizon for standard VOR, DPLC and stacked array antennas located at various heights above ground.

3.6 Filling Factor

The results in 3.5 indicate in general that for a given height Z_0, the depth of each minimum in the pattern of a large gradient antenna is less than the depth of the corresponding minimum in the standard VOR antenna. Thus it may be said that the large gradient antenna has a tendency to fill up the minimum in the pattern. We define the "filling factor" as the difference (in dB) between the depths of a given order of minimum in the patterns of standard and large gradient antennas. Thus the filling factor gives an indication of the amount of reduction in the depth of a minimum in the pattern obtained by using a large gradient antenna as compared with that obtained by a standard VOR antenna when the two antennas are located at the same height. Figures 3-15 through 3-19 give the variation of the filling factor for the first few minima in the pattern as a function of the height of the antenna above ground and for different antennas. It is found that initially the filling factor increases rapidly with height and then it approaches a constant value, e.g., 10dB for DPLC antennas. The saturation value of the filling factor

decreases as the field gradient value α_g decreases. The depth of the first minimum and the filling factor of the first minimum are shown in Figure 3-20 as functions of α_g for the stacked array antenna located 200' above ground.

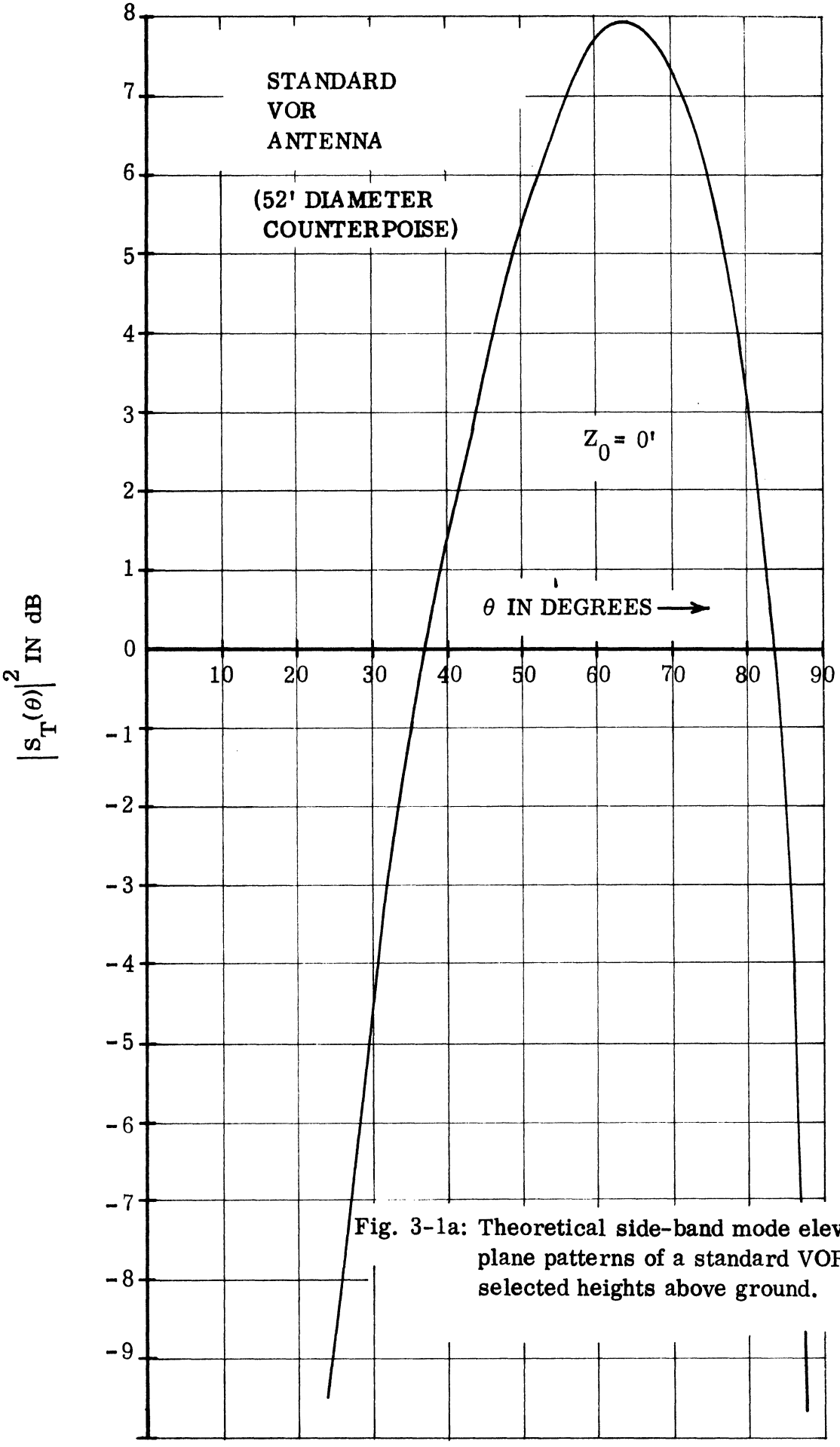

Fig. 3-1a: Theoretical side-band mode elevation plane patterns of a standard VOR antenna for selected heights above ground.

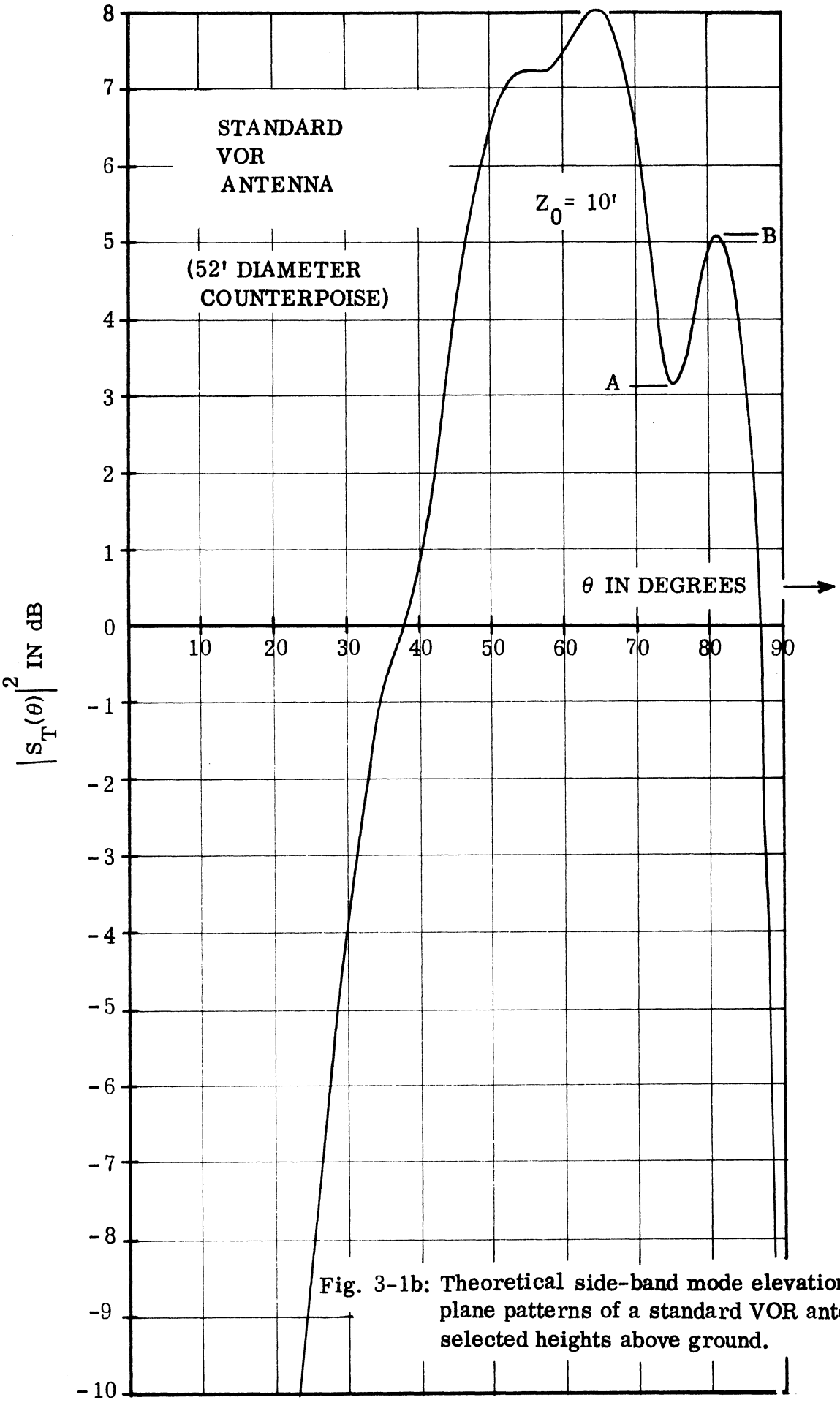

Fig. 3-1b: Theoretical side-band mode elevation plane patterns of a standard VOR antenna for selected heights above ground.

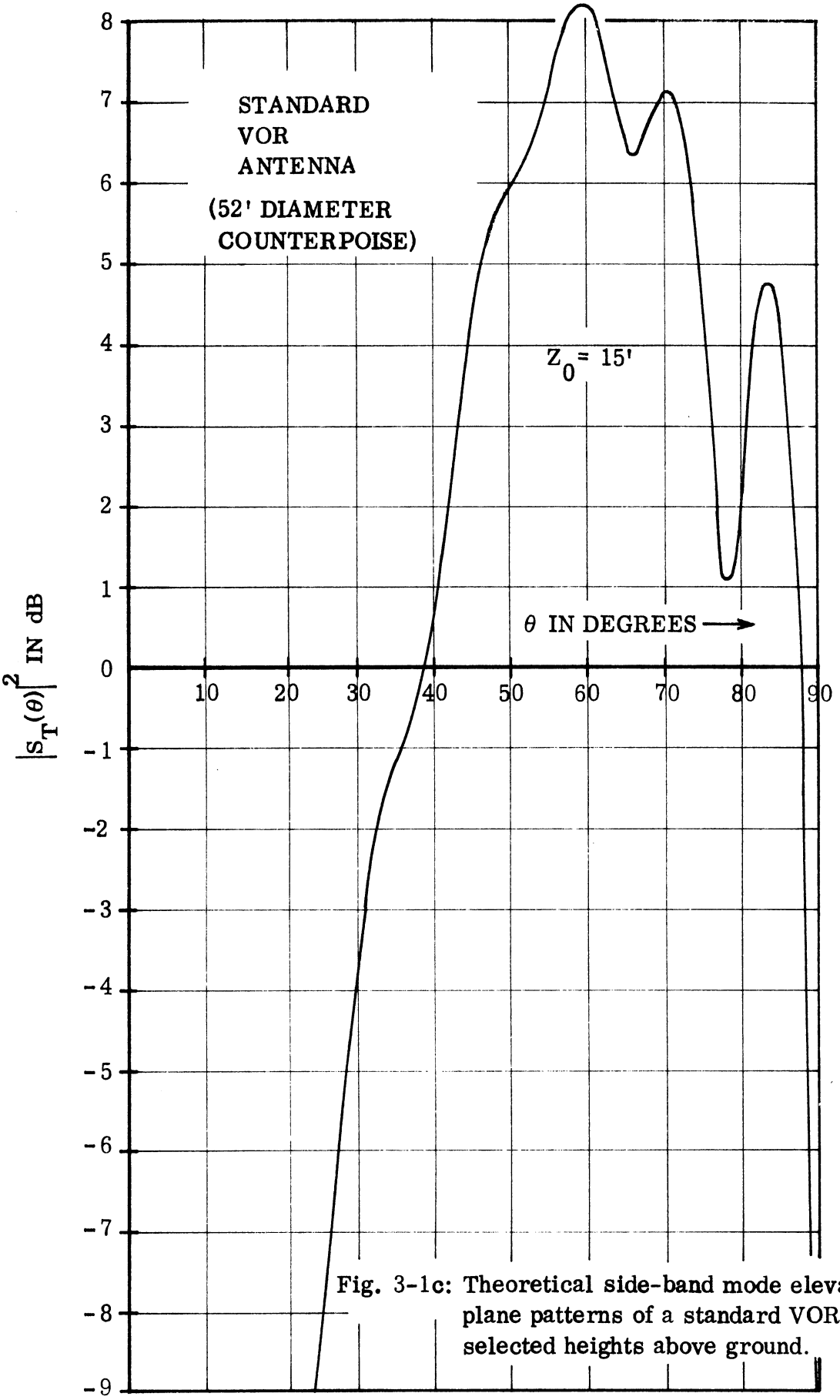

Fig. 3-1c: Theoretical side-band mode elevation plane patterns of a standard VOR antenna for selected heights above ground.

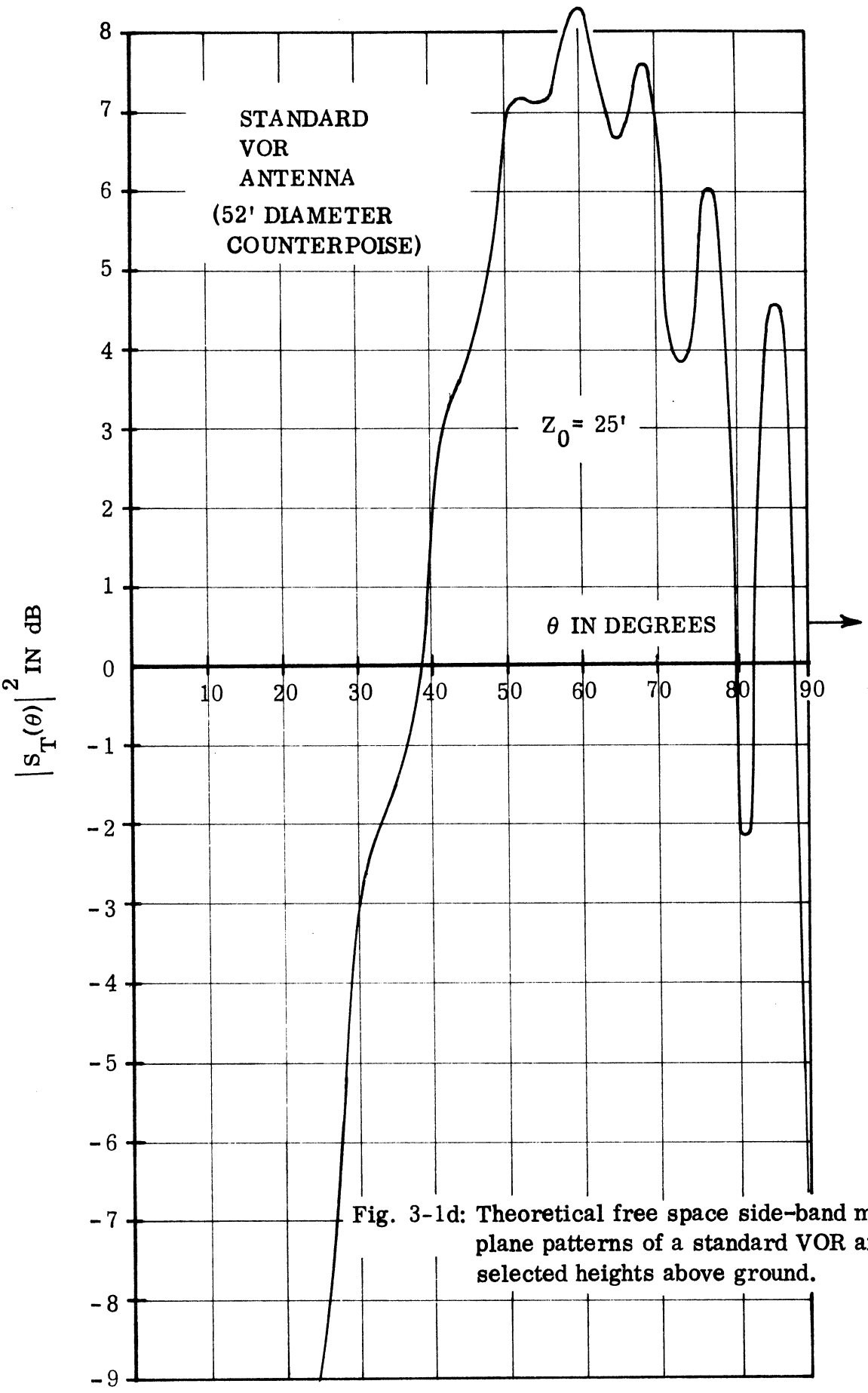

Fig. 3-1d: Theoretical free space side-band mode elevation plane patterns of a standard VOR antenna for selected heights above ground.

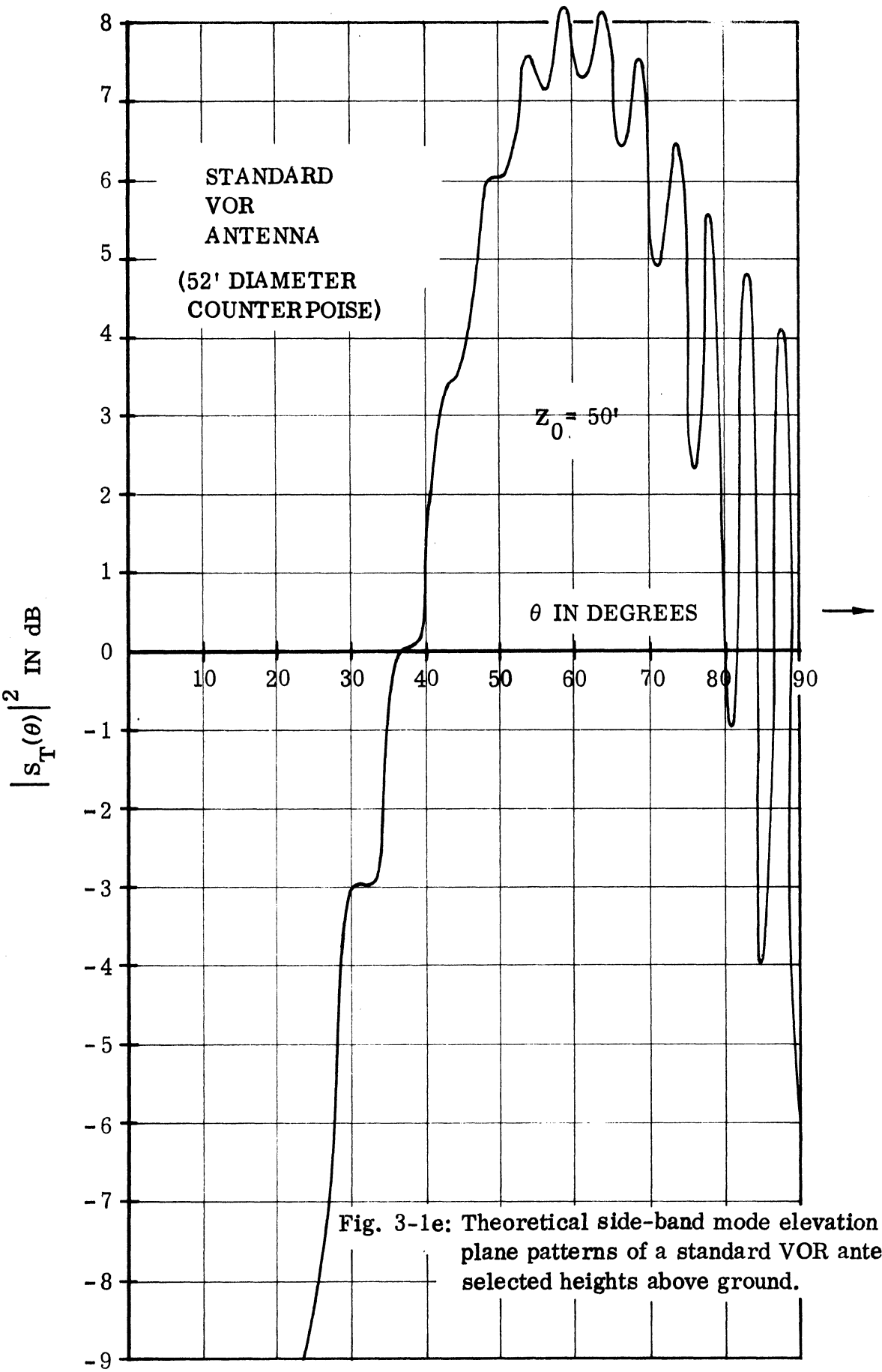

Fig. 3-1e: Theoretical side-band mode elevation plane patterns of a standard VOR antenna for selected heights above ground.

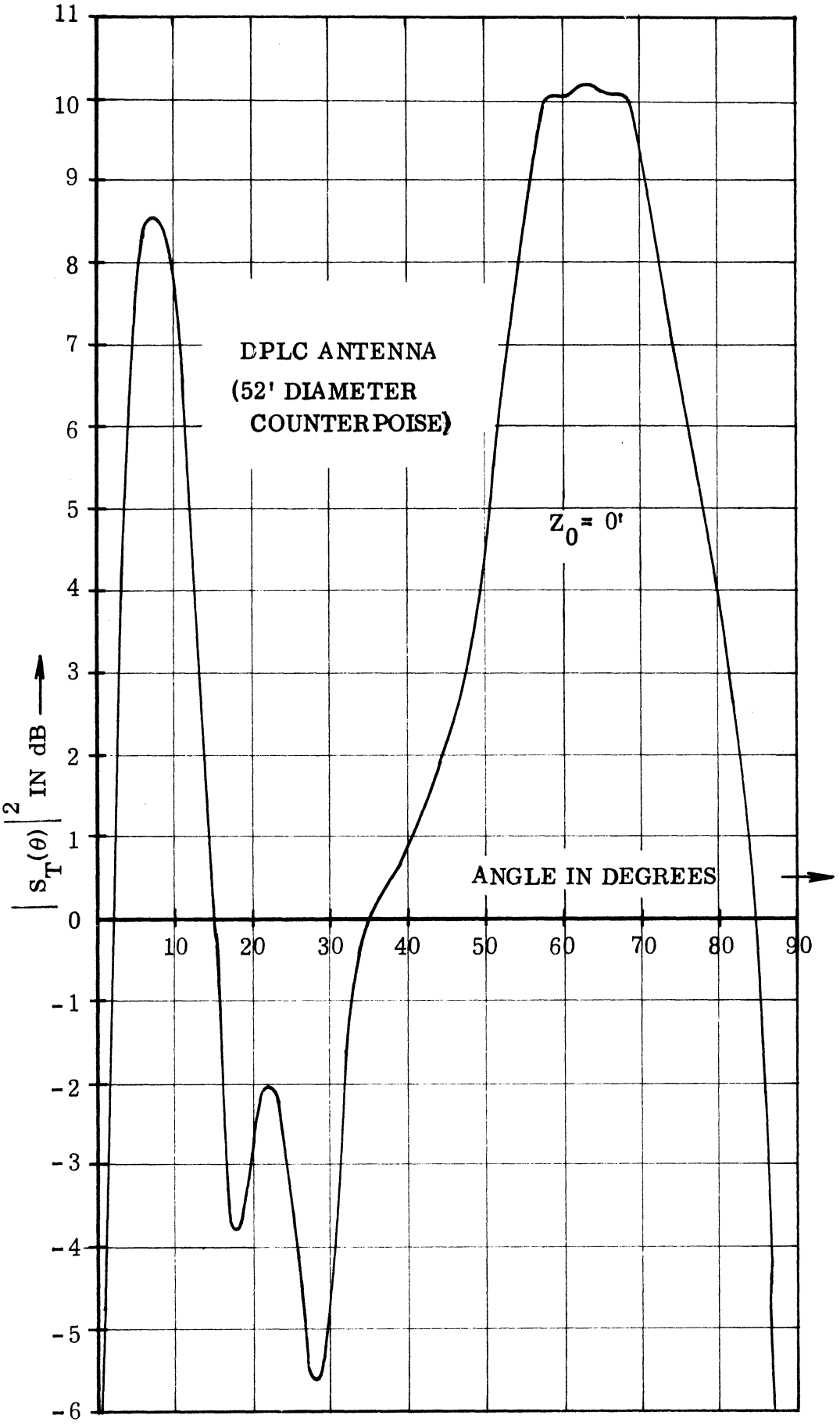

Fig. 3-2a: Theoretical side-band elevation plane patterns of a DPLC antenna for selected heights above ground.

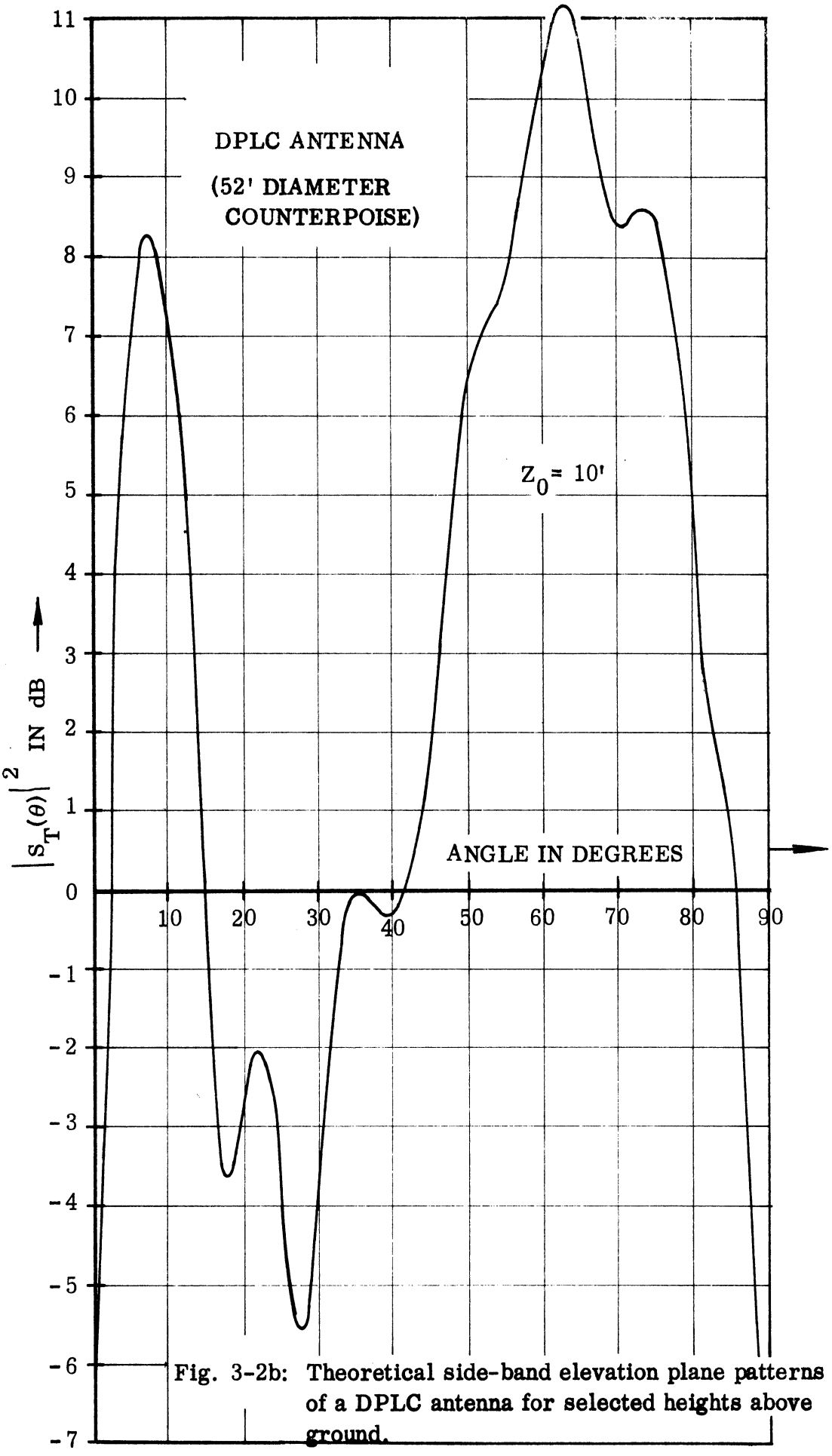

Fig. 3-2b: Theoretical side-band elevation plane patterns of a DPLC antenna for selected heights above ground.

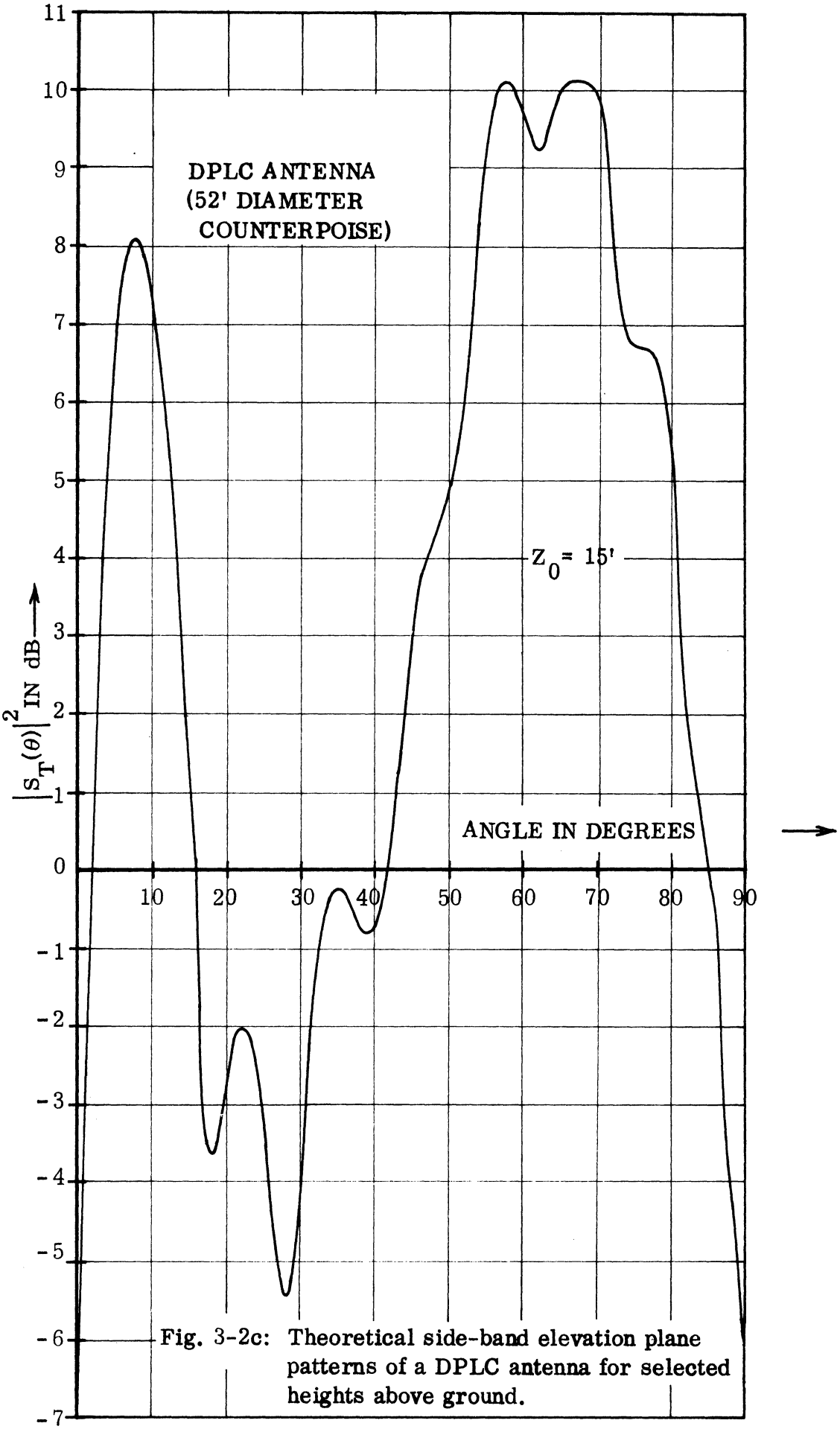

Fig. 3-2c: Theoretical side-band elevation plane patterns of a DPLC antenna for selected heights above ground.

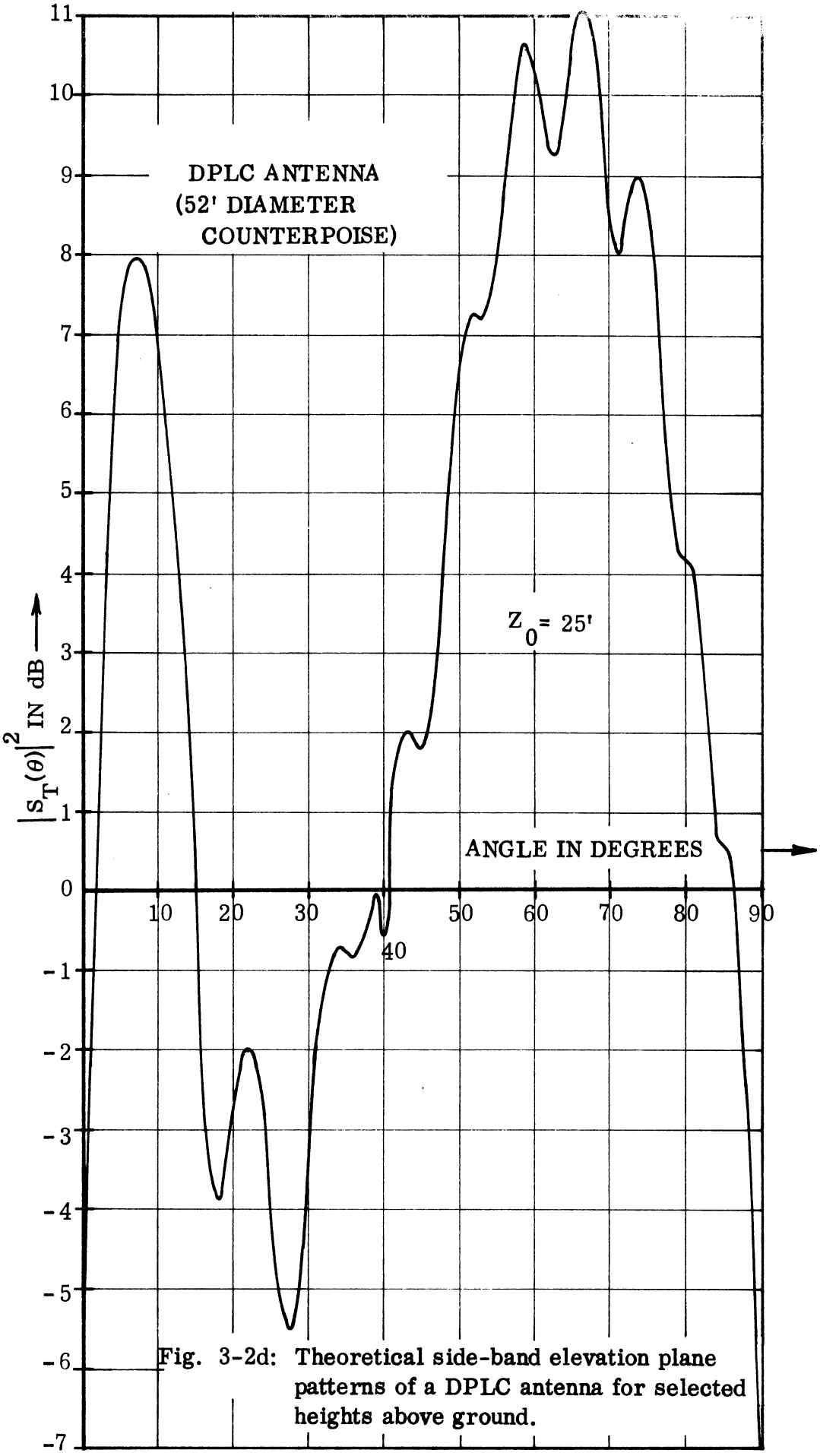

Fig. 3-2d: Theoretical side-band elevation plane patterns of a DPLC antenna for selected heights above ground.

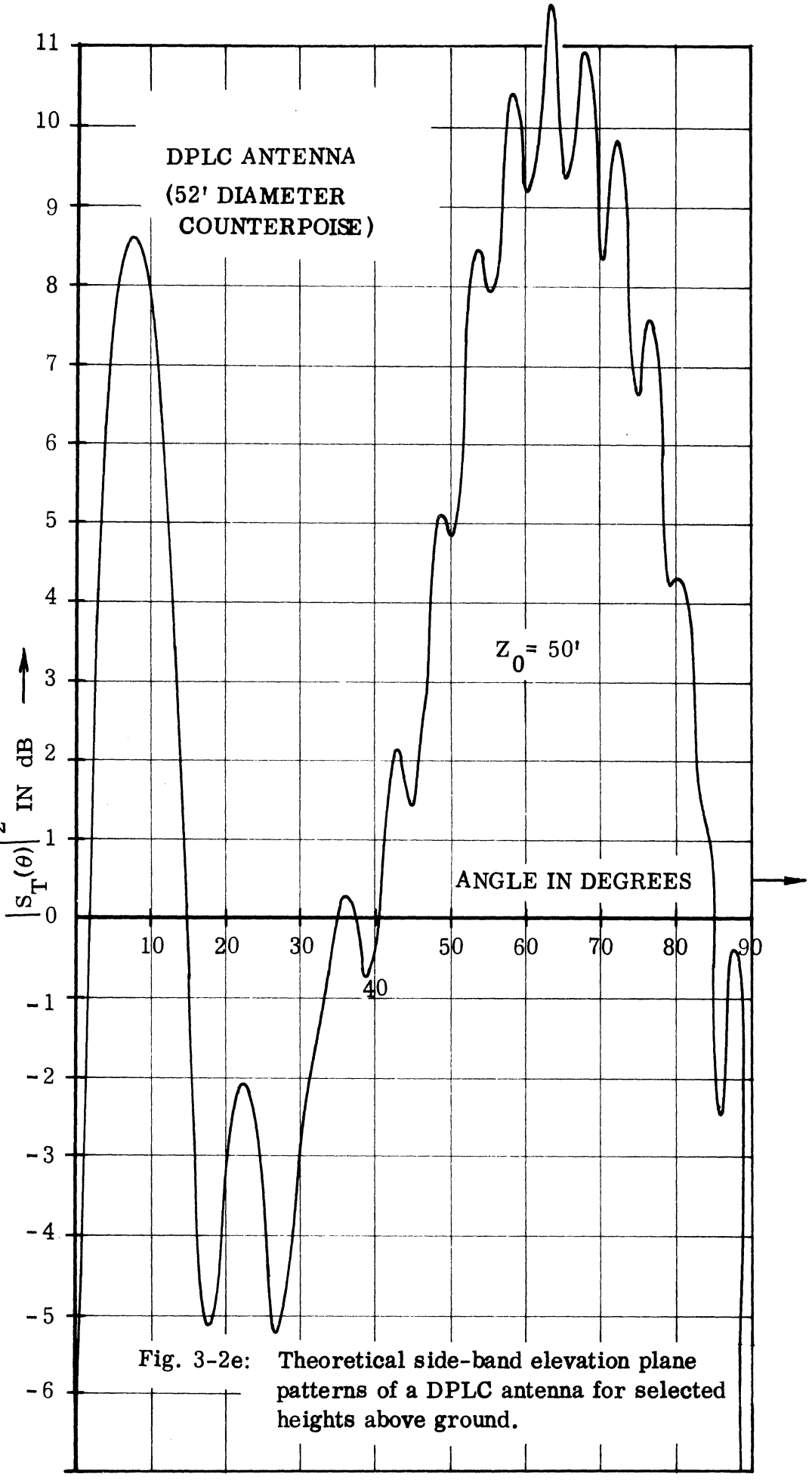

Fig. 3-2e: Theoretical side-band elevation plane patterns of a DPLC antenna for selected heights above ground.

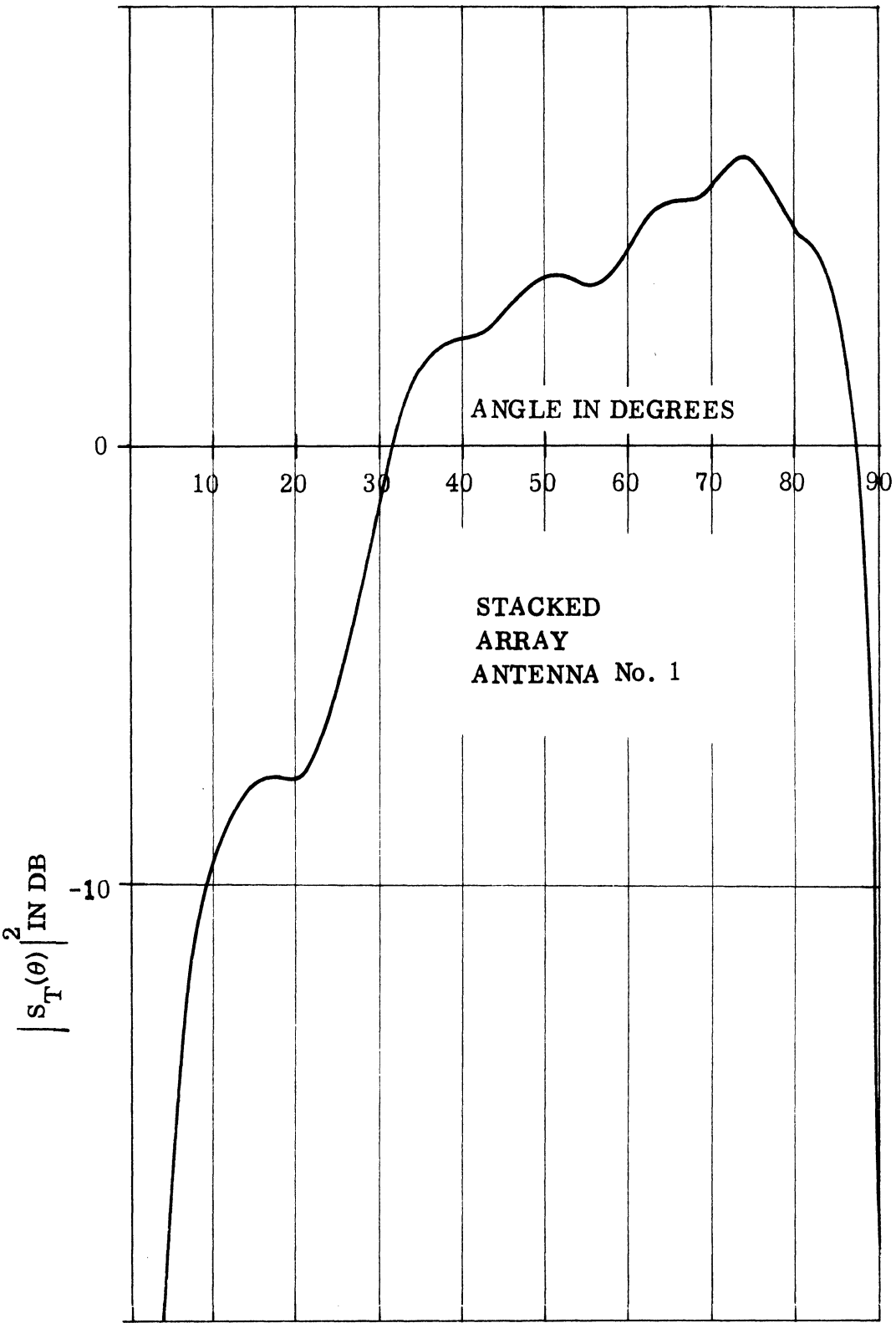

Fig. 3-3a: Theoretical elevation plane pattern of the optimum stacked array antenna above ground. $Z_0 = 15'$.

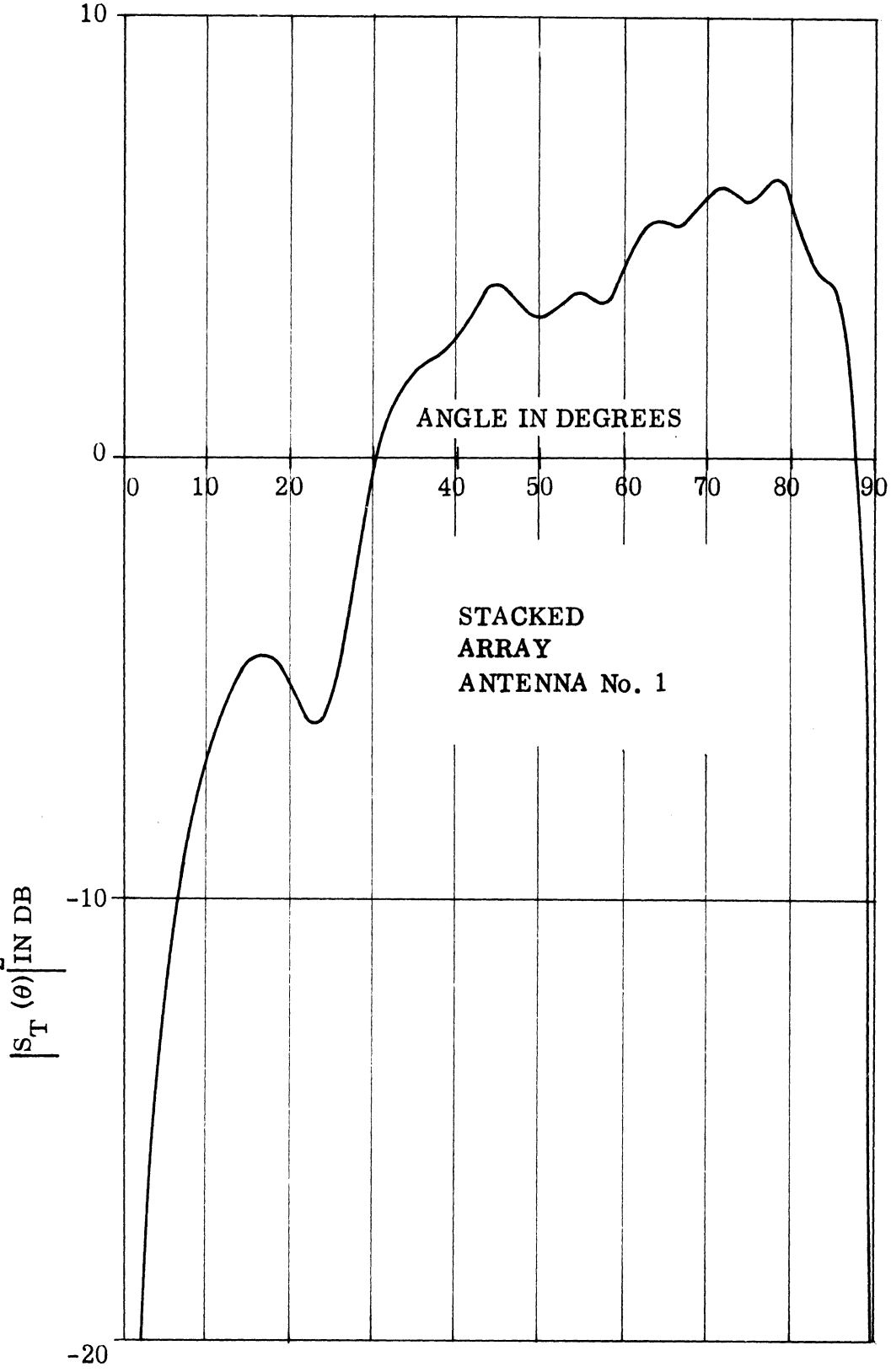

Fig. 3-3b: Theoretical elevation plane pattern of the optimum stacked array antenna above ground. $Z_0 = 25'$.

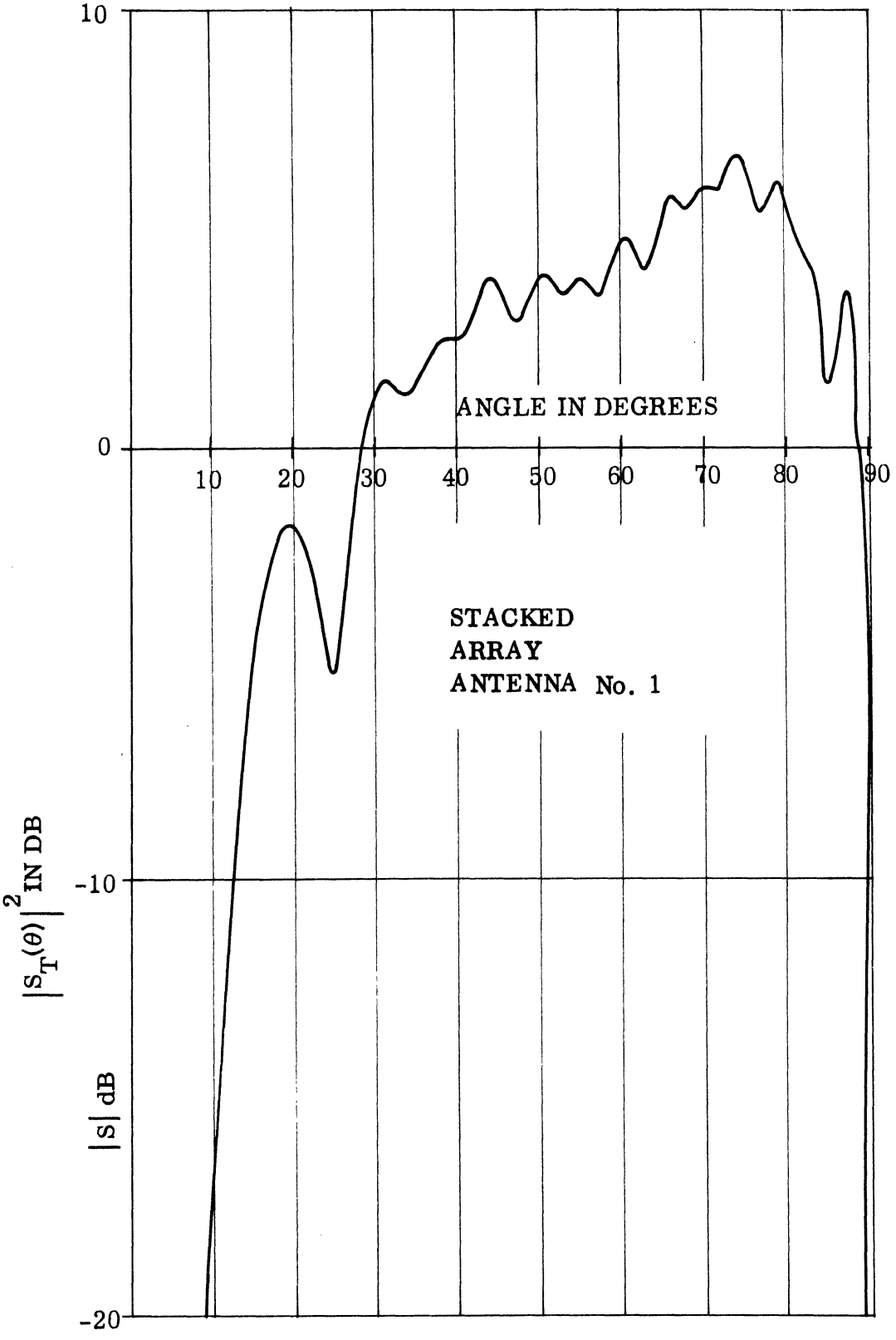

Fig. 3-3c: Theoretical elevation plane pattern of the optimum stacked array antenna. $Z_0 = 50'$.

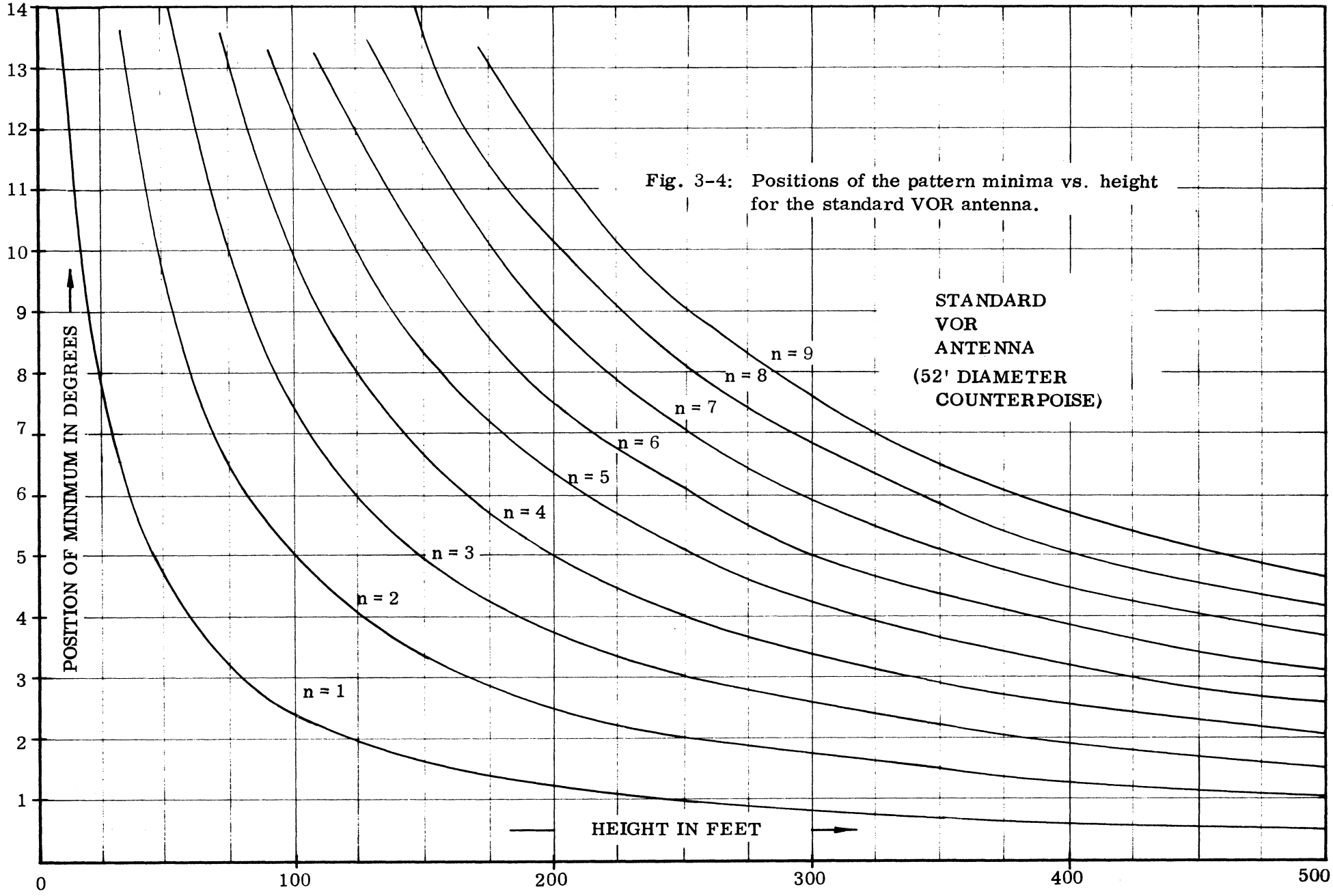

Fig. 3-4: Positions of the pattern minima vs. height for the standard VOR antenna.

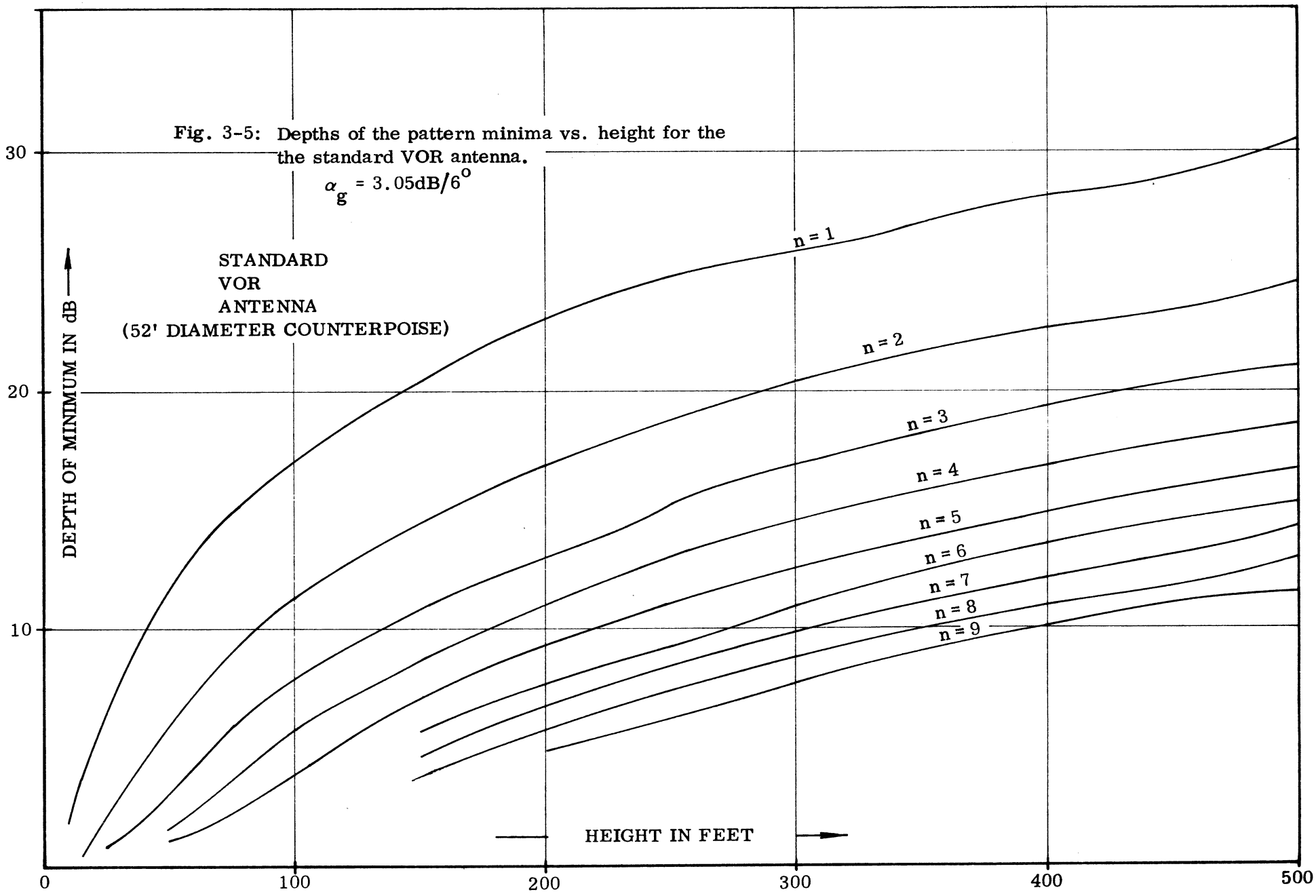

Fig. 3-5: Depths of the pattern minima vs. height for the the standard VOR antenna.
$\alpha_g = 3.05\text{dB}/6^o$

Fig. 3-6: Depths of the pattern minima vs. height for the DPLC antenna. $\alpha_g = 21.22\text{dB}/6^{\circ}$

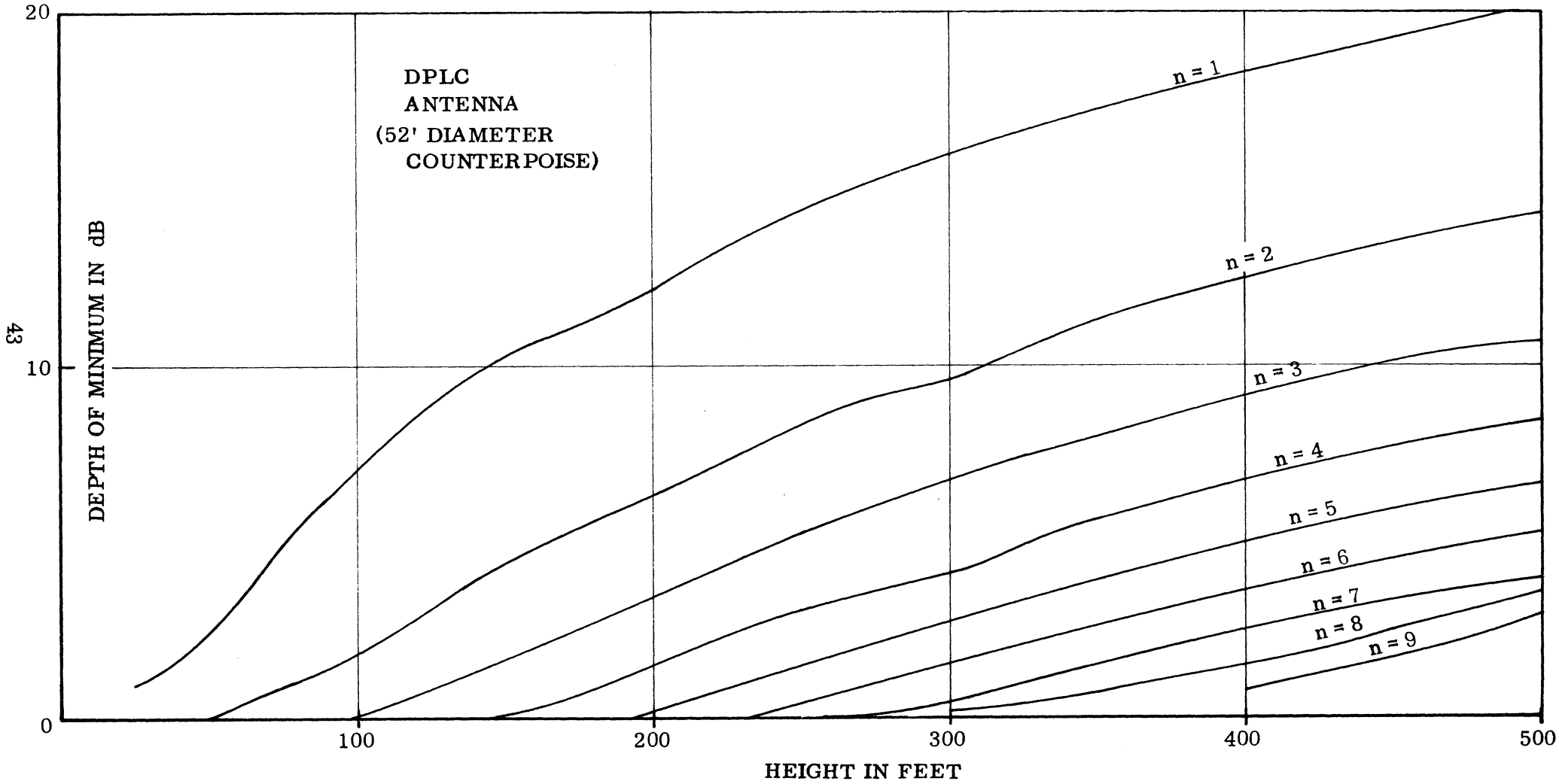

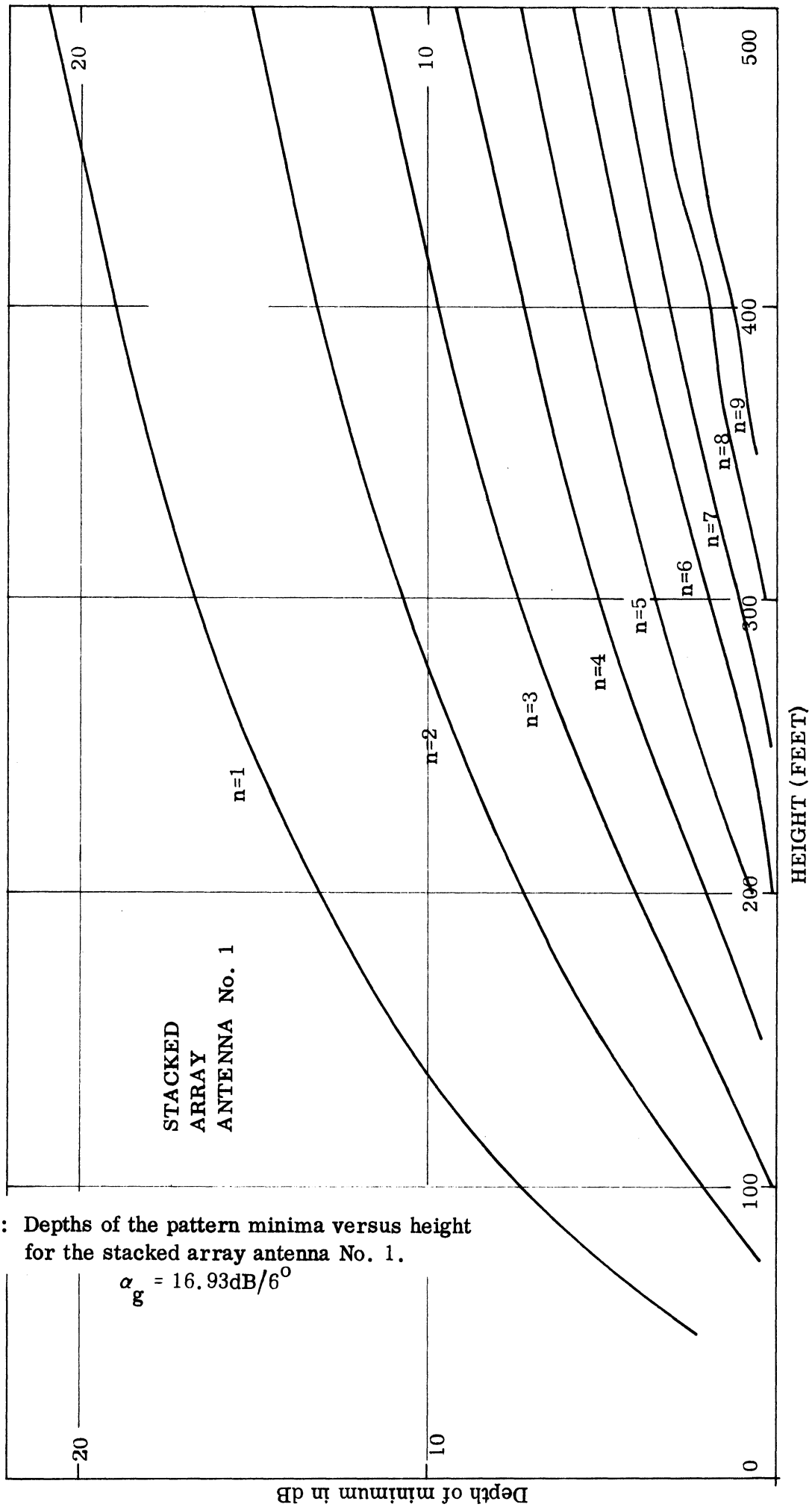

Fig. 3-7: Depths of the pattern minima versus height for the stacked array antenna No. 1.
$\alpha_g = 16.93\text{dB}/6^o$

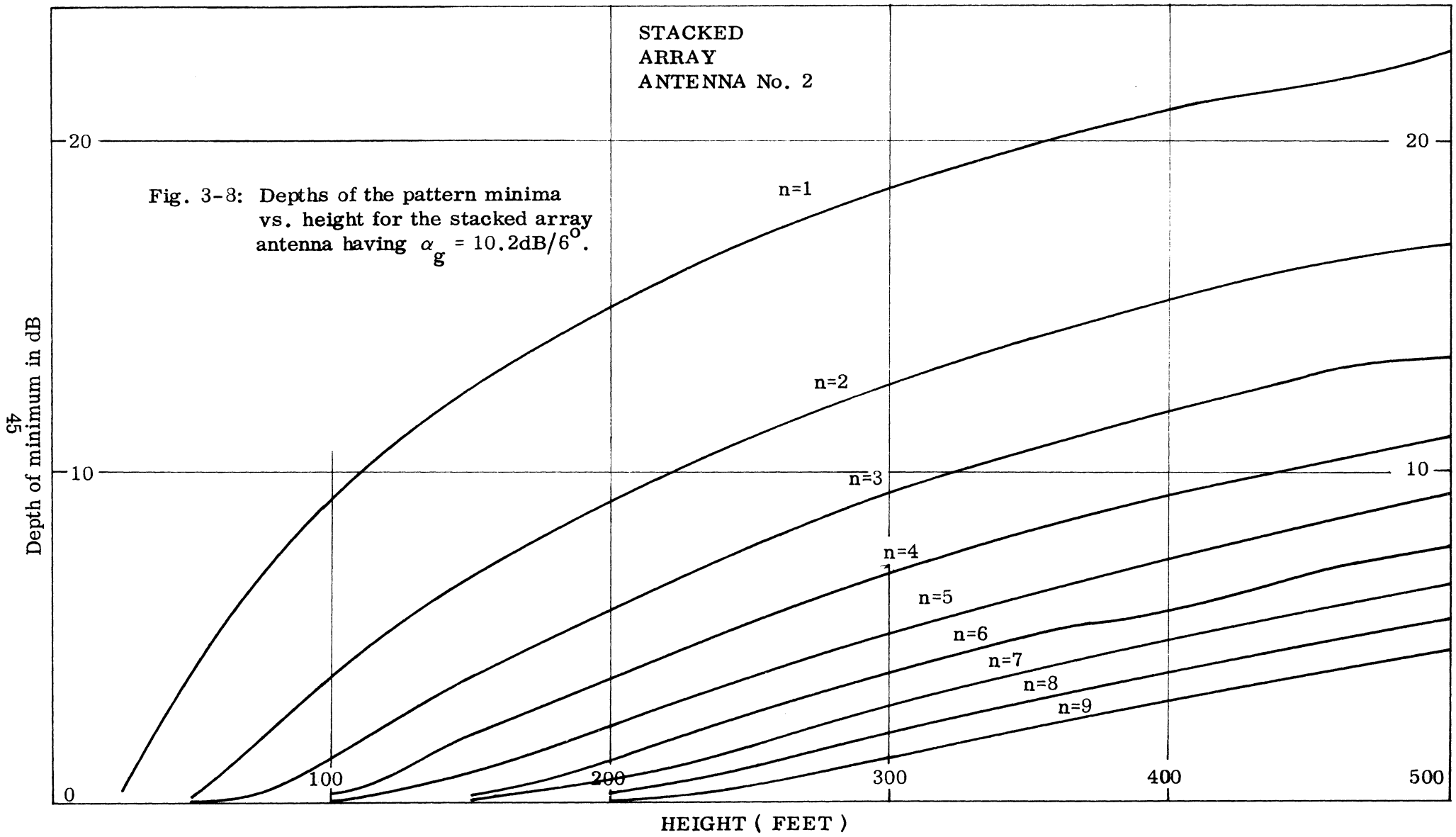

Fig. 3-8: Depths of the pattern minima vs. height for the stacked array antenna having α_g = 10.2dB/6°.

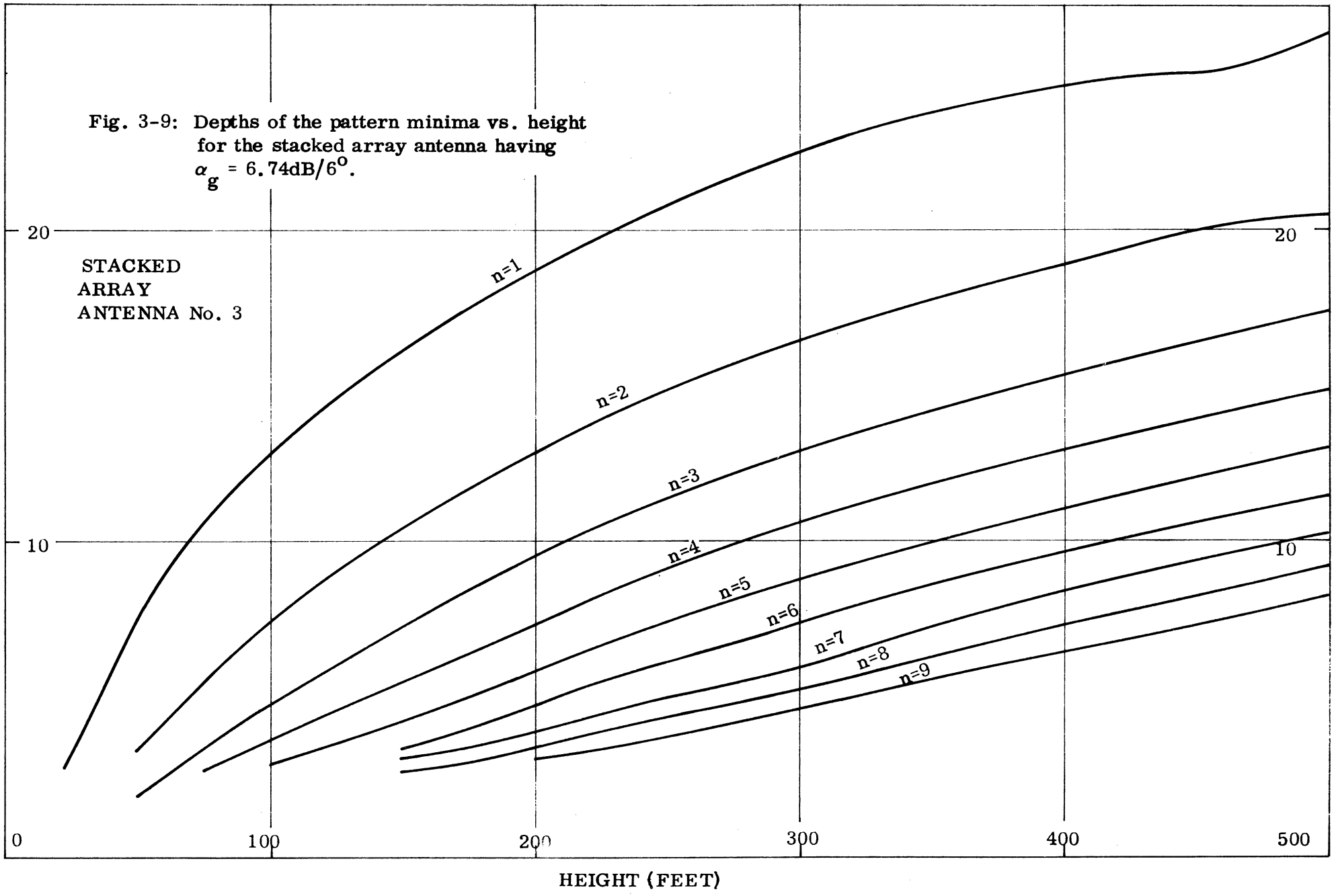

Fig. 3-9: Depths of the pattern minima vs. height for the stacked array antenna having $\alpha_g = 6.74\text{dB}/6^{\circ}$.

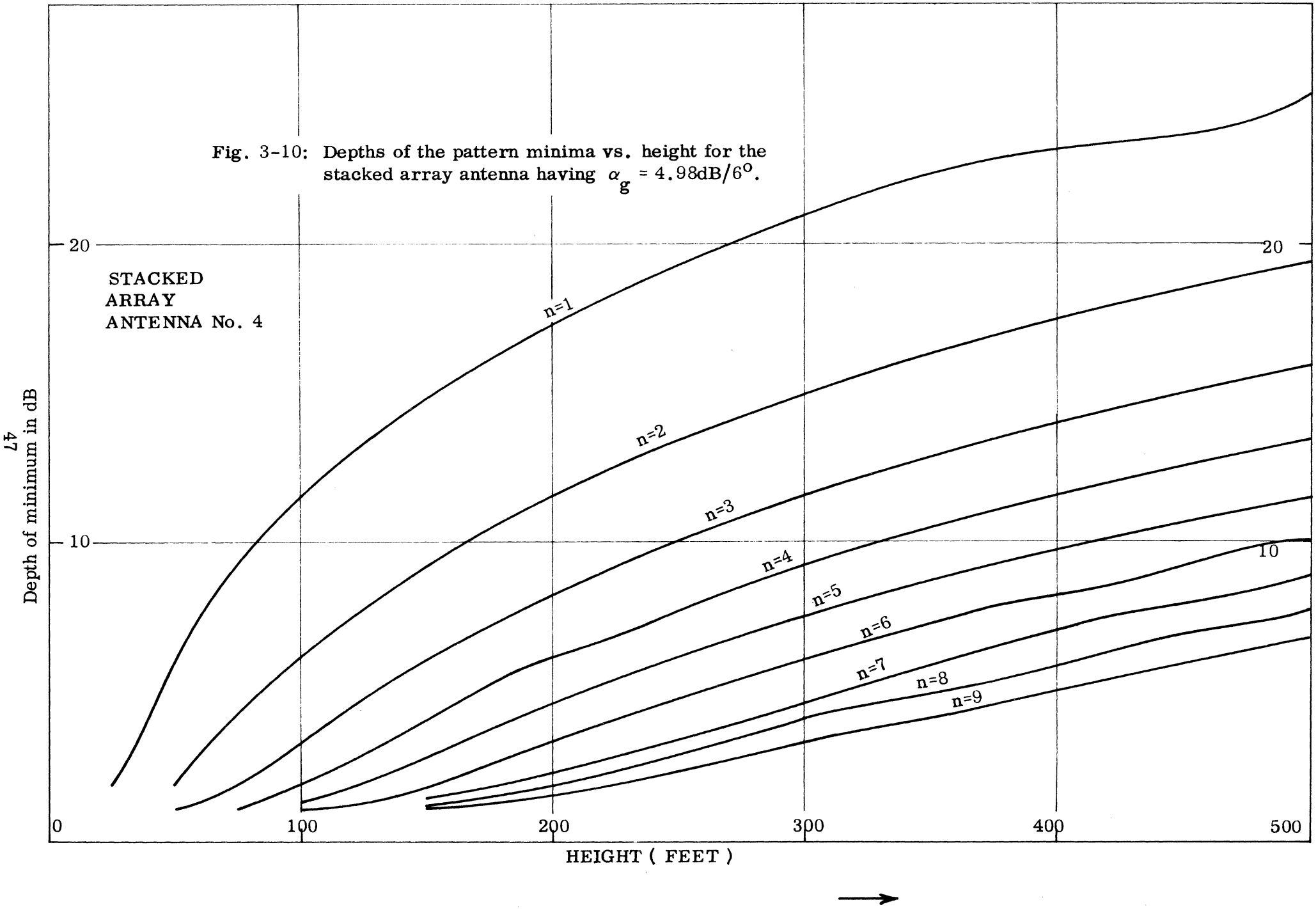

Fig. 3-10: Depths of the pattern minima vs. height for the stacked array antenna having $\alpha_g = 4.98\text{dB}/6^o$.

Fig. 3-11a: Side-band mode elevation plane radiation patterns near the horizon for $Z_0 = 450'$ (standard VOR antenna).

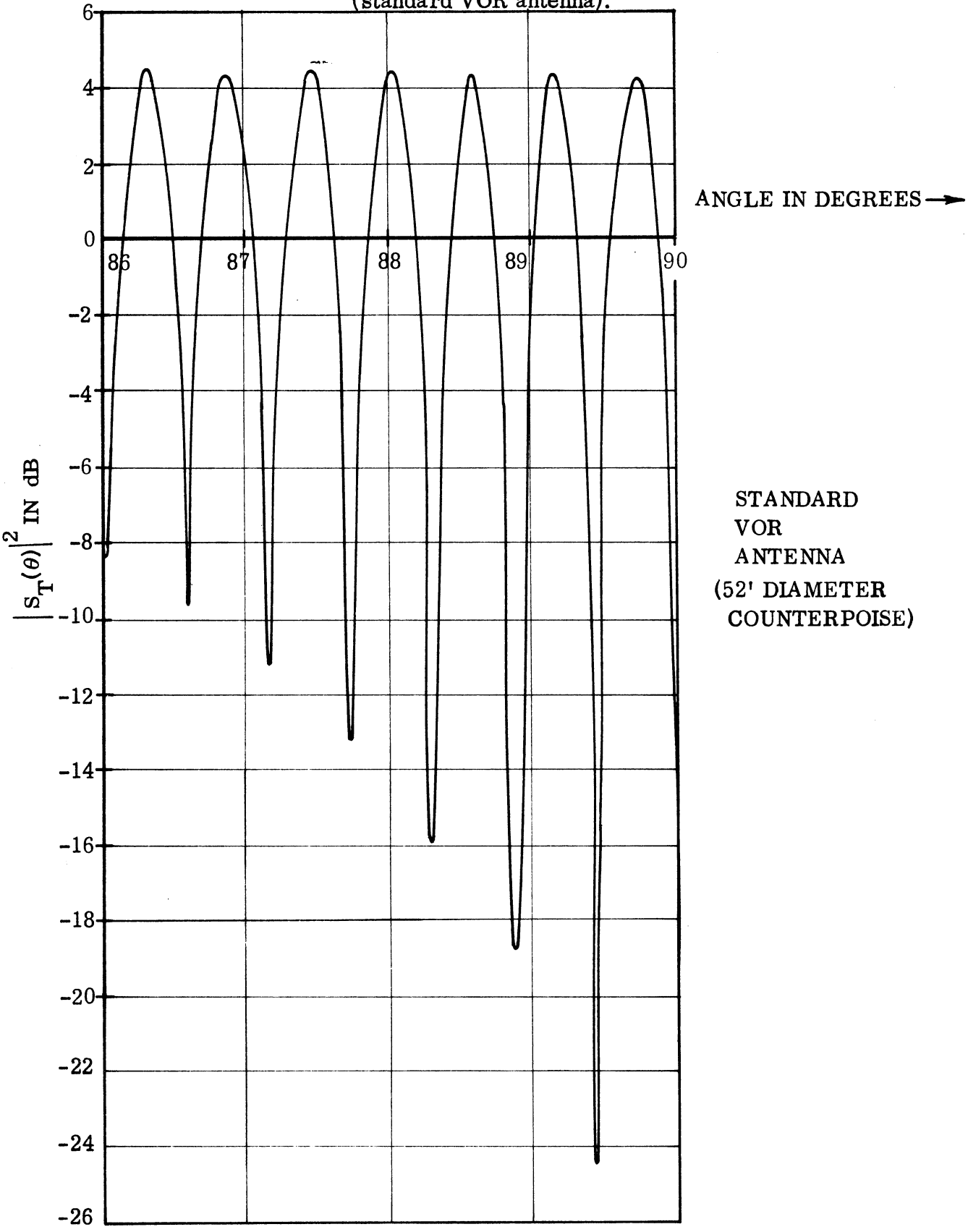

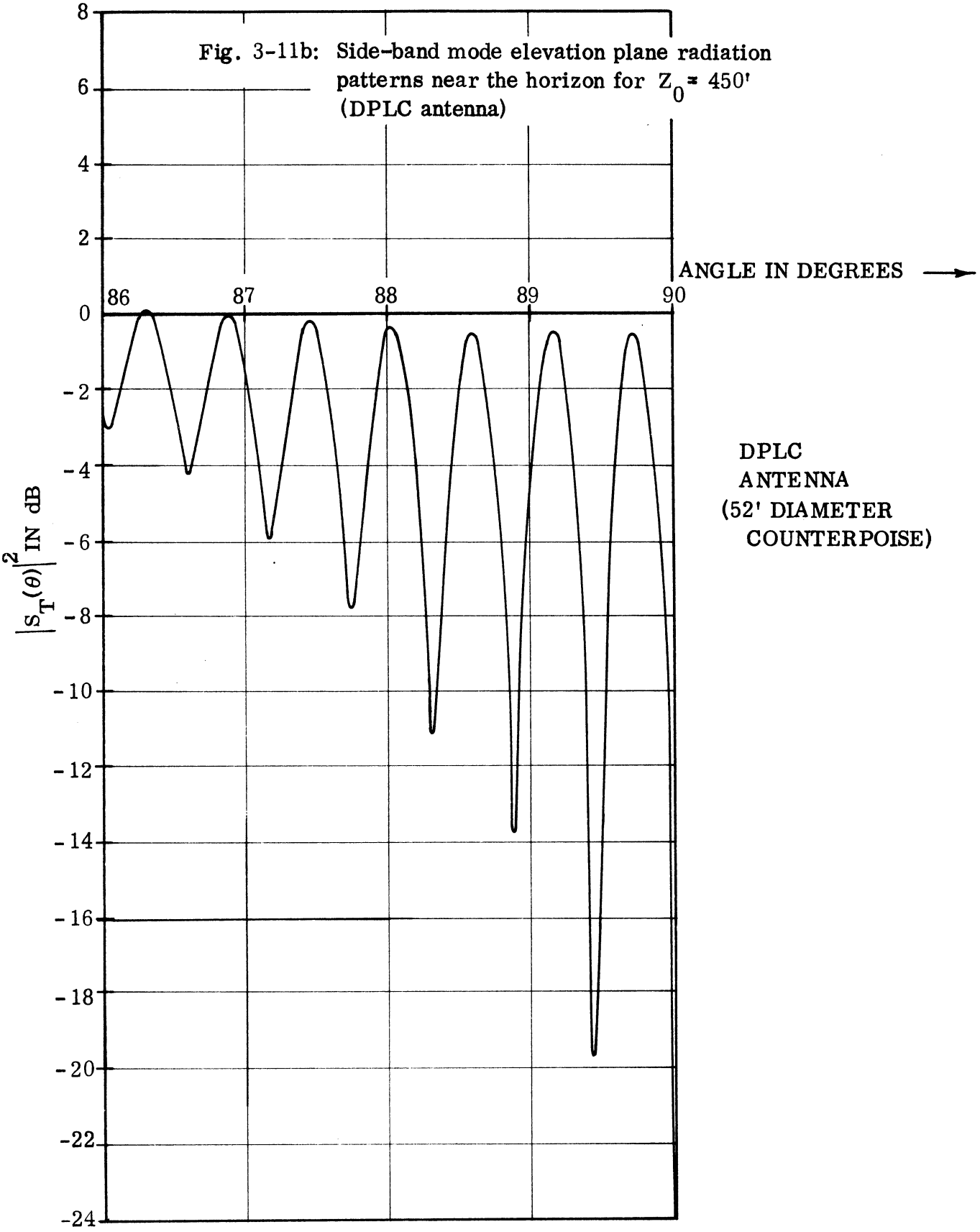

Fig. 3-11b: Side-band mode elevation plane radiation patterns near the horizon for $Z_0 = 450'$ (DPLC antenna)

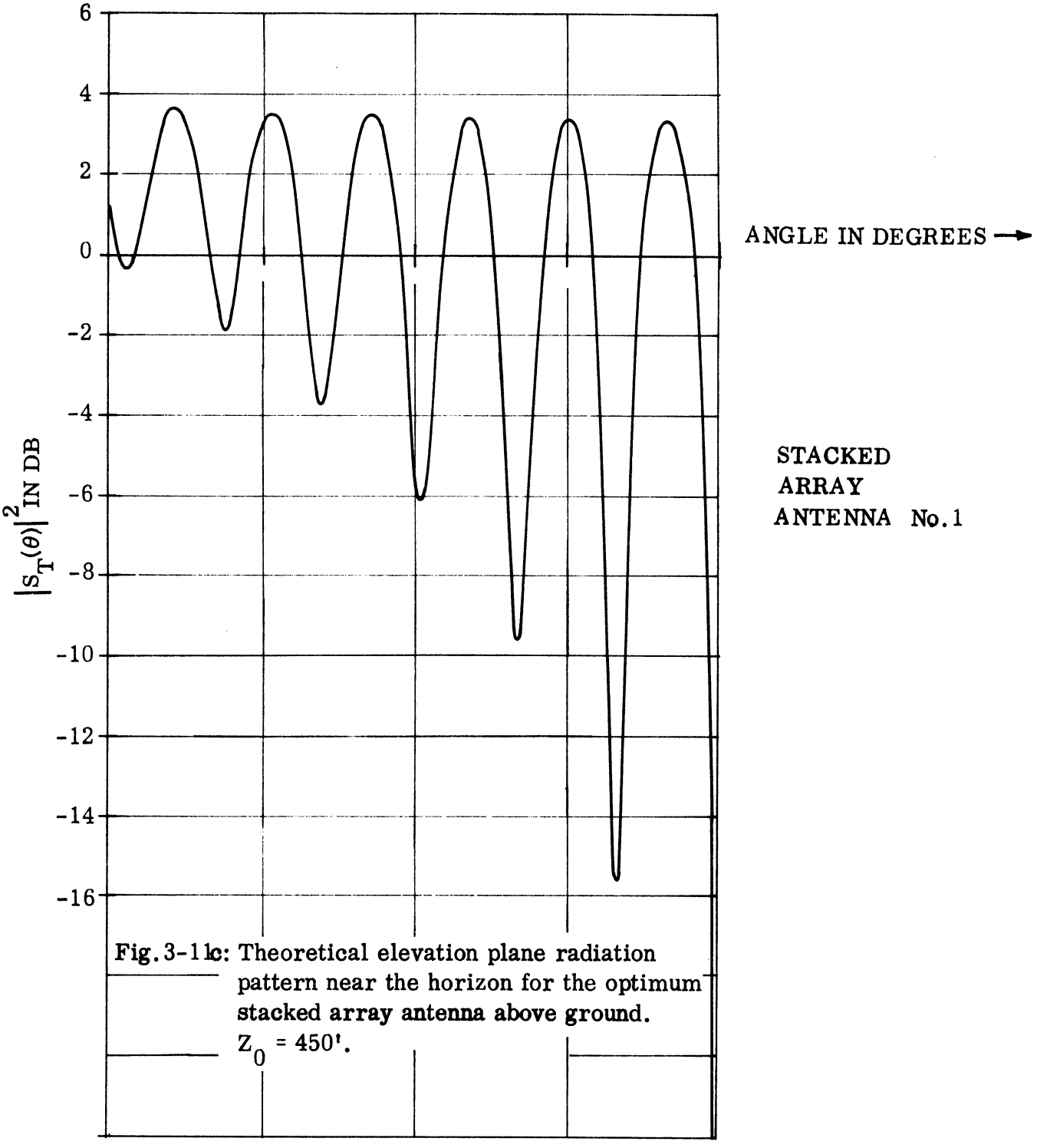

Fig. 3-11c: Theoretical elevation plane radiation pattern near the horizon for the optimum stacked array antenna above ground. $Z_0 = 450'$.

Fig. 3-12a: Side-band mode elevation plane radiation patterns near the horizon for $Z_0 = 350'$ (standard VOR antenna).

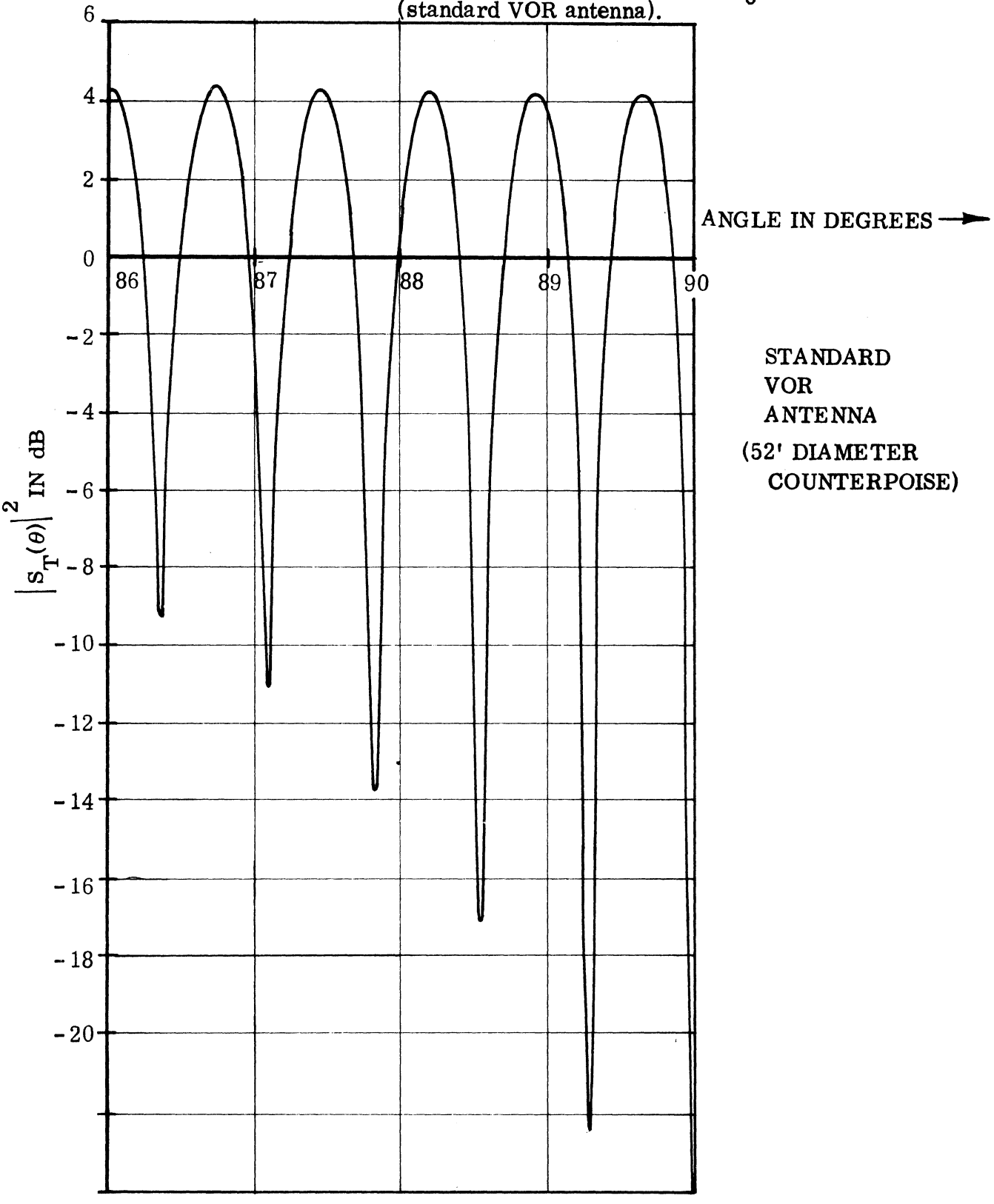

Fig. 3-12b: Side-band mode elevation plane radiation patterns near the horizon for $Z_0 = 350'$ (DPLC antenna).

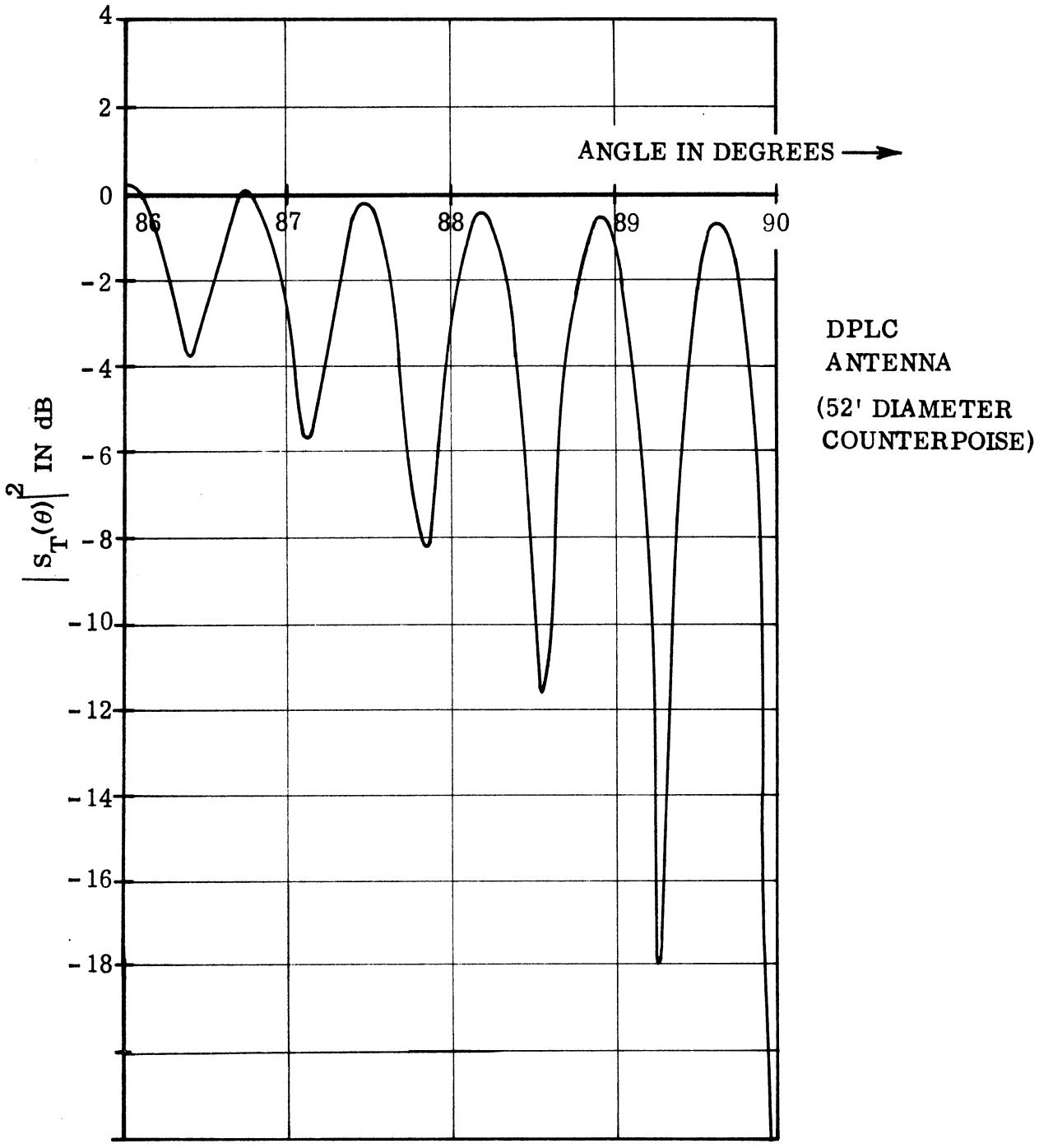

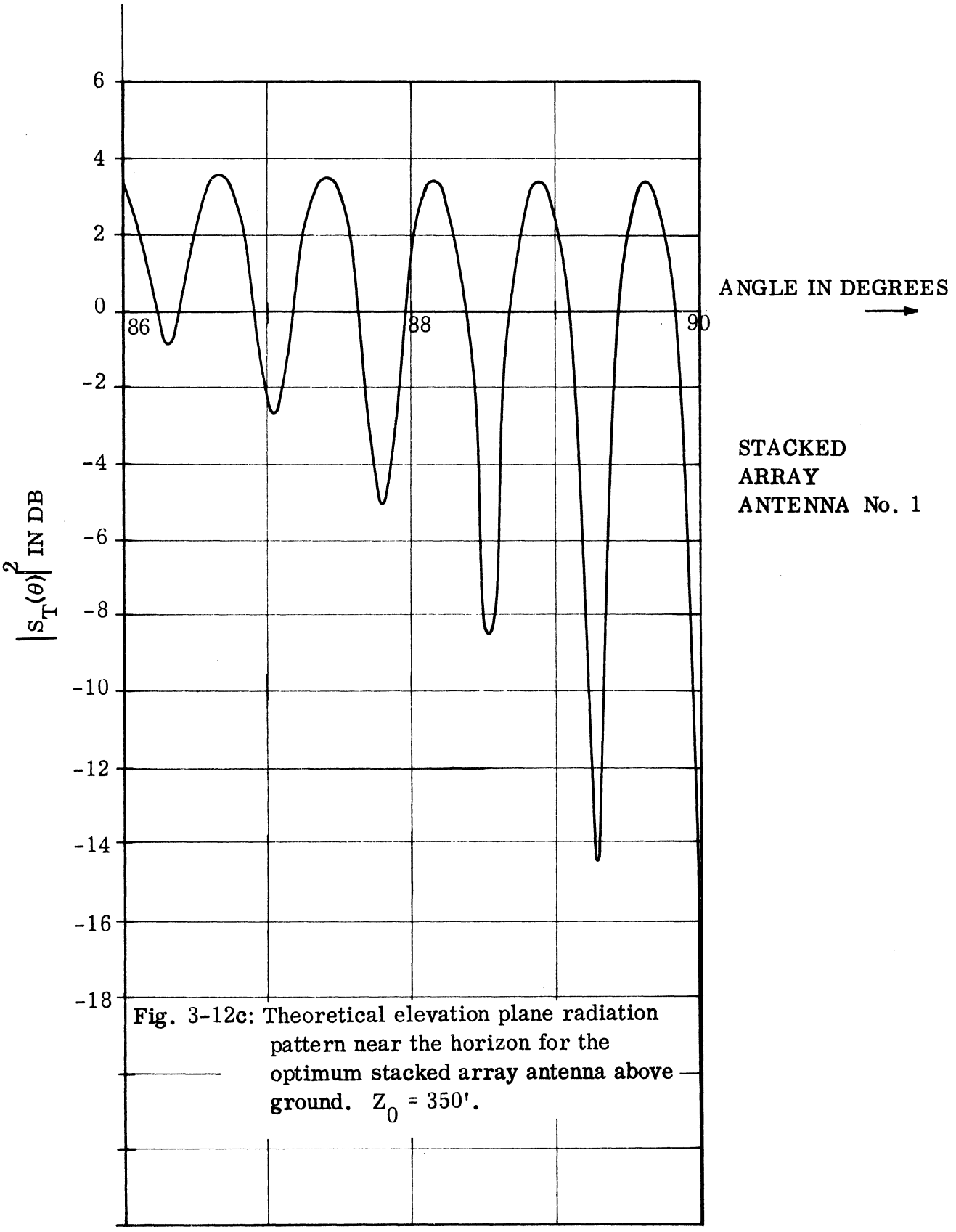

Fig. 3-12c: Theoretical elevation plane radiation pattern near the horizon for the optimum stacked array antenna above ground. $Z_0 = 350'$.

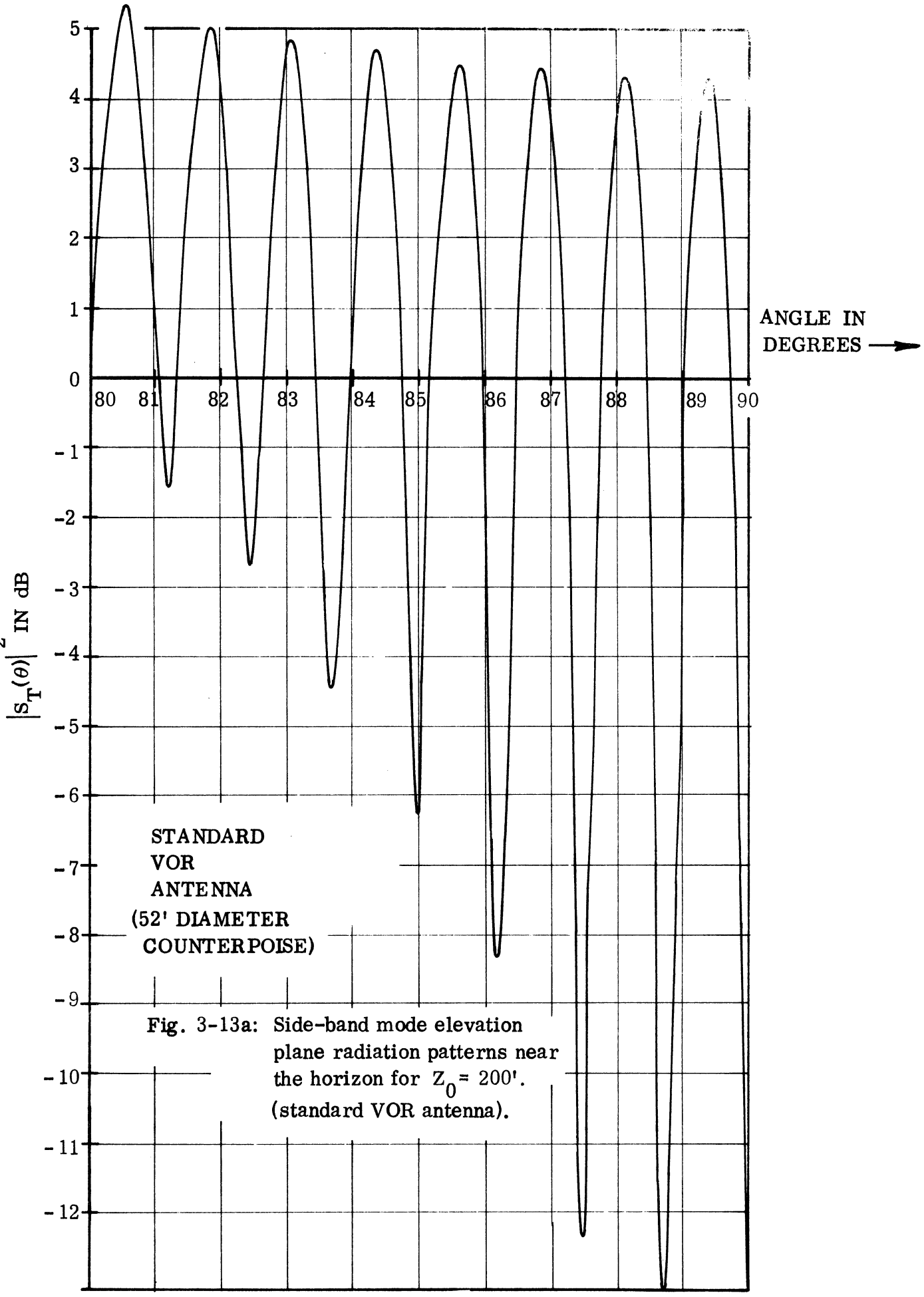

Fig. 3-13a: Side-band mode elevation plane radiation patterns near the horizon for Z_0 = 200'. (standard VOR antenna).

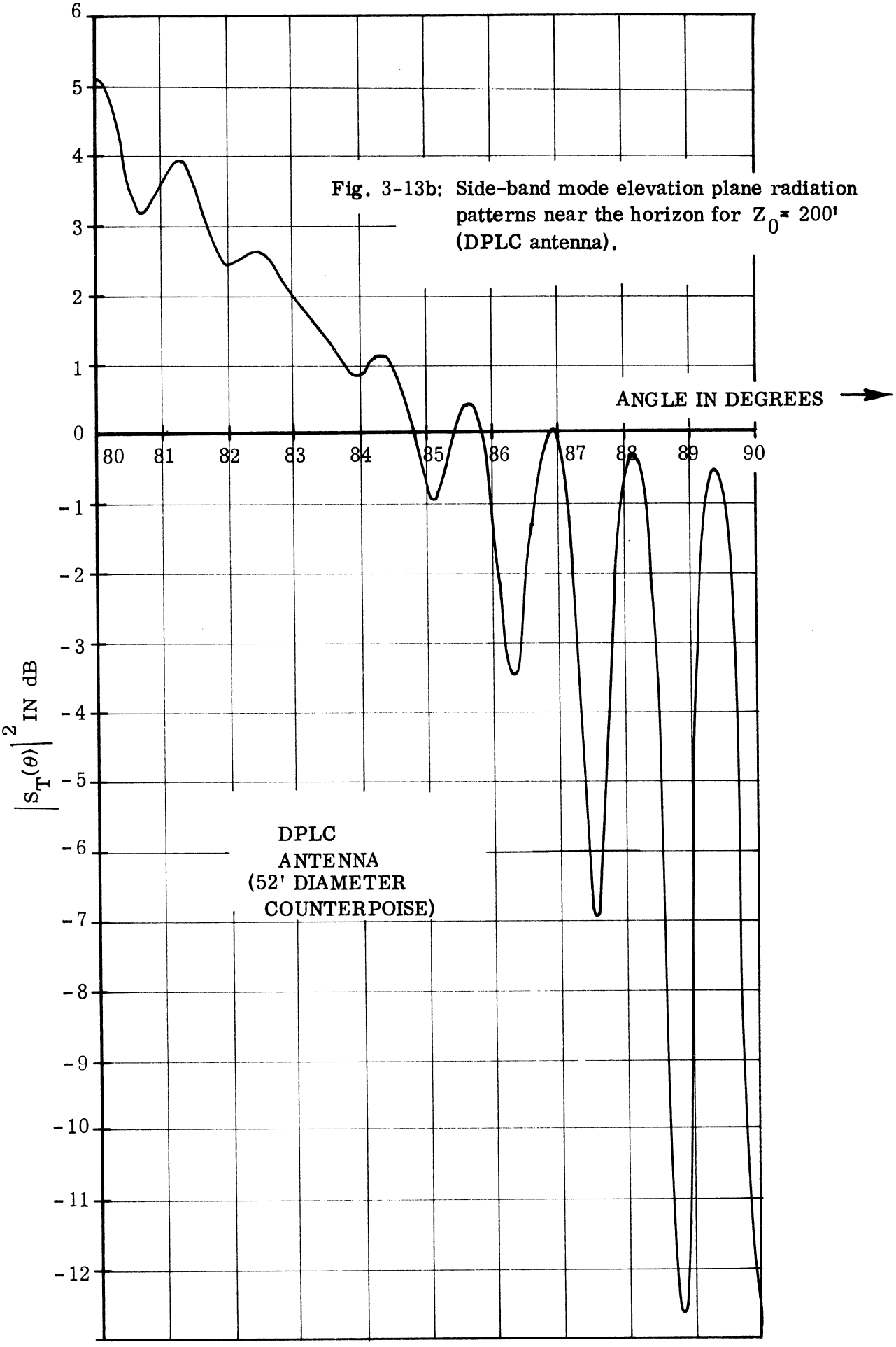

Fig. 3-13b: Side-band mode elevation plane radiation patterns near the horizon for $Z_0 = 200'$ (DPLC antenna).

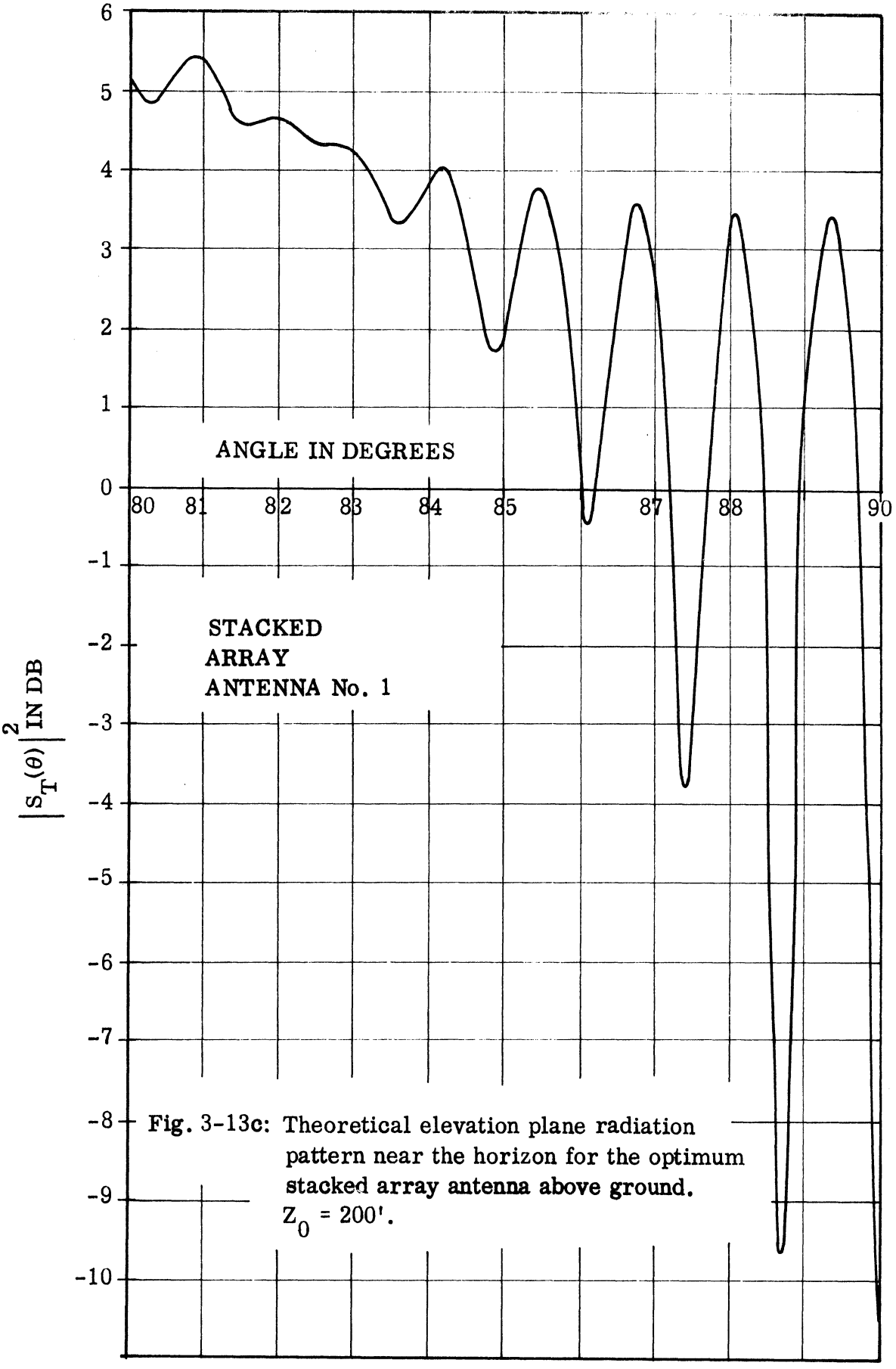

Fig. 3-13c: Theoretical elevation plane radiation pattern near the horizon for the optimum stacked array antenna above ground. $Z_0 = 200'$.

Fig. 3-14a: Side-band mode elevation plane radiation patterns near the horizon for Z_0 = 150' (standard VOR antenna).

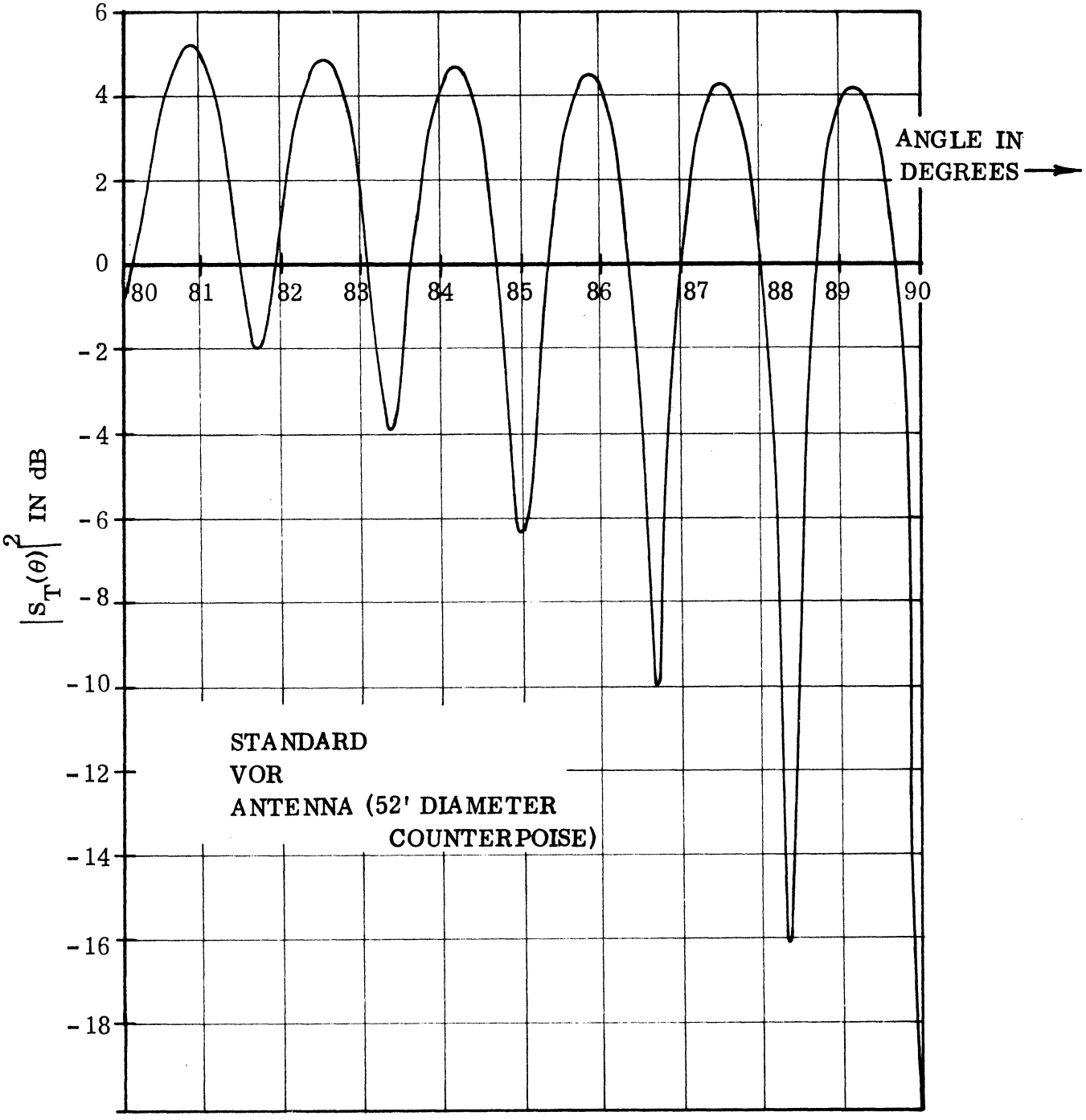

Fig. 3-14b: Side-band mode elevation plane radiation patterns near the horizon for Z_0 = 150' (DPLC antenna).

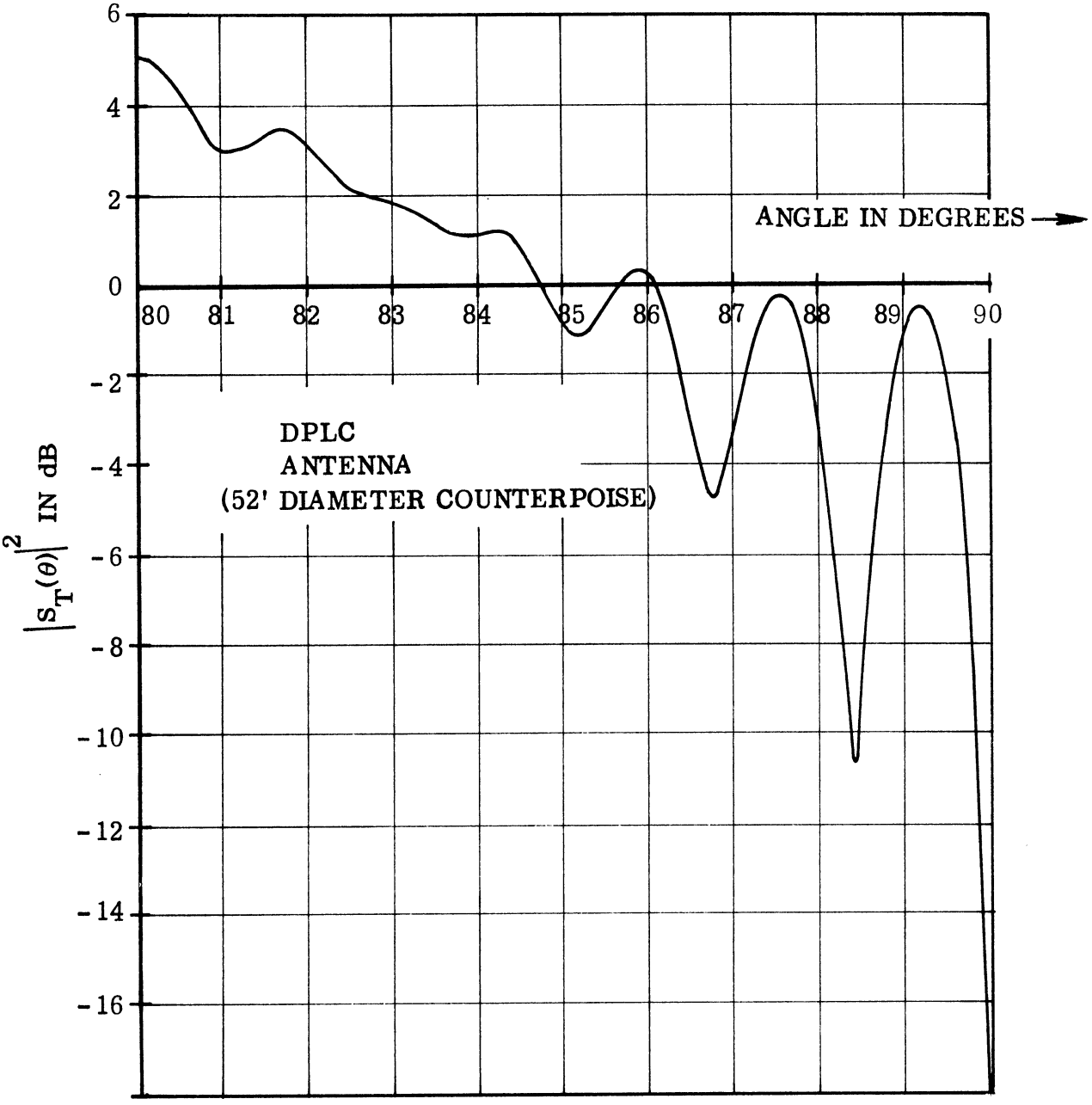

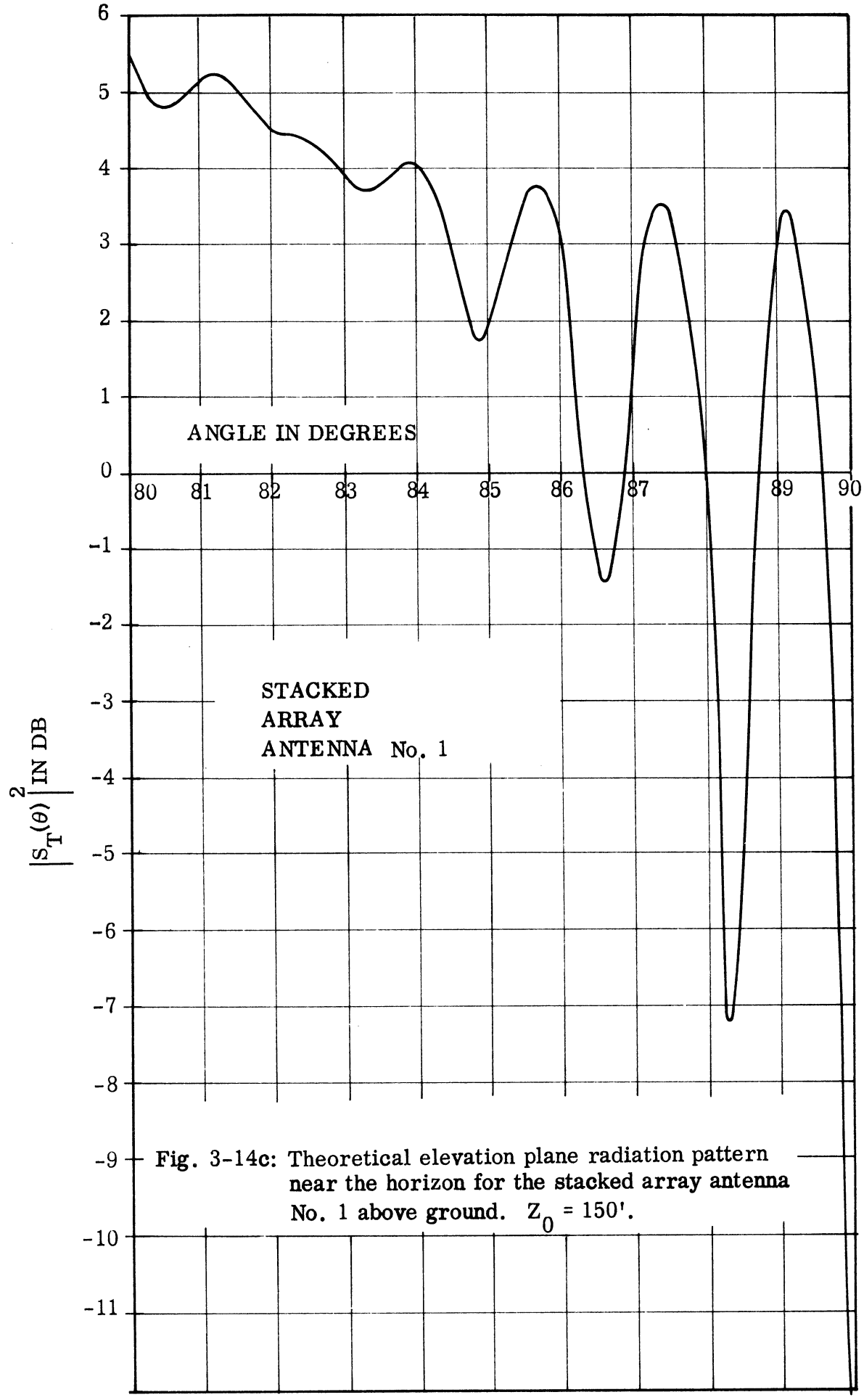

Fig. 3-14c: Theoretical elevation plane radiation pattern near the horizon for the stacked array antenna No. 1 above ground. Z_0 = 150'.

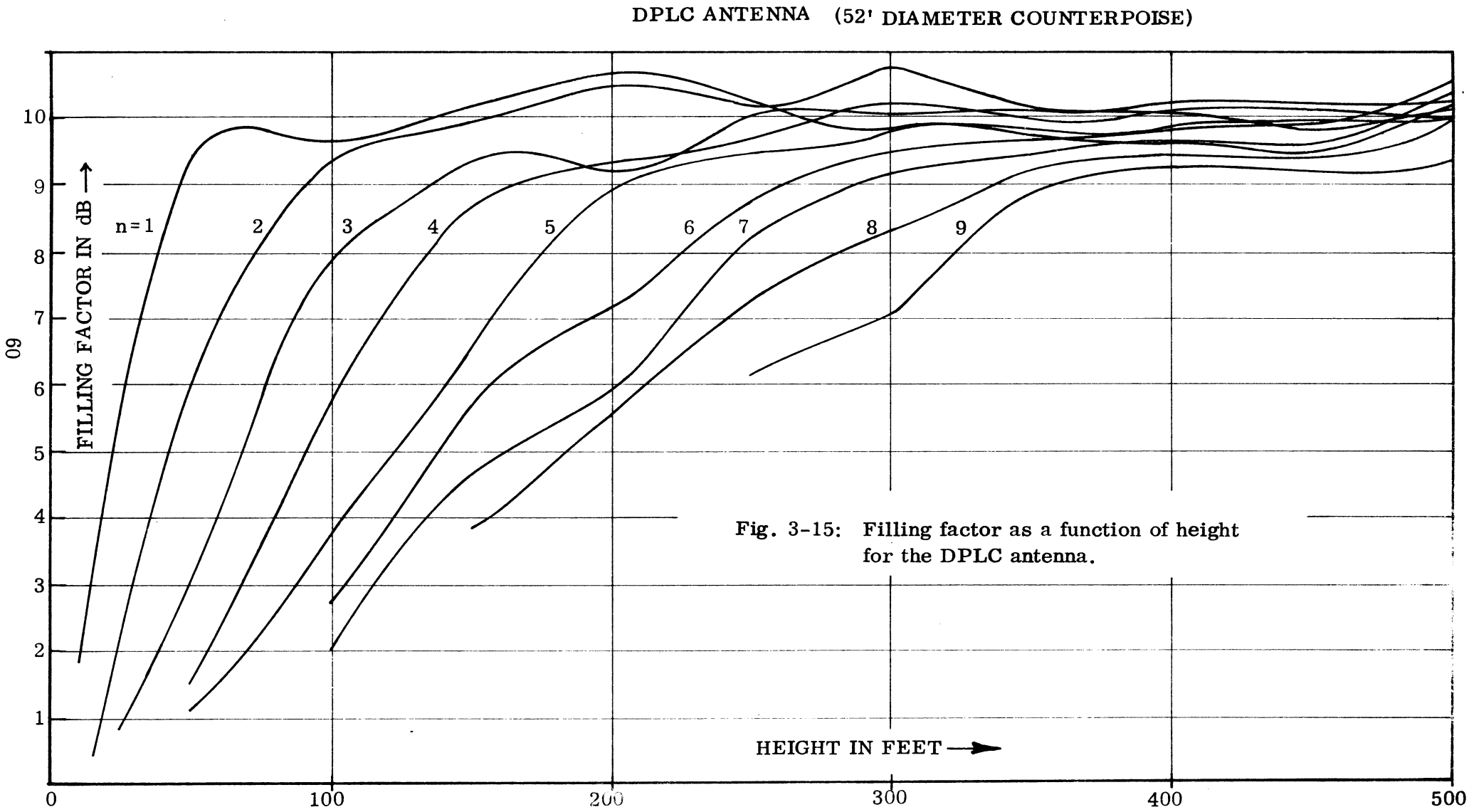

Fig. 3-15: Filling factor as a function of height for the DPLC antenna.

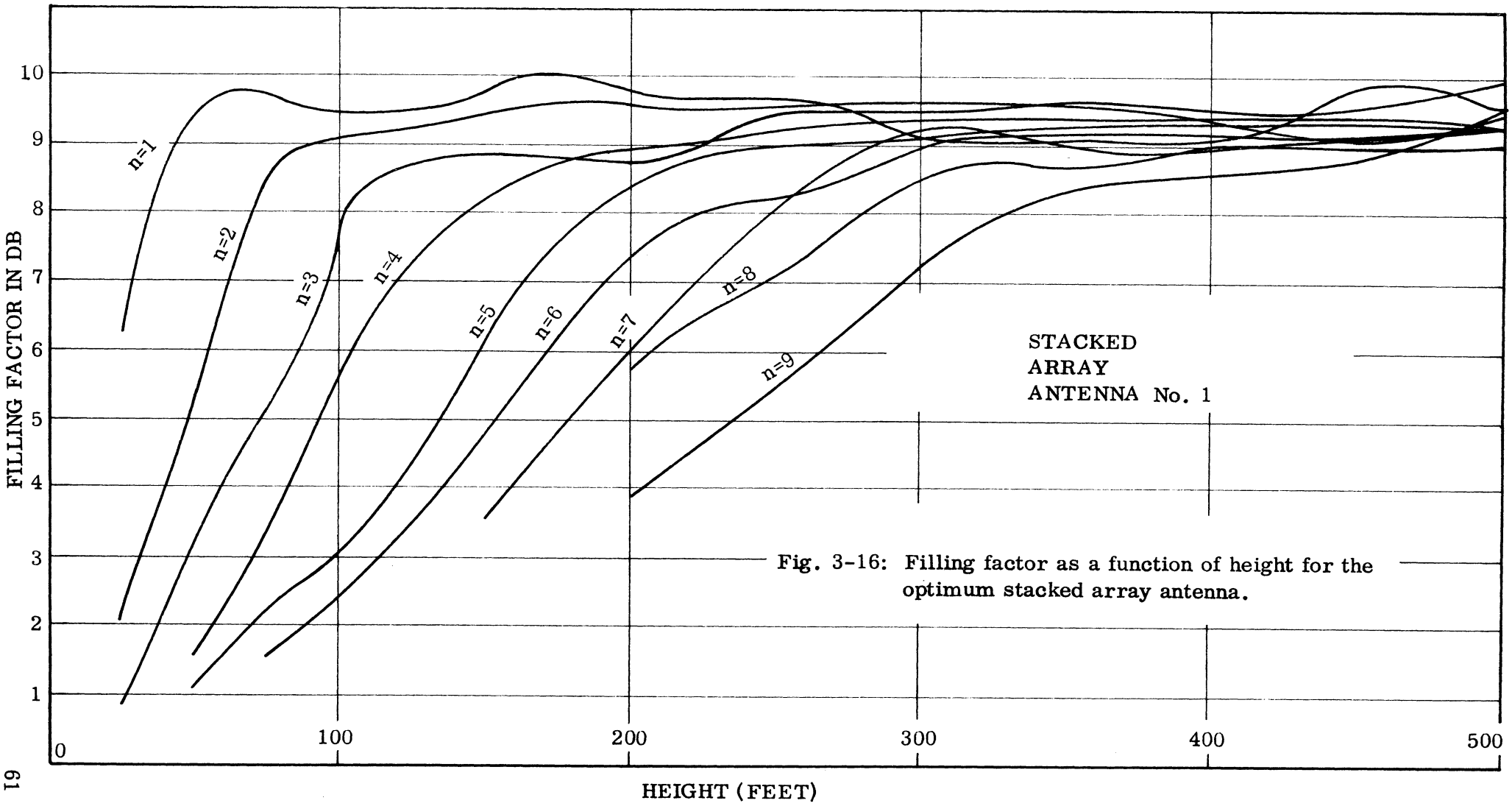

Fig. 3-16: Filling factor as a function of height for the optimum stacked array antenna.

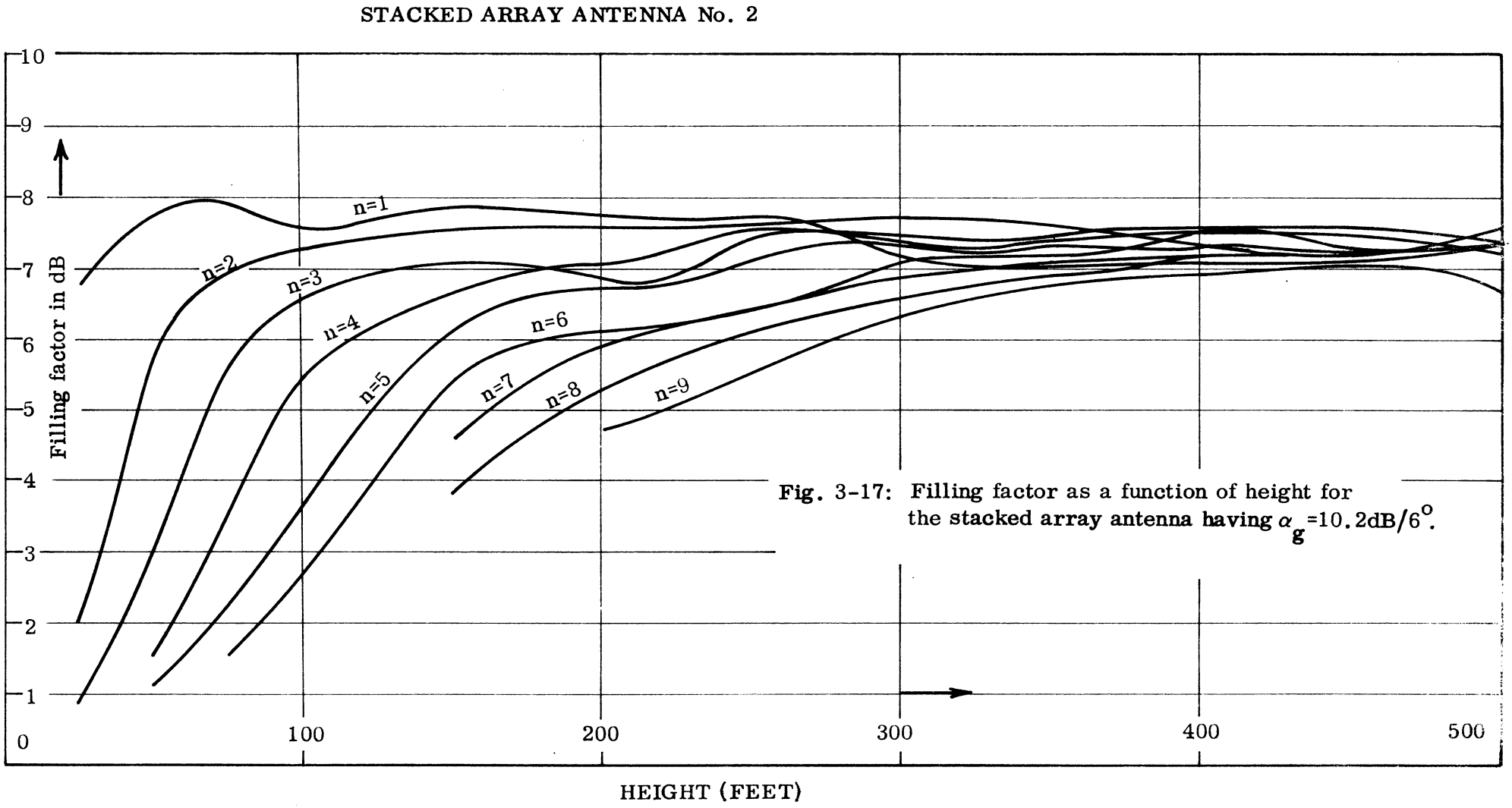

Fig. 3-17: Filling factor as a function of height for the stacked array antenna having α_g=10.2dB/6°.

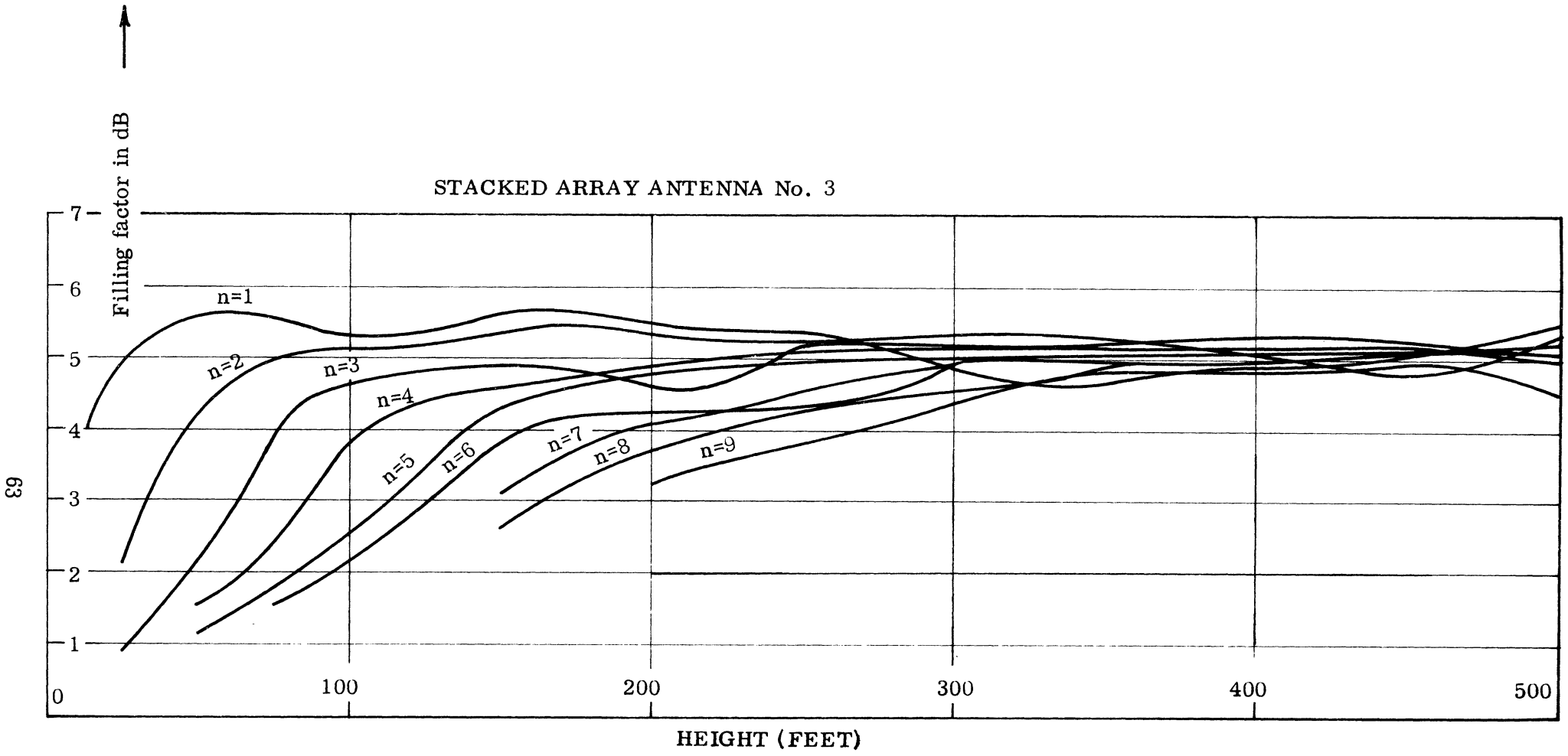

Fig. 3-18: Filling factor as a function of height for the stacked array antenna having $\alpha_g = 6.74\text{dB}/6^{\circ}$.

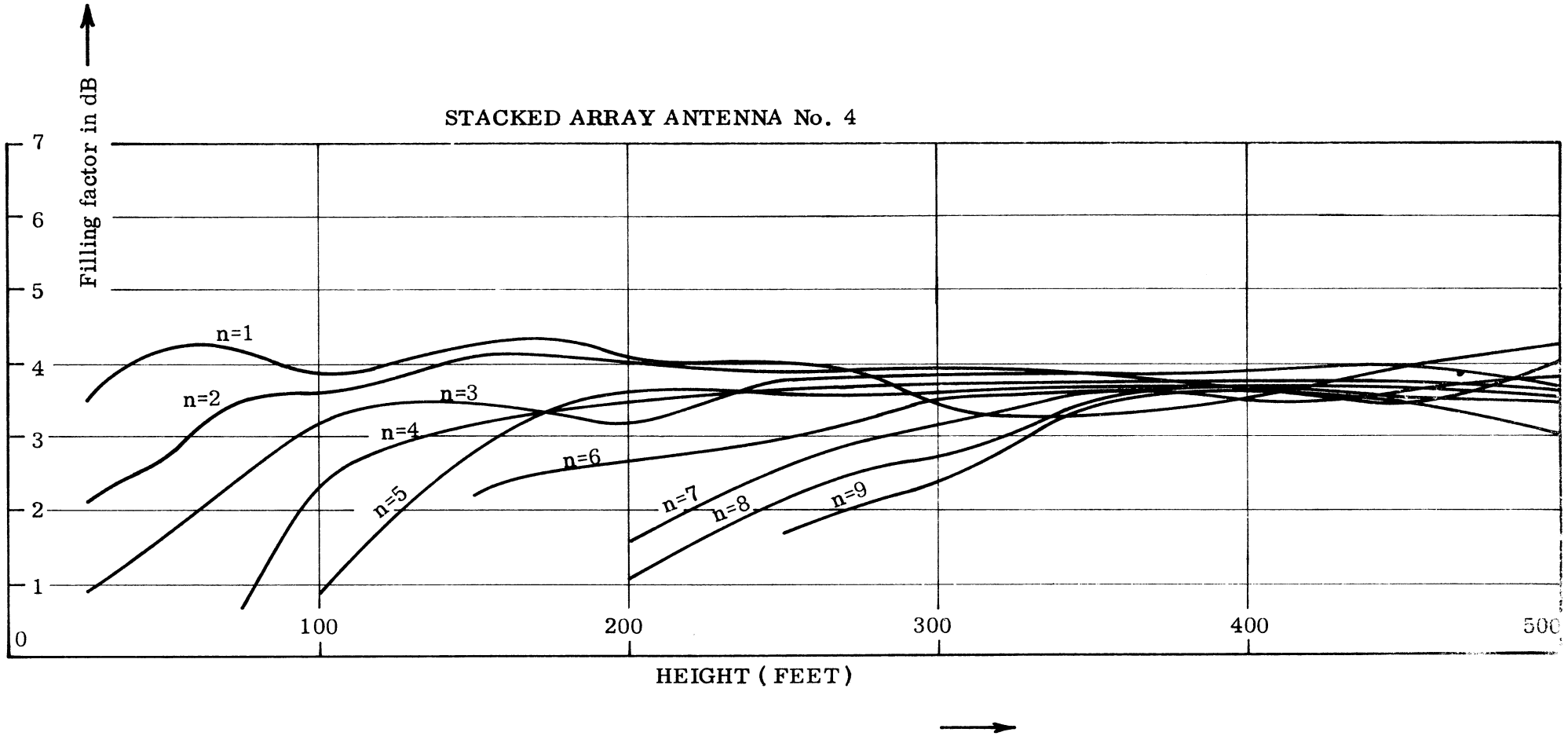

Fig. 3-19: Filling factor as a function of height for the stacked array antenna having $\alpha_g = 4.98\text{dB}/6^o$.

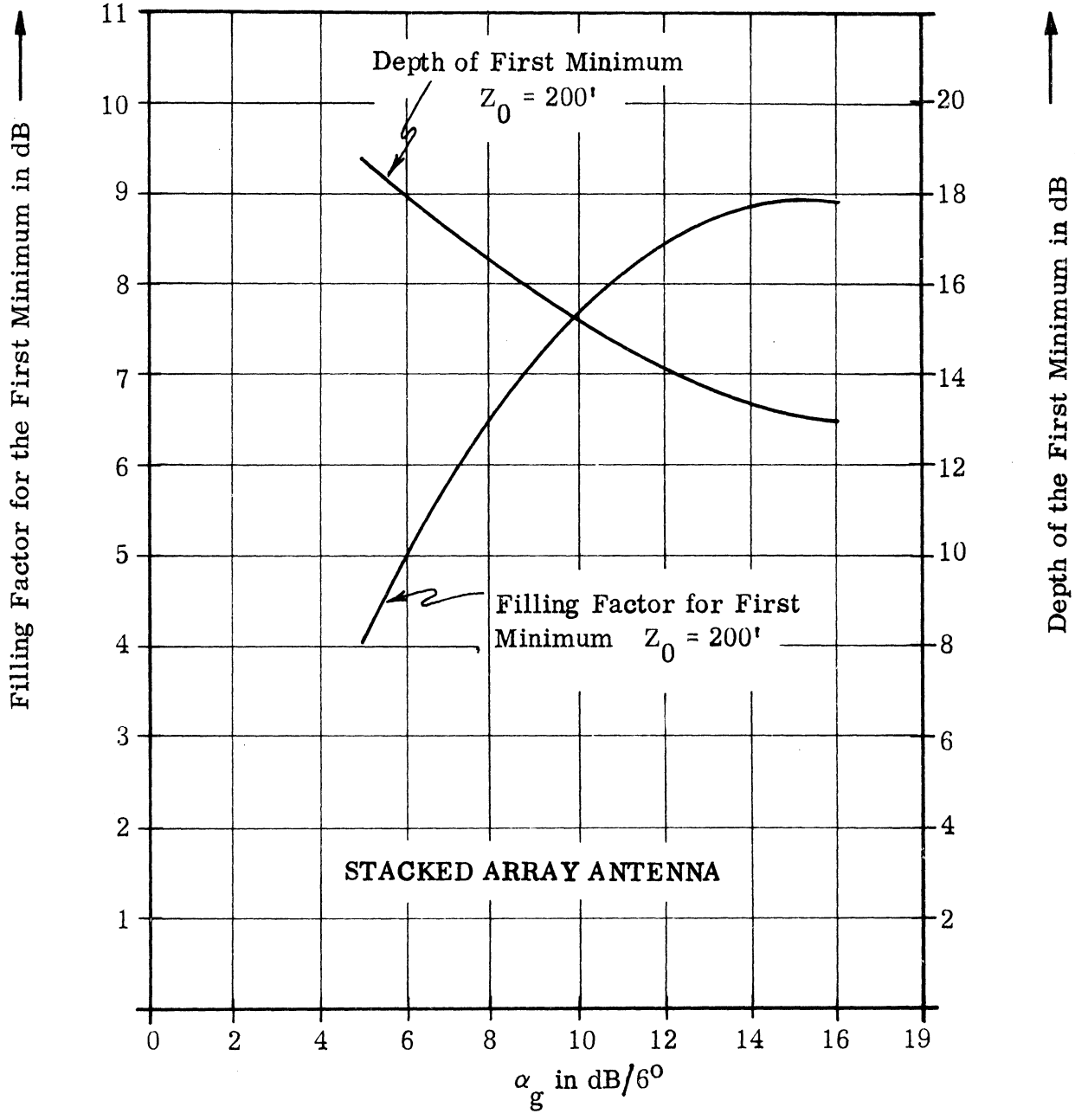

Fig. 3-20: Depth of the first minimum and the filling factor for the first minimum as functions of the field gradient α_g.

IV

VOR COURSE SCALLOPING AMPLITUDES IN BEARING INDICATIONS

4.1 Introduction

The present chapter discusses the numerical results for the course scalloping amplitudes in the bearing indications of a standard VOR system under various situations. The scatterer producing the scalloping errors is assumed to be isotropic and located at various heights above a perfectly conducting planar earth. Numerical results for the scalloping amplitudes are given when the VOR ground station uses standard VOR, large gradient DPLC and stacked array antennas with variable gradients. Detailed numerical results are given for the effects of the height of the VOR transmitting antenna above ground on the scalloping amplitudes.

4.2 Course Scalloping Amplitude Expression

The geometry of the VOR ground station antenna, the isotropic scatterer and the observation point located at a stationary aircraft are shown in Figure 4-1. The VOR antenna is located at $(Z_o, 0, 0)$, the scatterer at (d_1, θ_1, ϕ_1) and the ground plane is at $z = 0$; the coordinates of the observation point are (r, θ, ϕ). Sometimes it may be found convenient to represent the location of the scatterer by the parameters H and D as shown in Figure 4-1. Note that

$$\tan \theta_1 = \frac{D}{H} \quad . \tag{4.1}$$

It is assumed that at the observation point an ideal receiver receives the signal transmitted by the VOR ground station.

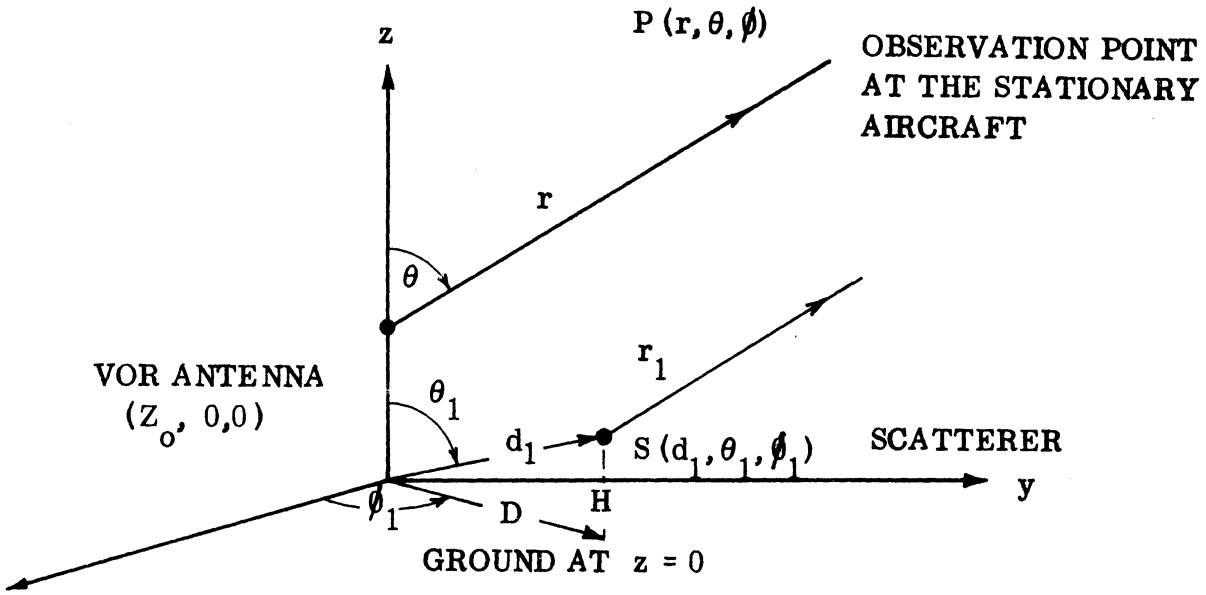

Figure 4-1: Location of the VOR transmitting antenna, the scatterer and the observation point at the stationary aircraft.

It can be shown (Sengupta and Chan 1973b, also see Appendix A), that in the presence of a scatterer the course scalloping amplitudes in the bearing indications of a standard VOR receiver at the observation point P are given by:

$$S_{\frac{1}{2}} = \mp \tan^{-1} \left[\frac{2A \left| \frac{S_s^T(\theta_1)}{S_s^T(\theta)} \right| \sin(kH \cos\theta) \sin(\phi - \phi_1)}{1 \pm 2A \left| \frac{S_s^T(\theta_1)}{S_s^T(\theta)} \right| \sin(kH \cos\theta) \cos(\phi - \phi_1)} \right], \quad (4.2)$$

where,

the upper sign pertains to S_1 and the lower sign to S_2,

$k = 2\pi/\lambda$ is the propagation constant in free space,

A is the generalized scattering coefficient for the scatterer and is, in general, a function of the coordinates of the scattering object and the observation point. In the present Handbook it is assumed that the scatterer is isotropic which implies that A is a constant and is less than unity. The quantity A is then a measure of the amplitude of the scattered field for unit amplitude field incident at the scatterer,

$S_s^T(\theta)$ is the side-band mode elevation plane complex pattern of the VOR transmitting antenna located above ground.

$S_s^T(\theta)$ is related to the corresponding free space pattern of the VOR antenna by the following:

$$S_s^T(\theta) = S_s(\theta)\, e^{-ikZ_o \cos\theta} - S_s(\pi-\theta)\, e^{ikZ_o \cos\theta}, \qquad (4.3)$$

where $S_s(\theta)$ is the side-band mode elevation plane complex pattern of the VOR transmitting antenna in free space.

Equation (4.2) indicates that during an orbital flight around the VOR station, the maximum bearing errors, i.e., the scalloping amplitudes as observed in the aircraft receiver will lie between the limits S_1 and S_2. We emphasize here the following basic assumptions made in obtaining Eq. (4.2): (i) the carrier and the side-band mode fields are in RF phase for all θ, (ii) the scatterer is located in the far zone of the VOR antenna. For simplicity we shall assume that the scatterer is isotropic, i.e., A is a constant and is independent of the coordinates of the scatterer and the observation point.

Equation (4.2) indicates that for orbital flights S_1 evaluated at $\pi + (\phi-\phi_1) = S_2$ evaluated at $(\phi - \phi_1)$ and vice versa. This implies that it is sufficient to calculate S_1 and S_2 in the range $0 \leq (\phi-\phi_1) \leq \pi$ in order to study the course scalloping amplitude variations during an orbital flight.

It is also interesting to observe from Eq. (4.2) that the course scalloping amplitude reduces to zero whenever the following relation is satisfied:

$$H \cos\theta = n\frac{\lambda}{2}, \quad n = 1, 2, 3, \ldots\ldots . \qquad (4.4)$$

4.3 General Discussion on Scalloping

On the basis of Eq. (4.2), the following observations can be made with regard to the general behavior of the course scalloping amplitudes in the VOR bearing indications observed by an aircraft in orbital flight around the VOR station:

(i) The scalloping amplitude is zero in directions $\phi = \phi_1$ and $\phi = \pi + \phi_1$. If the multipath source scatters energy isotropically (i.e., A = constant) then the amplitude of scalloping assumes maximum value in directions $\phi = \pi/2 + \phi_1$ and $\phi = 3\pi/2 + \phi_1$, only if $A << 1$.

(ii) The two envelopes of the bearing error (S_1, S_2) are opposite in sign but in general are not equal in amplitude.

(iii) In the case of a non-isotropic scattering by the multipath source, the directions of the scalloping amplitude maxima will be determined mainly by the parameter A.

(iv) The side-band mode pattern $\left|S_s^T(\theta)\right|$ is quite critical in determining the scalloping amplitudes. The scalloping amplitude increases in the directions of minima in the pattern $\left|S_s^T(\theta)\right|$. The carrier mode pattern of the antenna does not seem to have strong influence on $|S_1|$ and $|S_2|$. However, the relative rf phase difference between the side-band and carrier mode fields at the observation point influences considerably the amount of scalloping amplitudes (Sengupta and Chan 1973a).

4.4 Scalloping Amplitude Variation with Field Gradient

In this section we give a general discussion of the results obtained for scalloping amplitudes with VOR antennas having different values of the field gradient. The antennas considered are the standard VOR, DPLC and the five-bay stacked arrays discussed in Chapter II. The pertinent pattern information of these antennas are as given in Table I, page 20.

In order to present the results in a way meaningful in practical situations we characterize the scalloping amplitudes by two new parameters called the average maximum scalloping amplitude S and the scalloping improvement coefficient ρ. These two parameters are defined as follows:

$$S = \frac{|S_{1\,max}| + |S_{2\,max}|}{2} \quad , \tag{4.5}$$

where $S_{1\,max}$, $S_{2\,max}$ are the maximum values of S_1 and S_2 in Eq. (4.2) for a given observation angle θ,

and,

$$\rho = \frac{S \text{ for the test antenna}}{S \text{ for the standard VOR antenna}} \quad , \tag{4.6}$$

where it is assumed that the test and the VOR antennas are located at the same height above ground.

The variations of S and ρ with the field gradient for the stacked array antenna are shown in Fig.4-2a for an observation angle which corresponds to the first minimum in the pattern. The corresponding results for standard VOR and DPLC antennas with $2A_o = 52'$ and $Z_0 = 200'$ are also shown in Fig. 4-2a for comparison. For observation angle in the direction of the first maximum in the pattern, only the variation of S is shown in Fig. 4-2a for the stacked array antenna.

For the range of parameters considered in Fig.4-2a it is found that for an observation angle in the direction of the first pattern minimum both S and ρ decrease continuously with increase of the field gradient. In the direction of the first maximum in the pattern, S is found to be less than that in the direction of the pattern minimum and it is almost independent of the field gradient. In Chapter III, we found that the large gradient antenna produces improved filling factor. The results discussed here indicate that when the large gradient and the standard VOR antennas

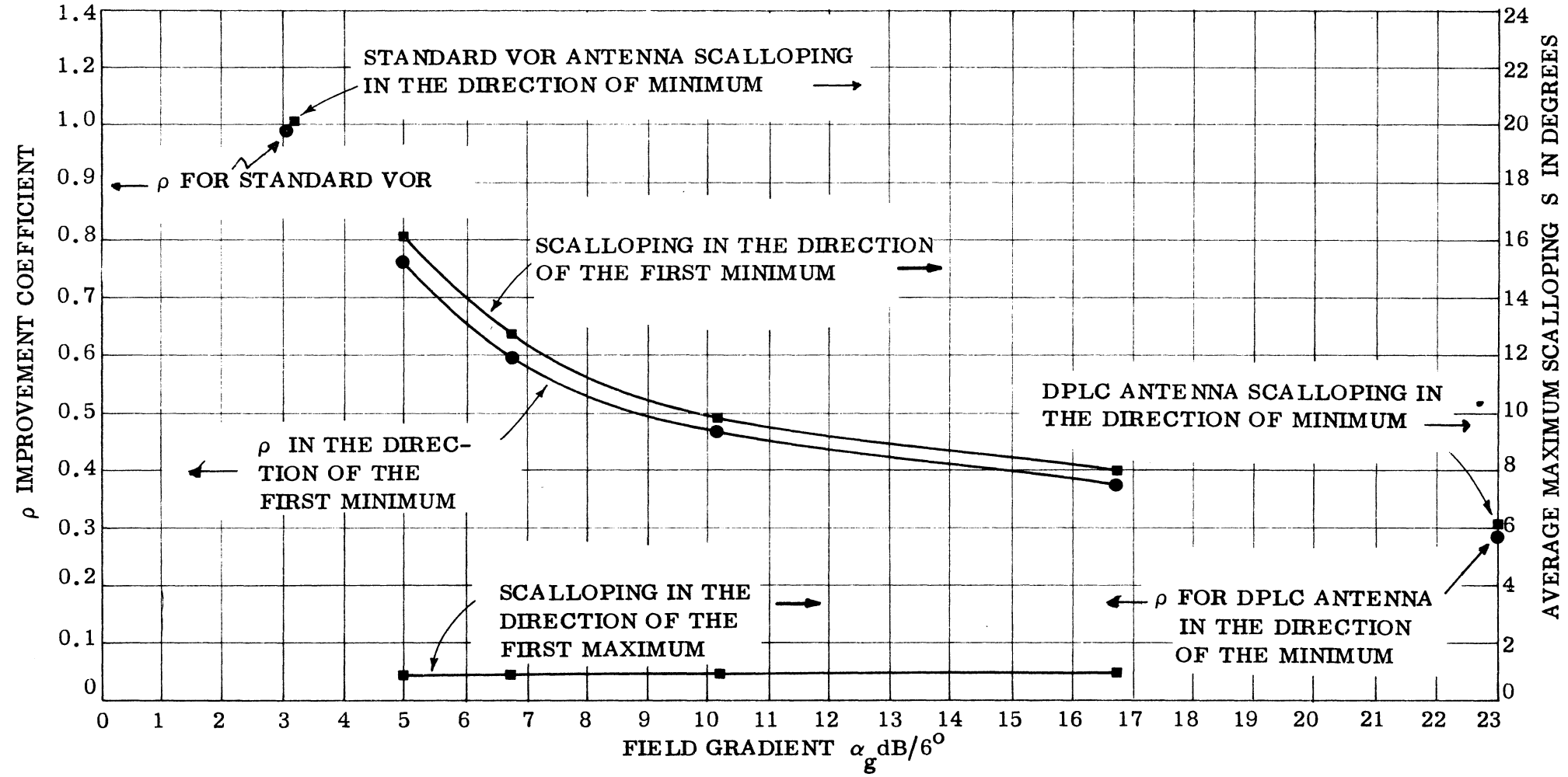

Fig. 4-2a: Improvement coefficient ρ and average maximum scalloping as functions of the field gradient α_g. This figure applies to stacked array antenna except where noted otherwise. Z_0 = 200', H = 60', D = 1000' and A = 0.02.

are located at the same height above ground, the former improves the siting errors in the first null. For example, it is found from Fig.4-2a that the DPLC antenna produces a siting error in the null which is about 0.28 times that produced by the standard VOR antenna. The Mannheim test results (Sengupta and Ferris, 1972) indicate that the DPLC antenna produces a siting error in the null which is about 0.17 times that produced by the standard VOR antenna. The discrepancy between these results are attributed to the different antenna height $Z_0 = 75'$ and the counterpoise size $2A_o = 150'$ used during the test. However, it can be said that the test results to confirm the improved performance of the large gradient antenna as predicted here.

Figure 4-2b shows S_2 versus $(\phi-\phi_1)$ in the range $0 \leq \phi - \phi_1 \leq 180^o$ for standard and DPLC antennas located 15' above ground and for orbital flights at $\theta = 83^o$. Notice that this flight angle corresponds to the first maximum in the elevation plane pattern of the standard VOR antenna (Fig. 3-1c); the DPLC antenna pattern does not have any such variation in this region (Fig. 3-2c). The isotropic scatterer is located 100' above ground. The results shown in Fig. 4-2b indicate that the difference between the scalloping amplitudes for the two antennas may be assumed to be negligible except near $(\phi - \phi_1) \sim 80^o$ where the DPLC antenna scalloping amplitude is about 0.5^o less.

4.5 Variation of S and ρ with Relative Location of the Antenna and Scatterer

The variations of the average maximum scalloping amplitude S and the scalloping improvement coefficient ρ as functions of the relative location of the antenna and the scatterer above ground are discussed in the present section. Results have been obtained for (see Figure 4-1 for notation) D = 500', 1000', 2000' and 3000' and for H = 25', 50', 75' and 100'. The antennas considered are the standard VOR and the DPLC antennas. In all cases the antenna heights have been varied from $Z_o = 15'$ to $Z_o = 500'$. In the following sections we first discuss the results obtained when the scatterer is located at a distance D = 1000' from the antenna.

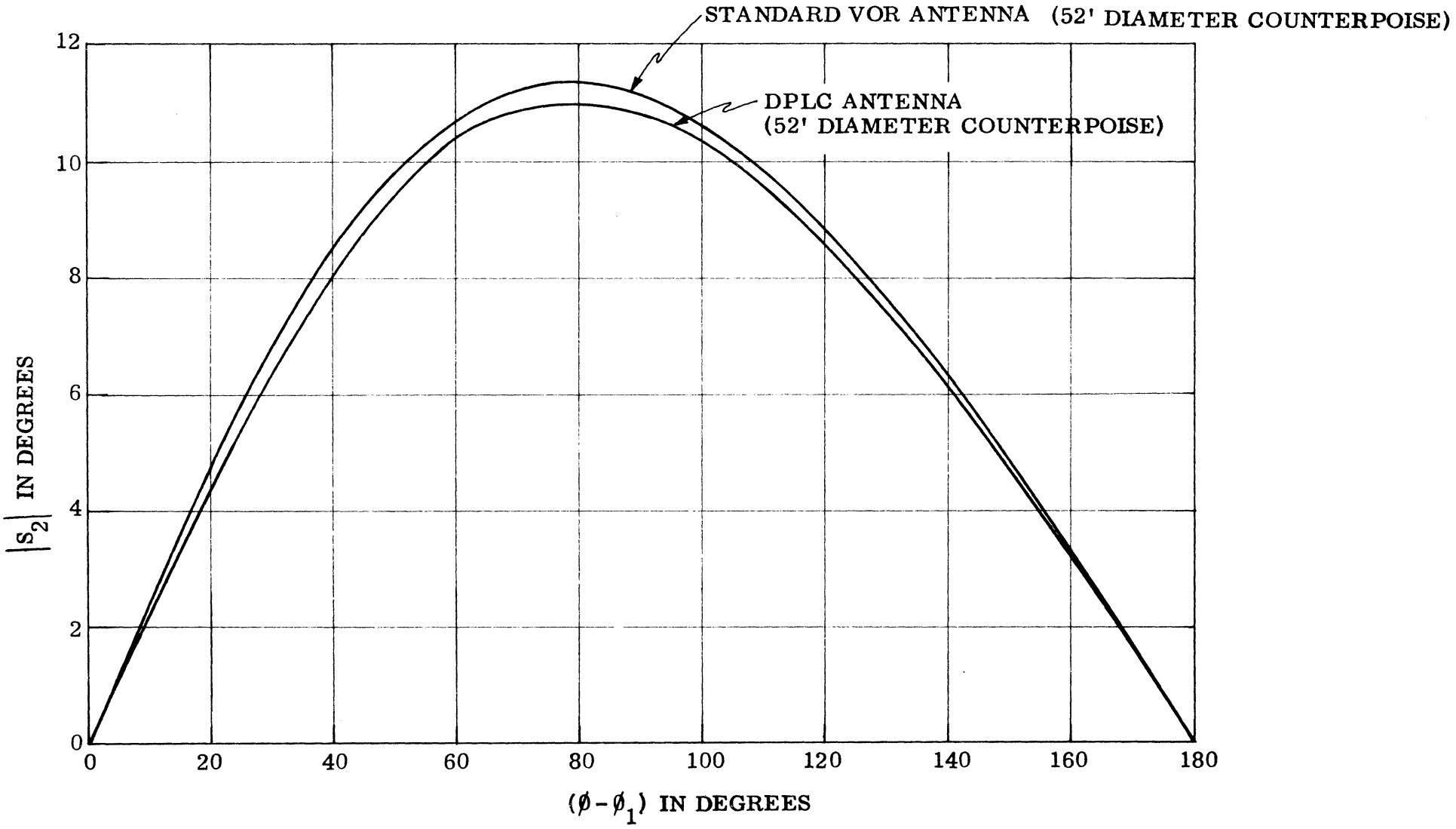

Fig. 4-2b: S_2 as functions of $(\phi - \phi_1)$ for a standard VOR and DPLC antenna located 15' above ground for a scatterer located 100' above ground. Orbital flight at $\theta = 83^{o}$, D = 1000', A = 0.1, H = 100'.

Results for D = 1000'

Average maximum scalloping amplitude versus antenna height for two observation angles and for different heights of the scatterer are shown in Figures 4-3a and 4-3b for a standard VOR antenna. In general, for a given scatterer height the average maximum scalloping S is found to be an oscillating function of the height of the antenna above ground. This is indicative of the image effects on the field radiated by the antenna which in turn affects the scalloping. The average value of S tends to increase with the increase of the scatterer height. This may be attributed to the fact that in this particular case with D = 1000' the field incident at the scatterer increases with the height of the scatterer. It should also be observed from Eq. (4.2) that for a given antenna height the scalloping goes to zero if the height of the scatterer is such that $H = \frac{n\lambda}{2 \cos \theta}$, where n = 1, 2,....,. This is due to the image effects on the scattered field at the observation point. The corresponding results for DPLC antennas are shown in Figures 4-4a and 4-4b. Observe that the curves in Figs. 4-4a - 4-4c start at $Z_0 = 50'$. This was done because for $Z_0 < 50'$ the free space patterns of the DPLC antenna do not develop any appreciable maximum and minimum near the horizon.

Results for D = 500', 2000' and 3000'

Similar results for D = 500', 2000' and 3000' are shown in Figures 4-5 through 4-7. The elevation of the flight path is assumed to correspond to the first minimum in the elevation plane pattern of the antenna. The general behavior of the results is similar to that of the results for D = 1000'. Note that in Figs. 4-5a and 4-5c the curves for H = 100' and H = 75' are terminated at $Z_0 = 200$. For these combinations of Z_0 and H the S_1 and S_2 values for standard VOR antennas, as computed from Eq. (4.2), change sign for $Z_0 > 200$. This would require re-definition of Z. To avoid this the curves are not continued beyond 200'.

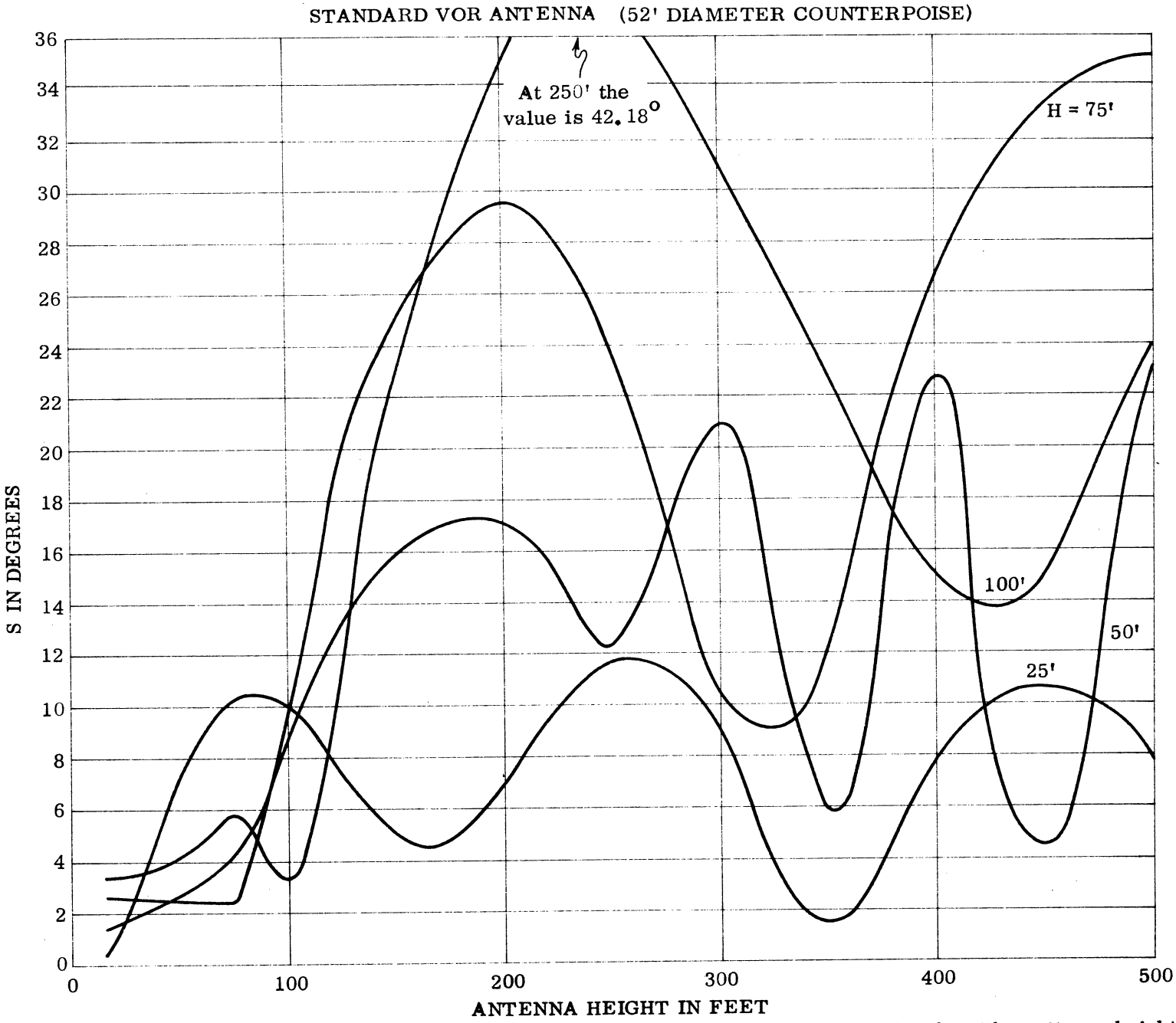

Fig. 4-3a: Average maximum scalloping as a function of standard VOR antenna height with scatterer height as the parameter. Observation angle is in the direction of the first pattern minimum. D=1000', A=0.02.

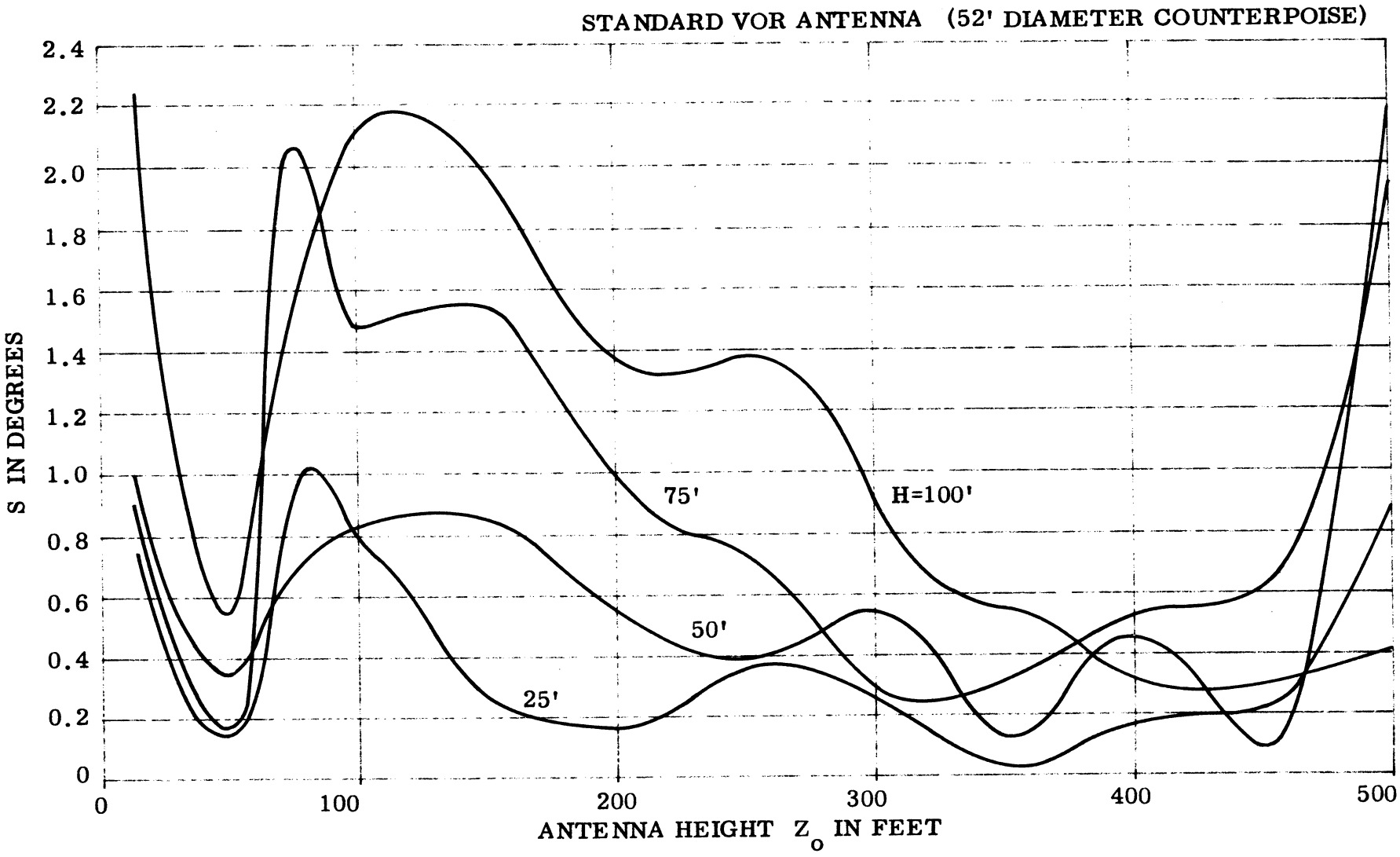

Fig. 4-3b: Average maximum scalloping as a function of standard VOR antenna height with scatterer height as the parameter. Observation angle is in the direction of the first pattern maximum. D = 1000', A = 0.02.

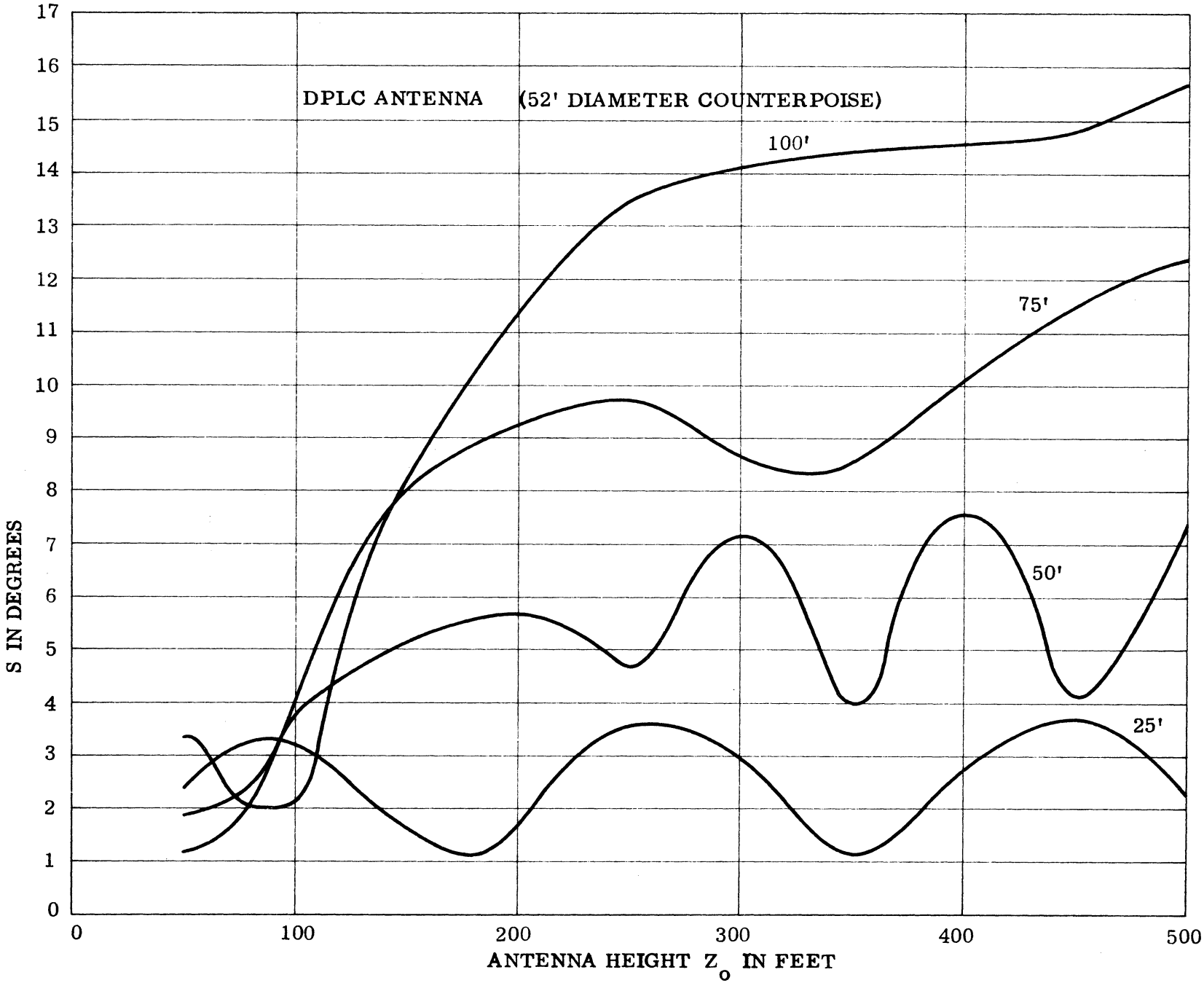

Fig. 4-4a: Average maximum scalloping as a function of DPLC antenna height with scatterer height as the parameter. Observation angle is in the direction of the first pattern minimum. D=1000', A=0.02.

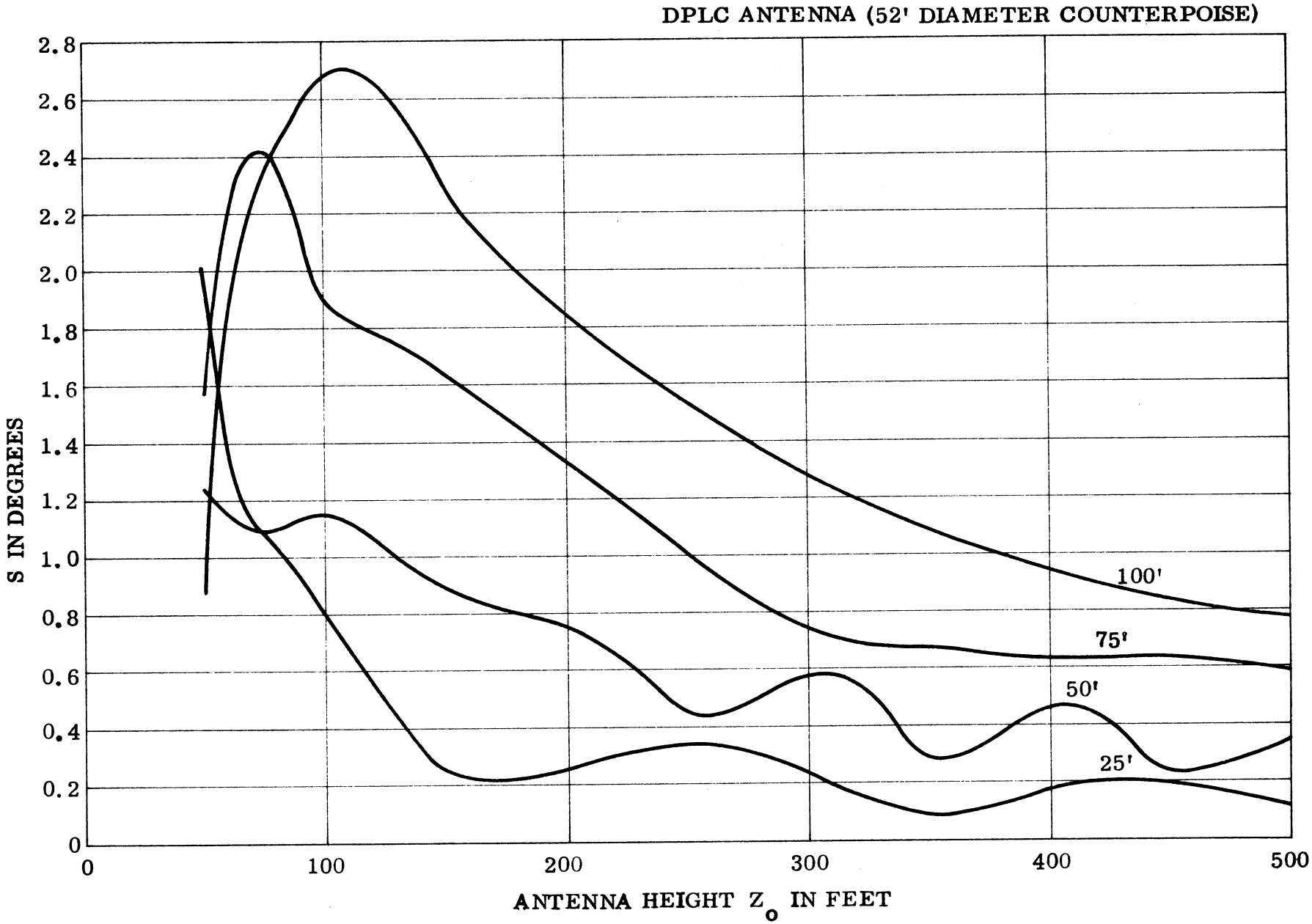

Fig. 4-4b: Average maximum scalloping as a function of DPLC antenna height with scatterer height as the parameter. Observation angle is in the direction of the first pattern maximum. D=1000', A=0.02.

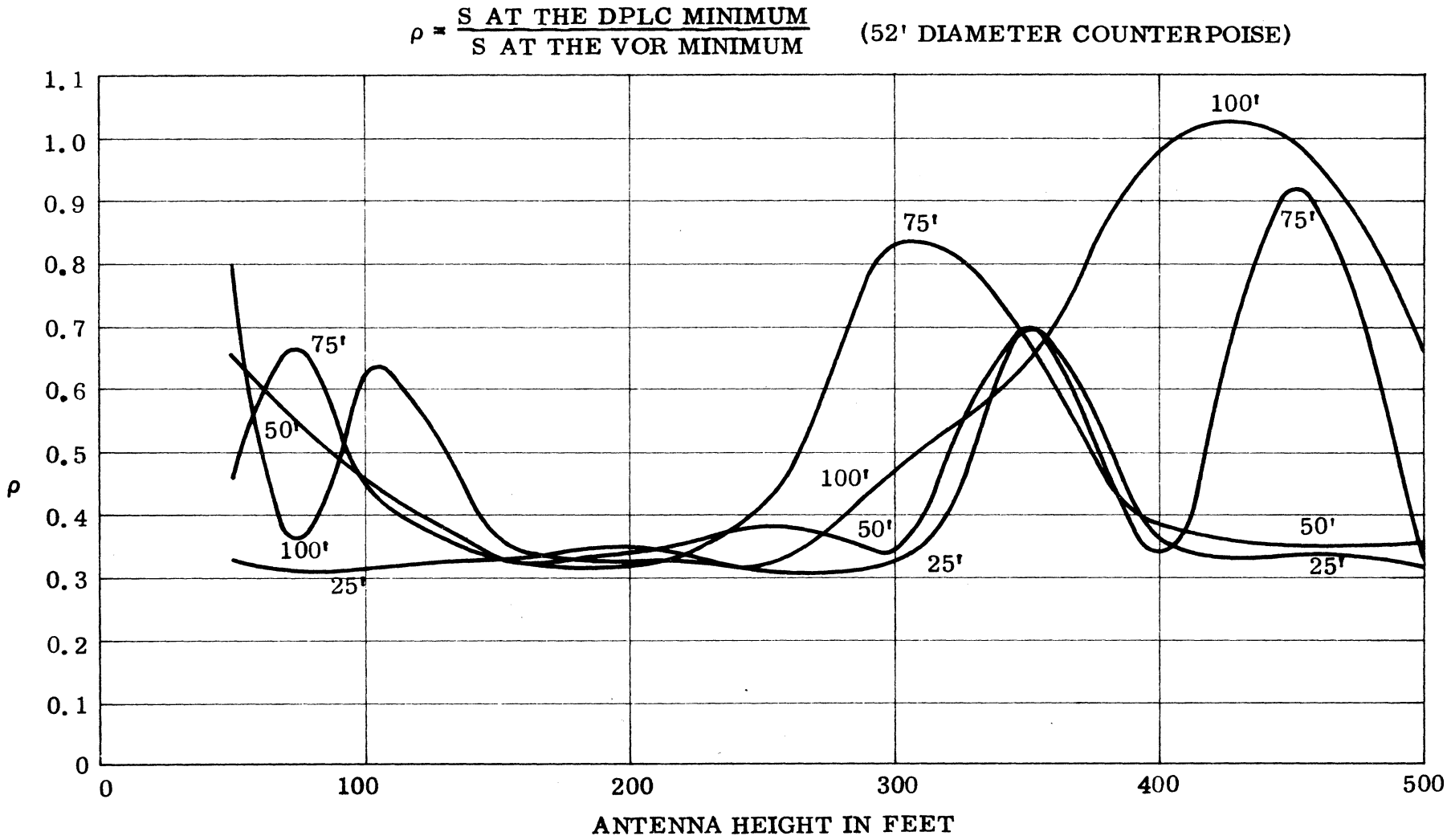

Fig. 4-4c: The DPLC antenna improvement coefficient ρ as a function of the antenna height with scatterer height as the parameter. Observation angle is in the direction of the first pattern minimum. D = 1000', A = 0.02.

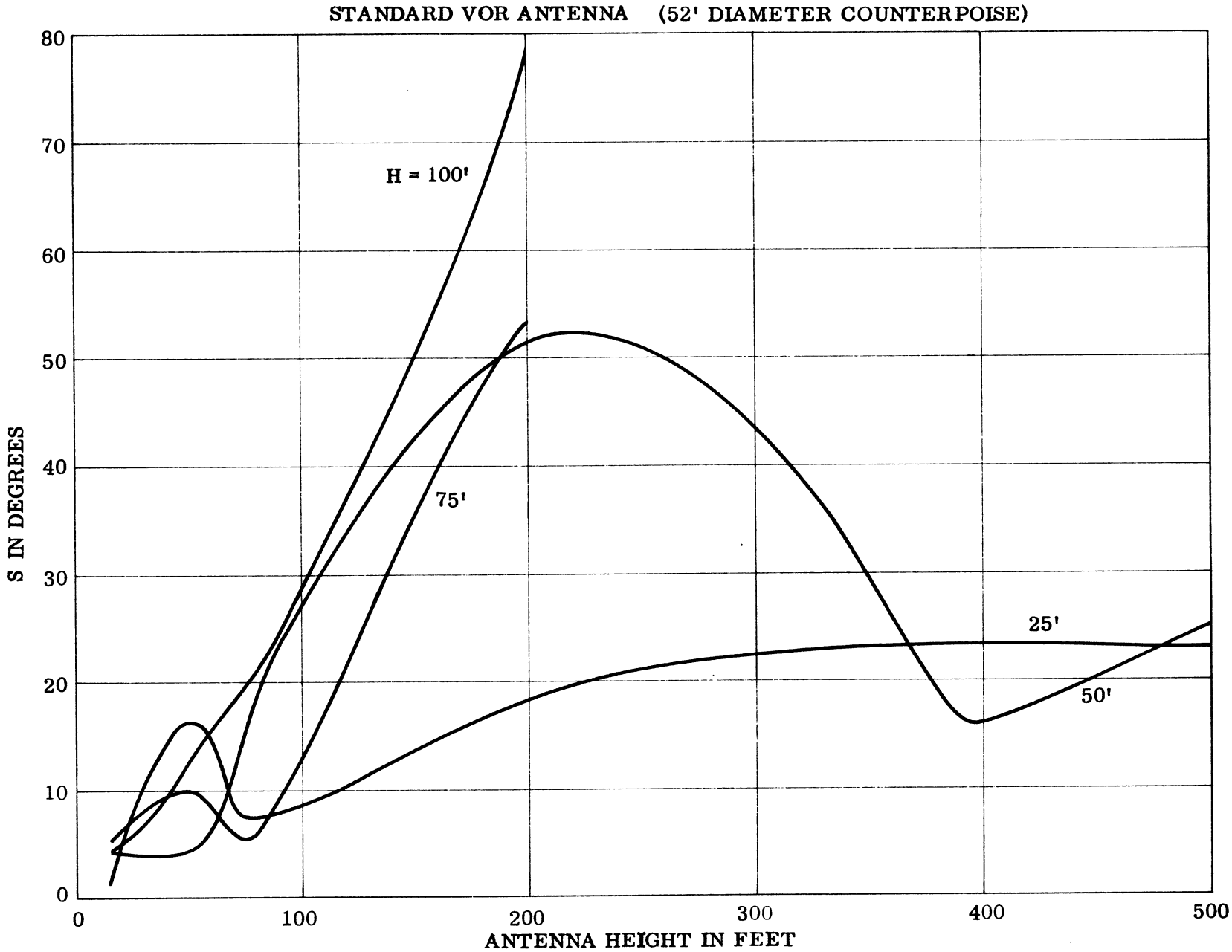

Fig. 4-5a: Average maximum scalloping as a function of standard VOR antenna height with scatterer height as the parameter. Observation angle is in the direction of the first pattern minimum. D = 500', A = 0.02.

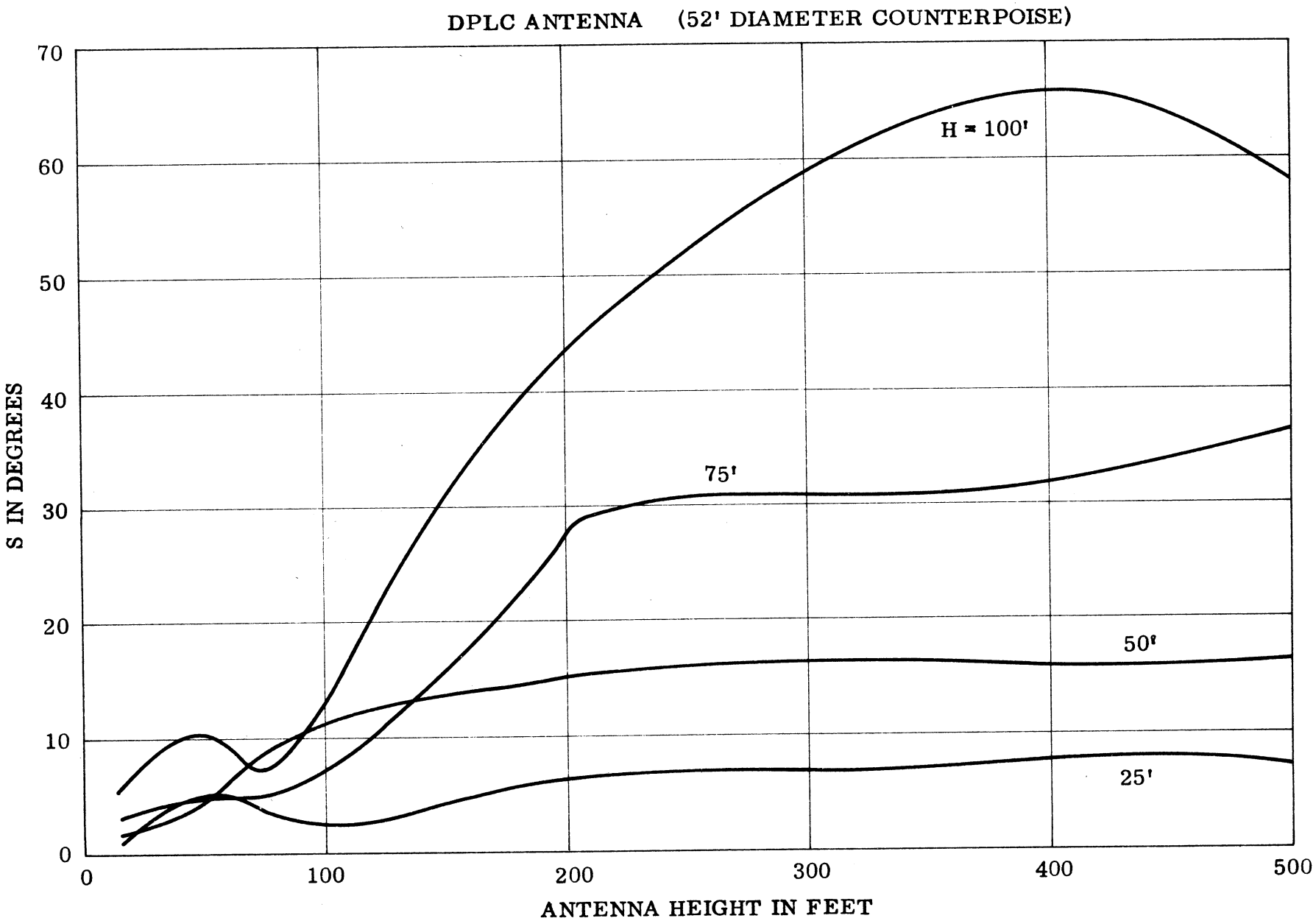

Fig. 4-5b: Average maximum scalloping as a function of the DPLC antenna height with scatterer height as the parameter. Observation angle is in the direction of the first pattern minimum. D=500', A=0.02.

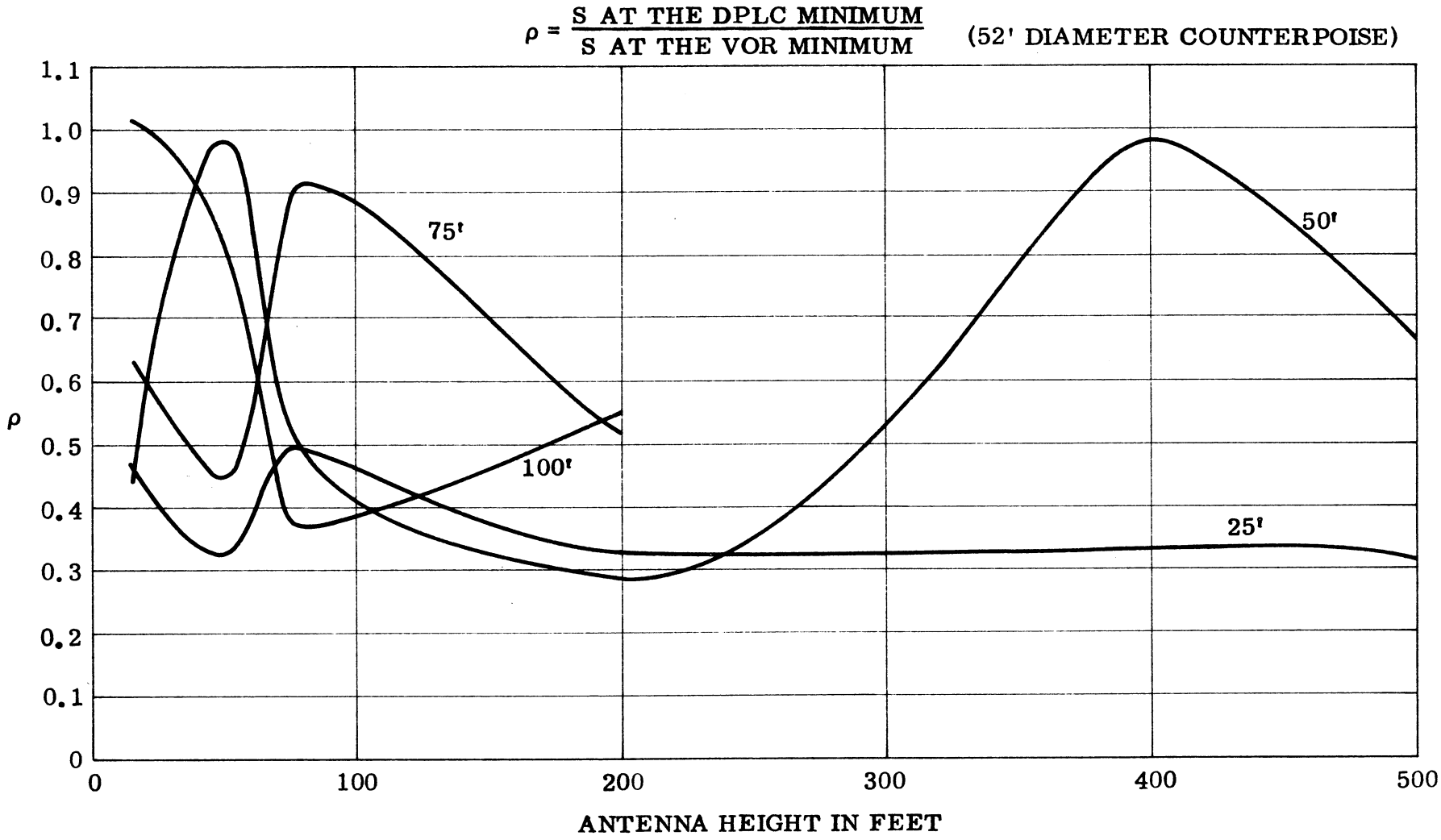

Fig. 4-5c: The DPLC antenna improvement coefficient ρ as a function of the antenna height with scatterer height as the parameter. Observation angle is in the direction of the first pattern minimum. D = 500', A = 0.02.

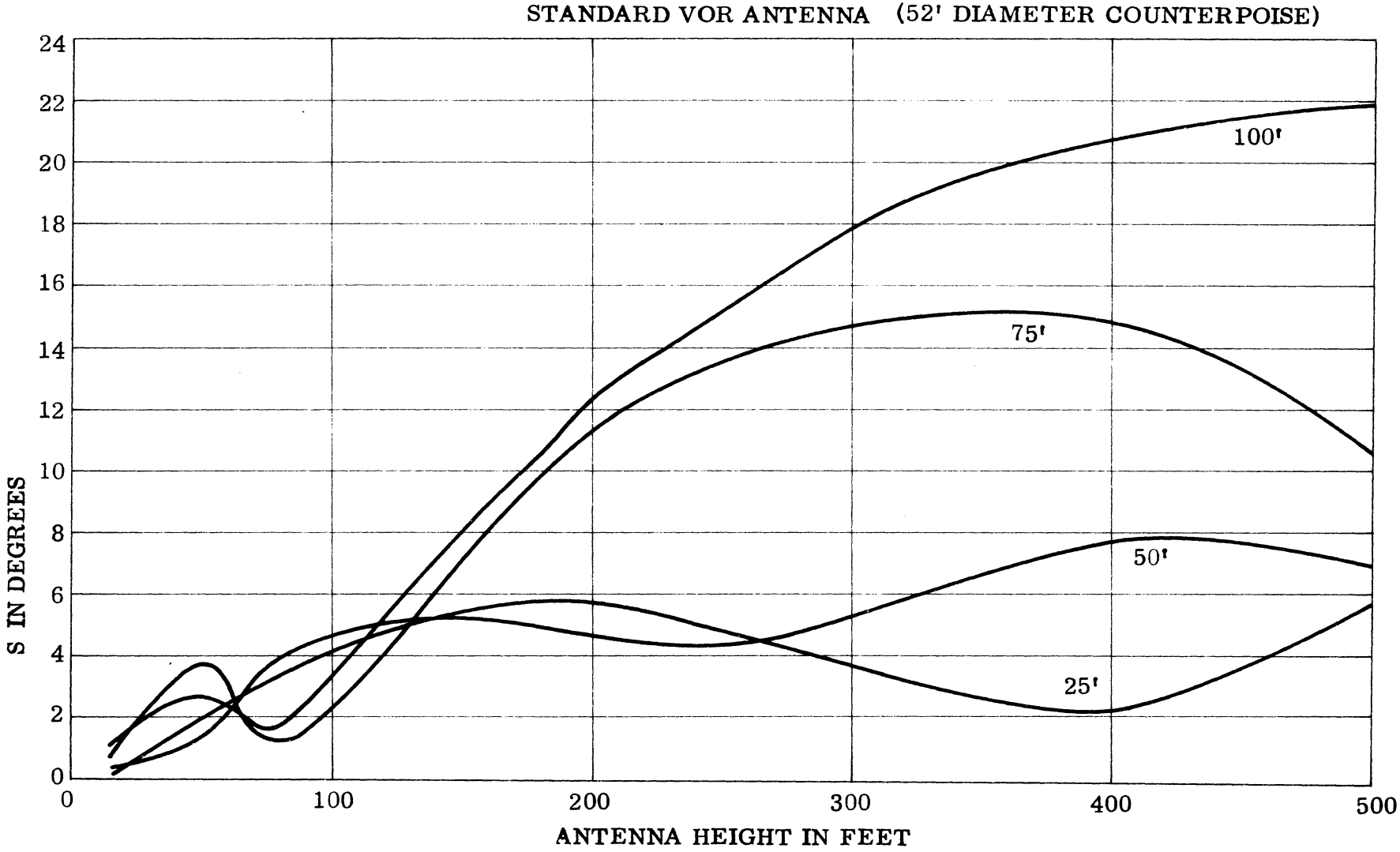

Fig. 4-6a: Average maximum scalloping as a function of standard VOR antenna height with scatterer height as the parameter. Observation angle is in the direction of the first pattern minimum. D = 2000', A = 0.02.

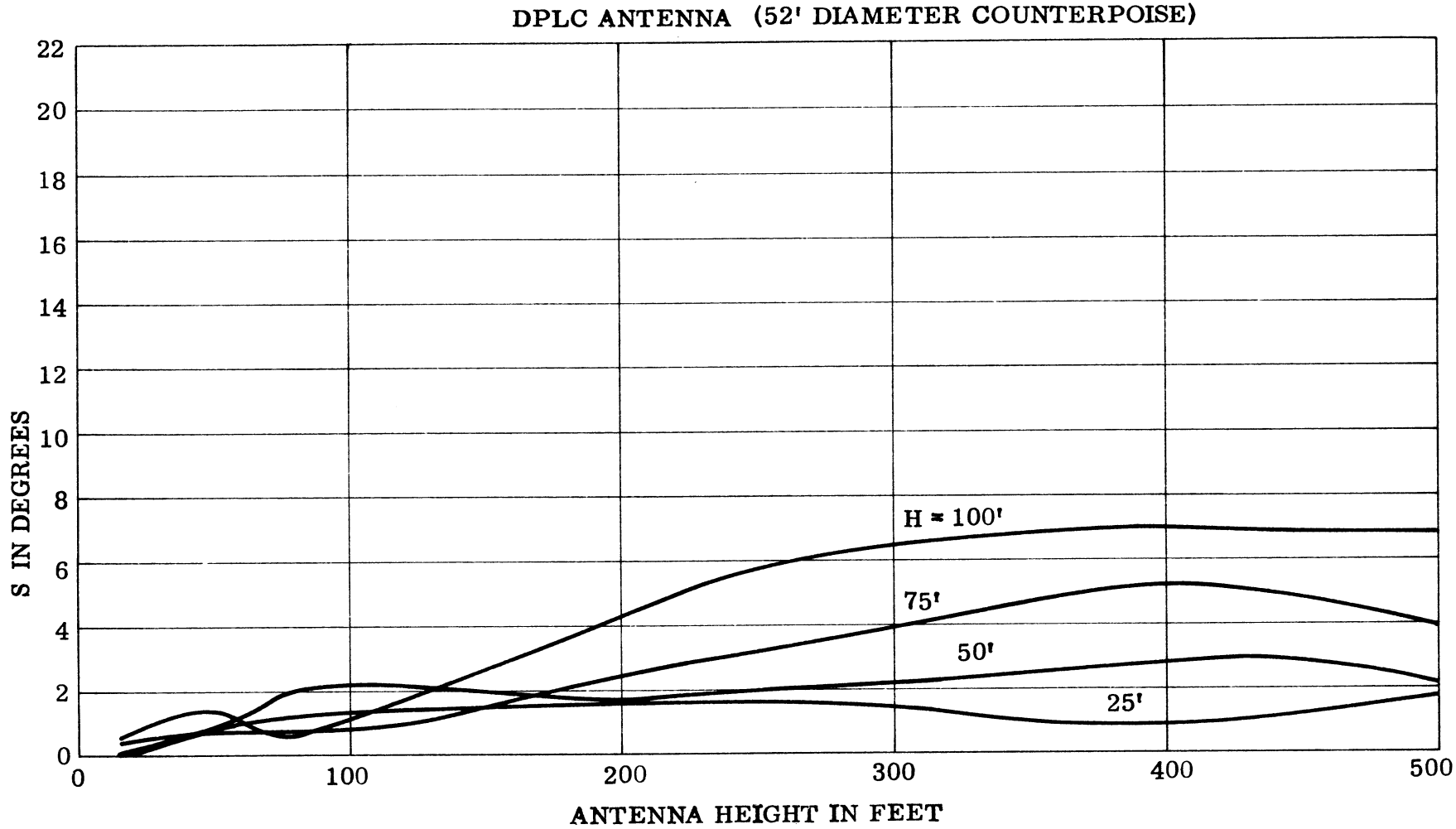

Fig. 4-6b: Average maximum scalloping as a function of the DPLC antenna height with scatterer height at the parameter. Observation angle is in the direction of the first pattern minimum. D = 2000', A = 0.02.

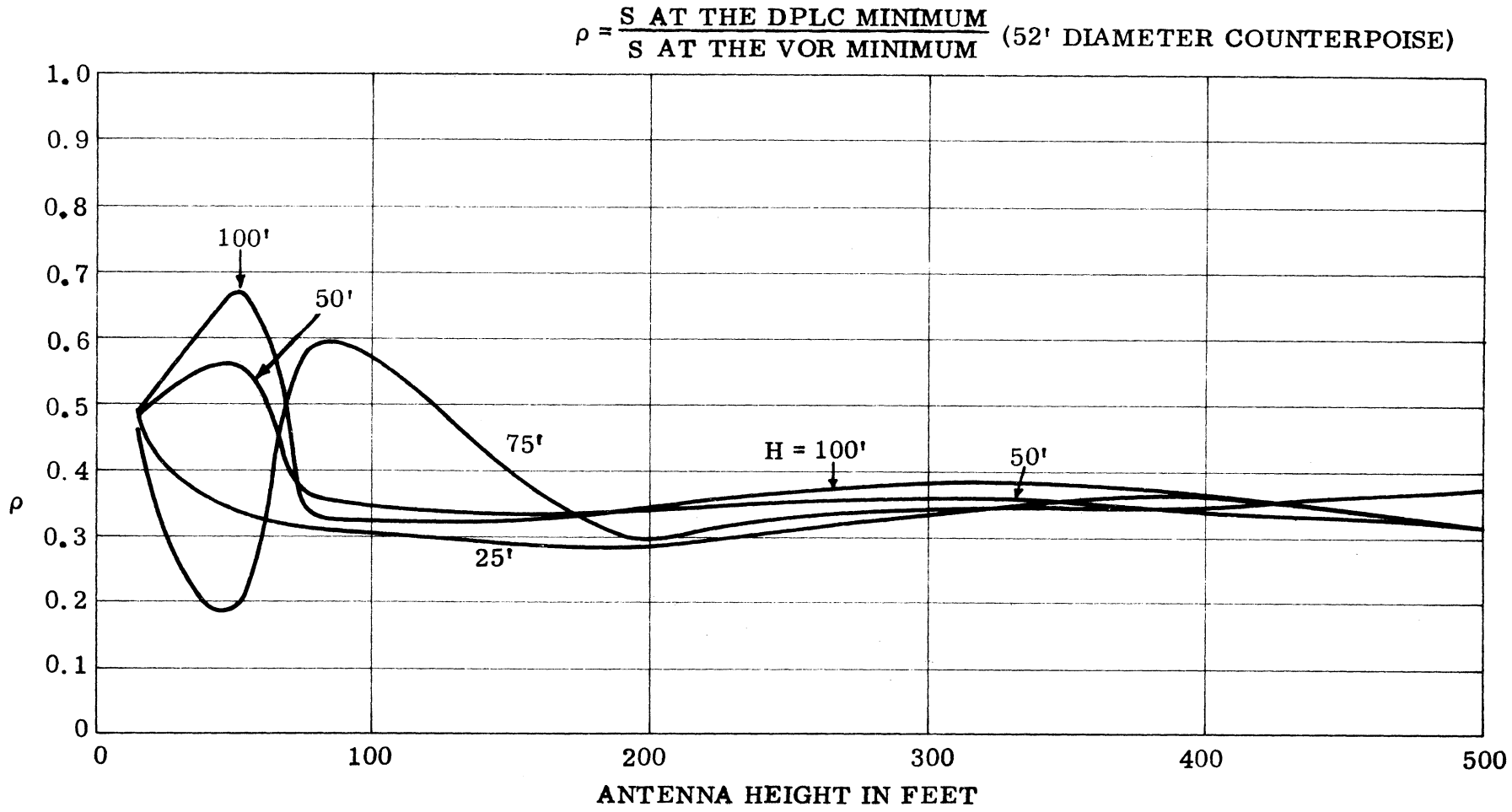

Fig. 4-6c: The DPLC antenna improve coefficient ρ as a function of the antenna height with scatterer height as the parameter. Observation angle is in the direction of the first pattern minimum. D = 2000', A = 0.02.

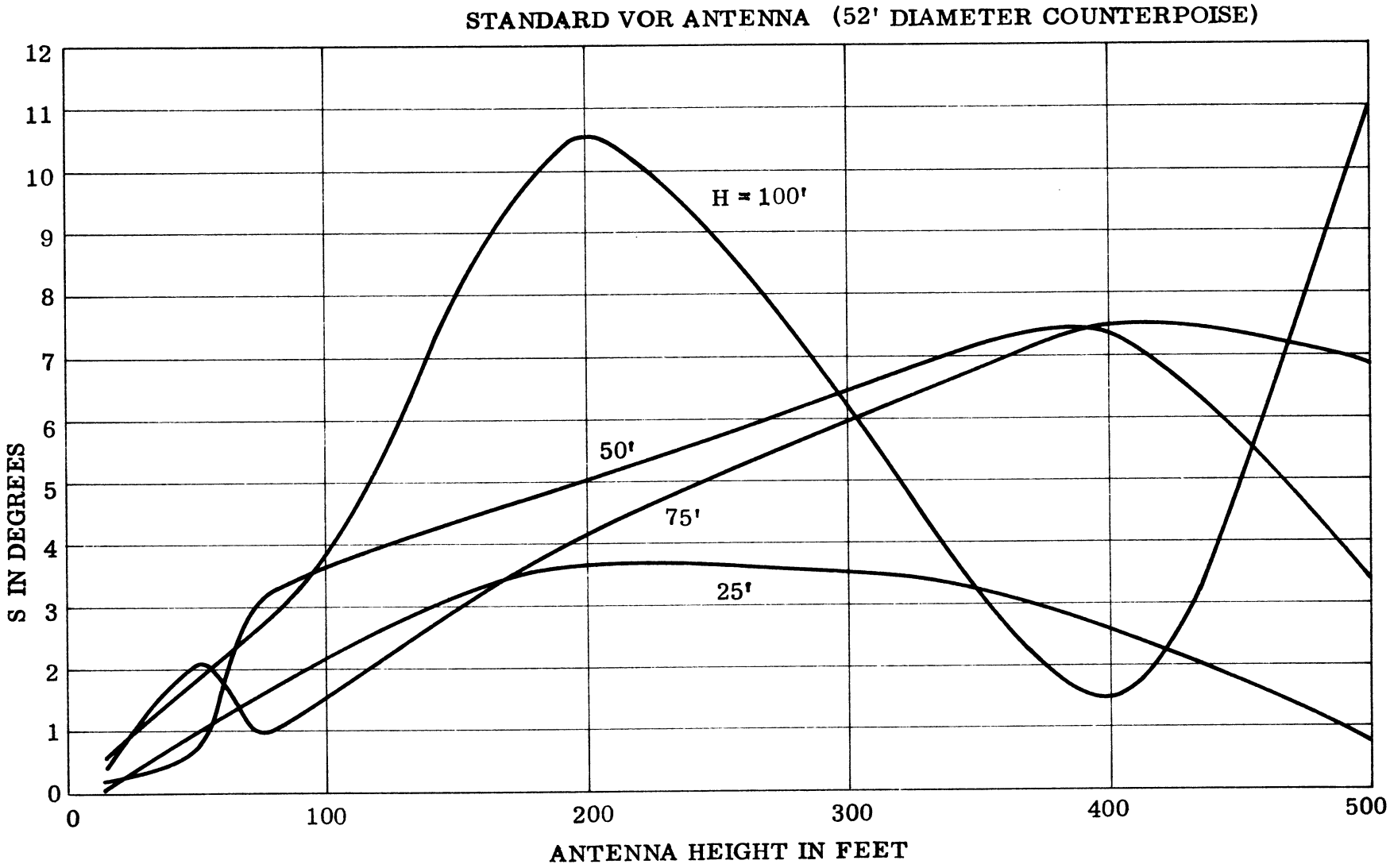

Fig. 4-7a: Average maximum scalloping as a function of the standard VOR antenna height with scatterer height as the parameter. Observation angle is in the direction of the first pattern minimum. D = 3000', A = 0.02.

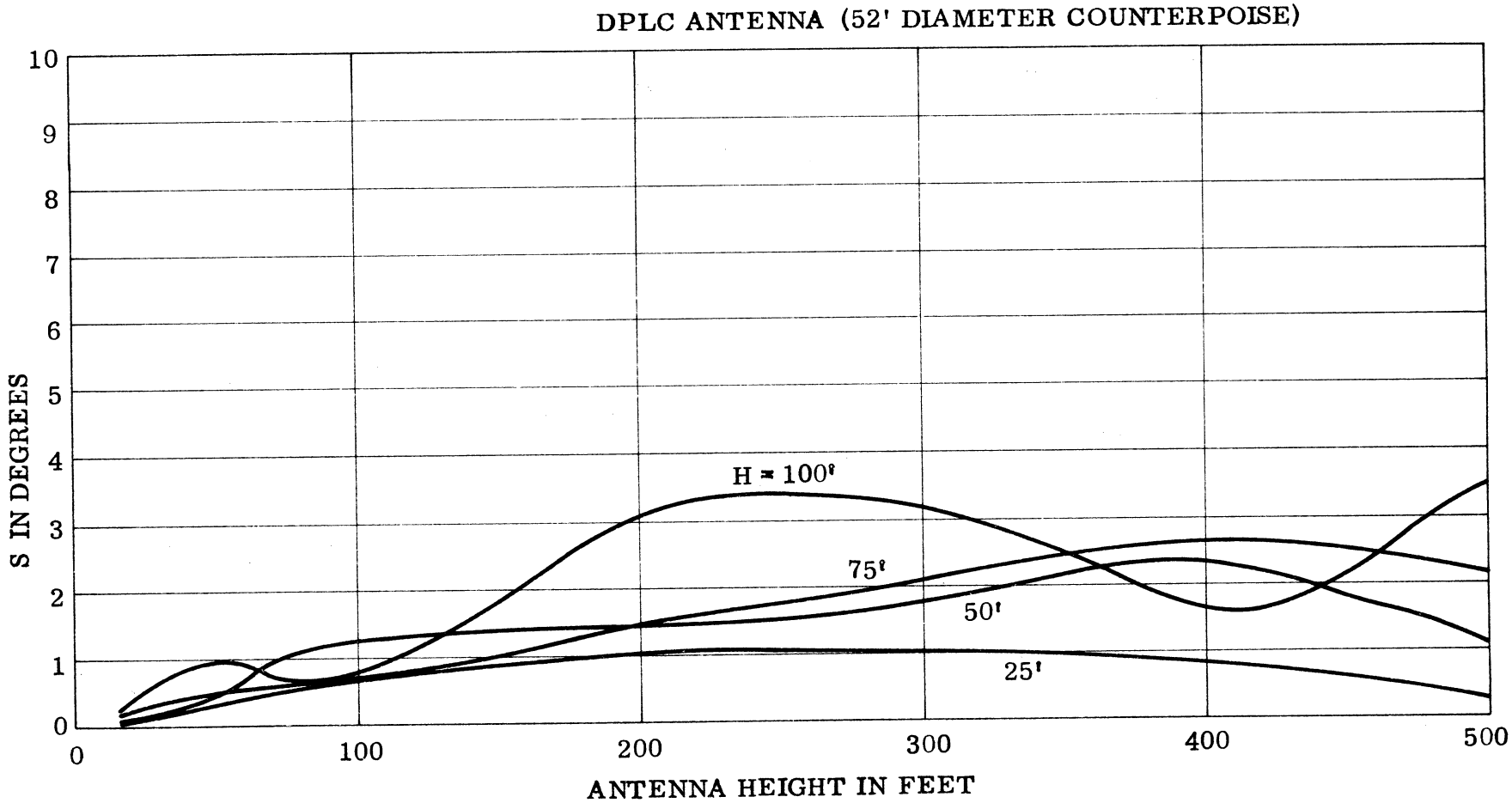

Fig. 4-7b: Average maximum scalloping as a function of the DPLC antenna height with scatterer height as parameter. Observation angle is in the direction of the first pattern minimum. D = 3000', A = 0.02.

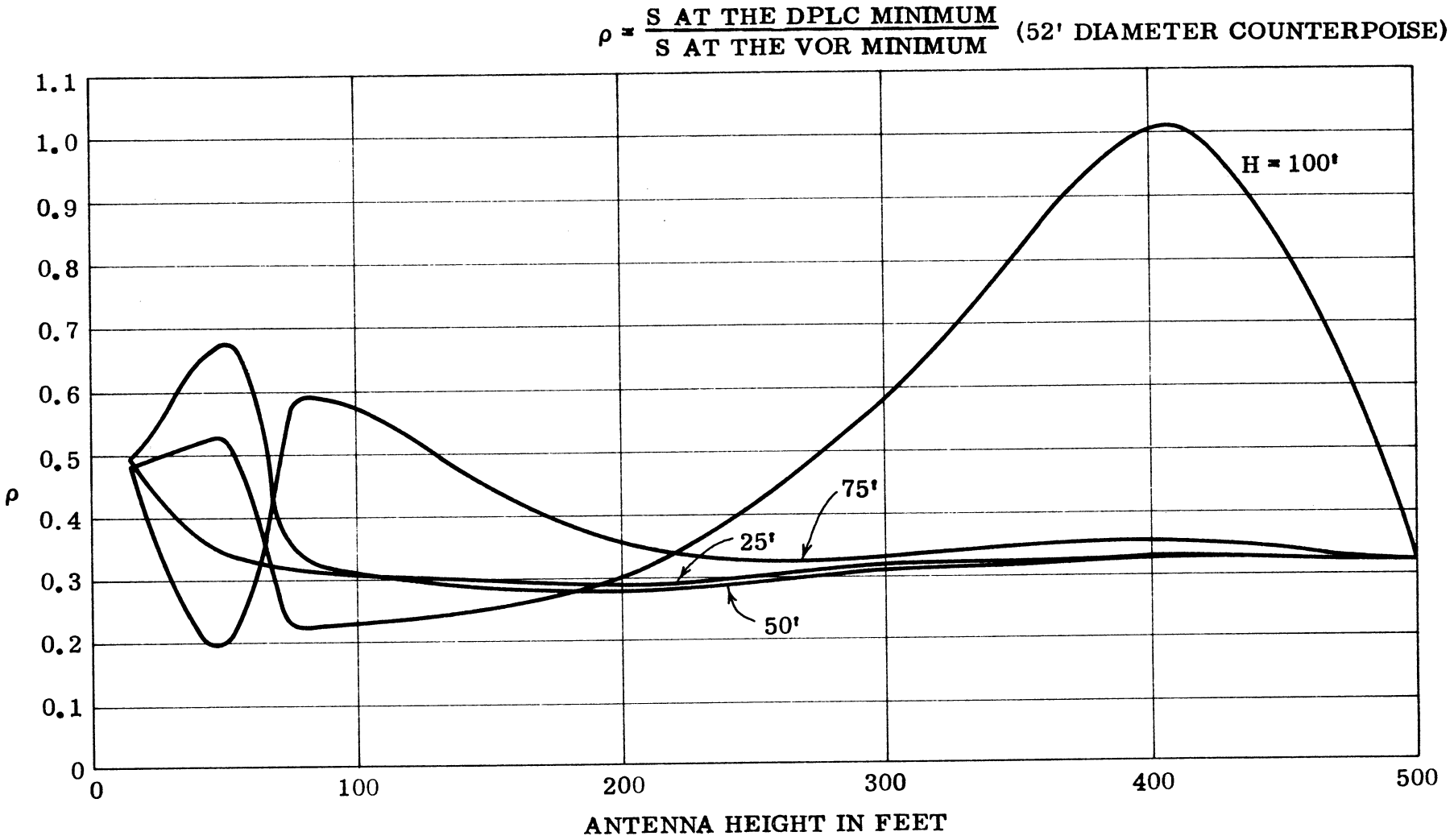

Fig. 4-7c: The DPLC antenna improvement coefficient σ as a function of the antenna height with scatterer height as the parameter. Observation angle is in the direction of the first pattern minimum. D = 3000', A = 0.02.

4.6 Standardized Scalloping Results

Sometimes it may be found convenient to represent the scalloping amplitudes in a given direction observed with a test antenna in terms of the scalloping amplitudes observed in the direction of the lowest pattern minimum with a standard VOR antenna located at a standard height 15' above ground. For this purpose we define a new parameter, called the standardized scalloping amplitude ρ_s, as follows:

$$\rho_s = \frac{S \text{ observed with the test antenna at variable height}}{S \text{ observed with the standard VOR antenna located 15' above ground}} \qquad (4.7)$$

where the observation angles correspond to the lowest minima or maxima in the pattern.

Figures 4-8a through 4-8d show the standardized scalloping amplitude ρ_s as functions of the standard VOR antenna height above ground with the scatterer height as the parameter and for a variable distance D of the scatterer from the antenna. The observation angles in each case correspond to the lowest pattern minima.

Corresponding results for the DPLC antenna are shown in Figures 4-9a through 4-9d.

The results shown in Figures 4-8 - 4-9 indicate that in general ρ_s increases with increase of the antenna height.

Figure 4-10 shows the variation of S as a function of the scatterer height with D as the parameter and for a standard VOR antenna located 15' above ground. The observation angle in each case is in the direction of the lowest pattern minimum. From Fig. 4-10 it is found that in general for a given height of the scatterer, the scalloping amplitude decreases as D increases and for a given distance D of the scatterer the scalloping amplitude increases with the increase of scatterer height H.

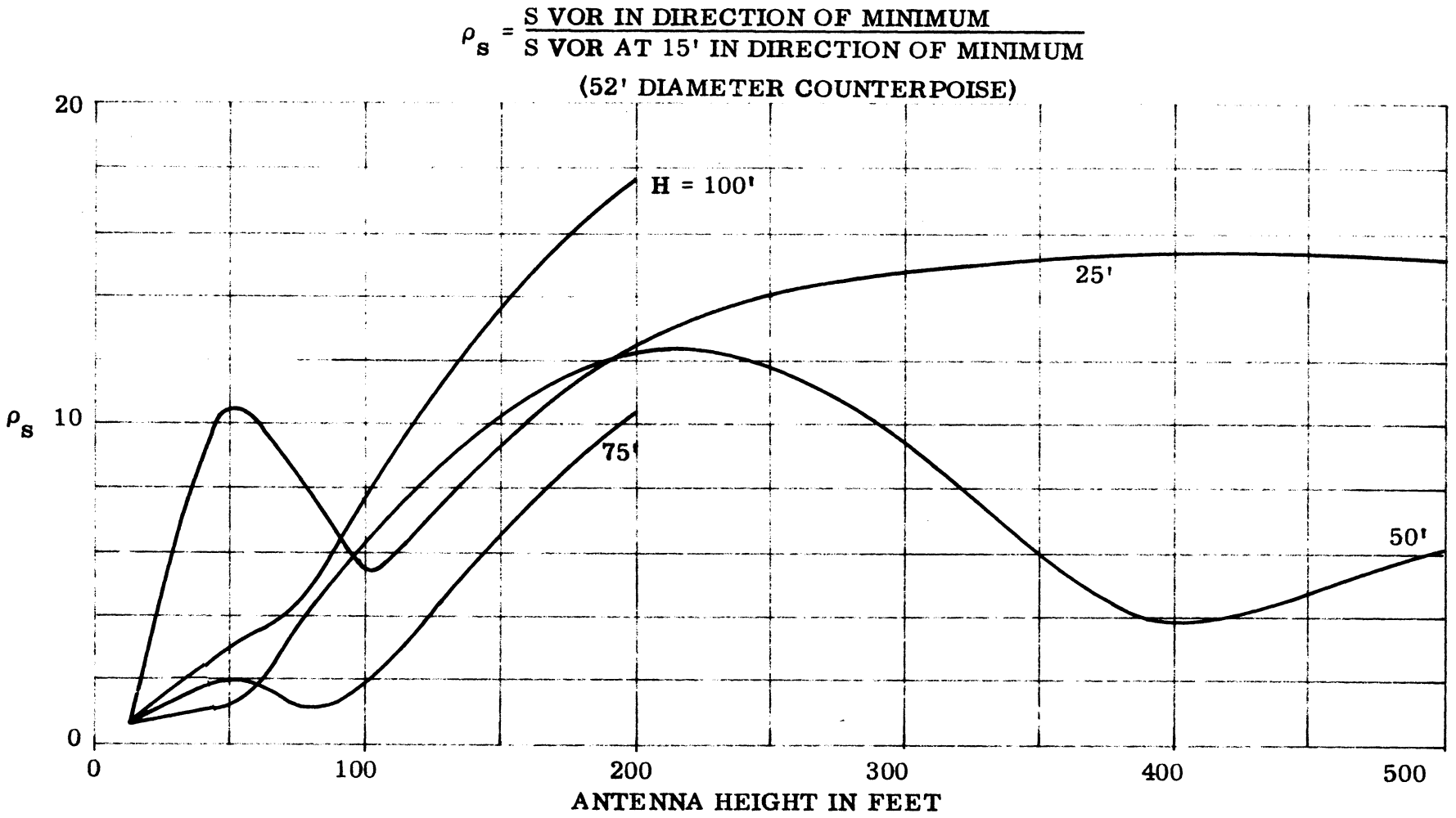

Fig. 4-8a: The standardized scalloping amplitude for standard VOR antenna as a function of the antenna height with scatterer height as the parameter. Observation angle is in the direction of the first pattern minimum. D = 500', A = 0.02.

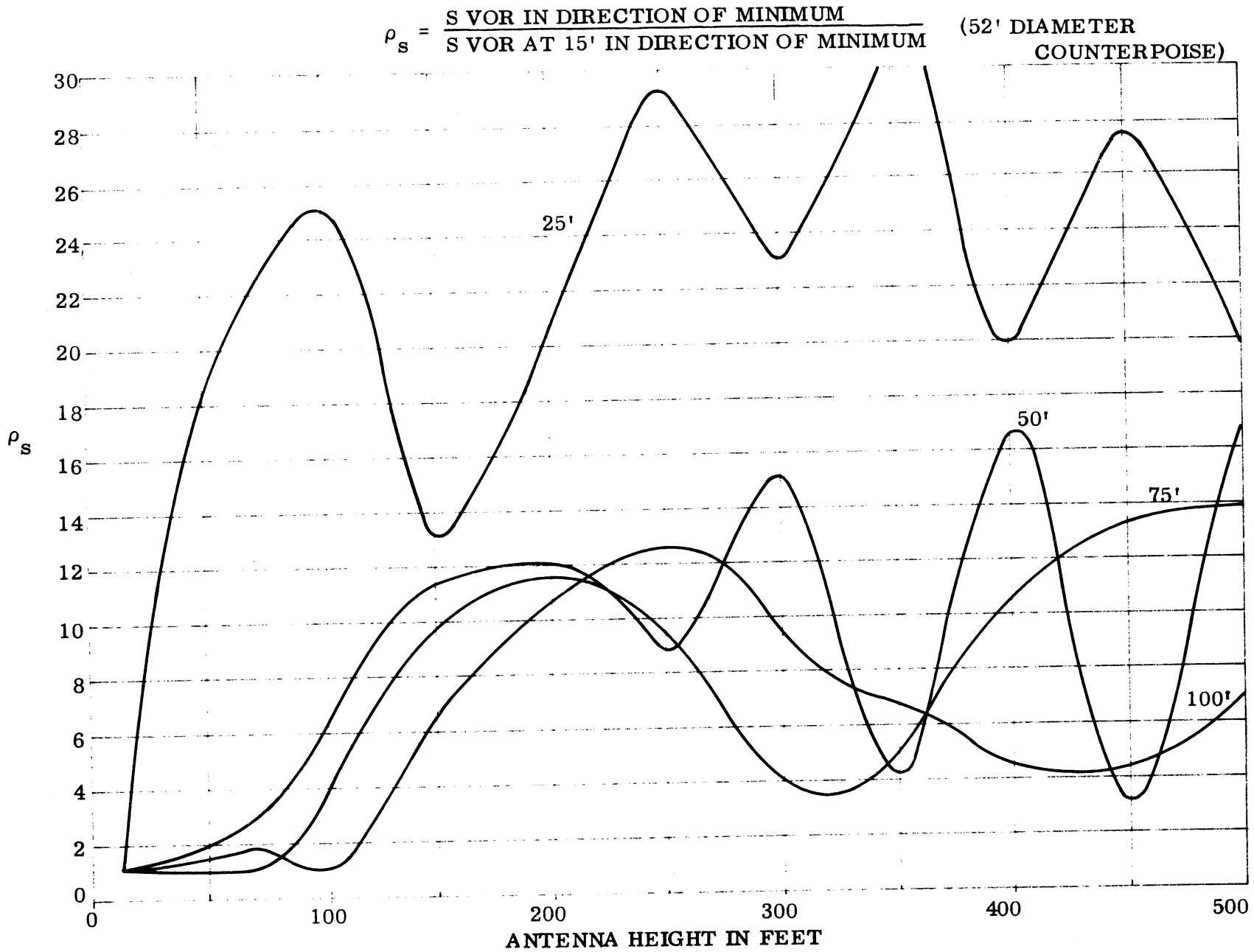

Fig. 4-8b: The standardized scalloping amplitude for standard VOR antenna as functions of the antenna height with scatterer height as the parameter. Observation angle is in the direction of the first pattern minimum. D = 1000', A = 0.02.

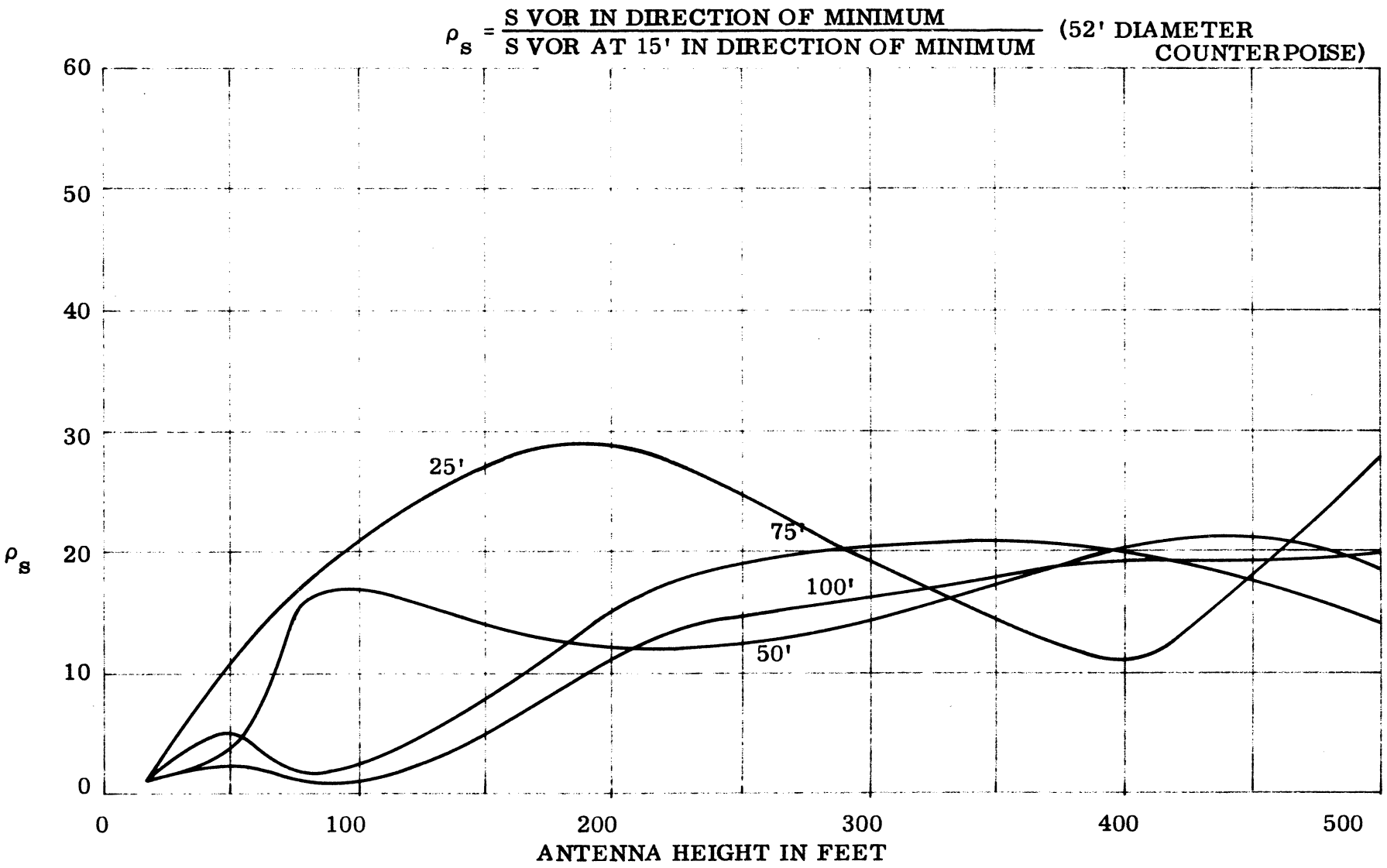

Fig. 4-8c: The standardized scalloping amplitude for standard VOR antenna as function of the antenna height with scatterer height as the parameter. Observation angle is in the direction of the first pattern minimum. D = 2000', A = 0.02.

ρ_s = S VOR IN DIRECTION OF MINIMUM / S VOR AT 15' IN DIRECTION OF MINIMUM (52' DIAMETER COUNTERPOISE)

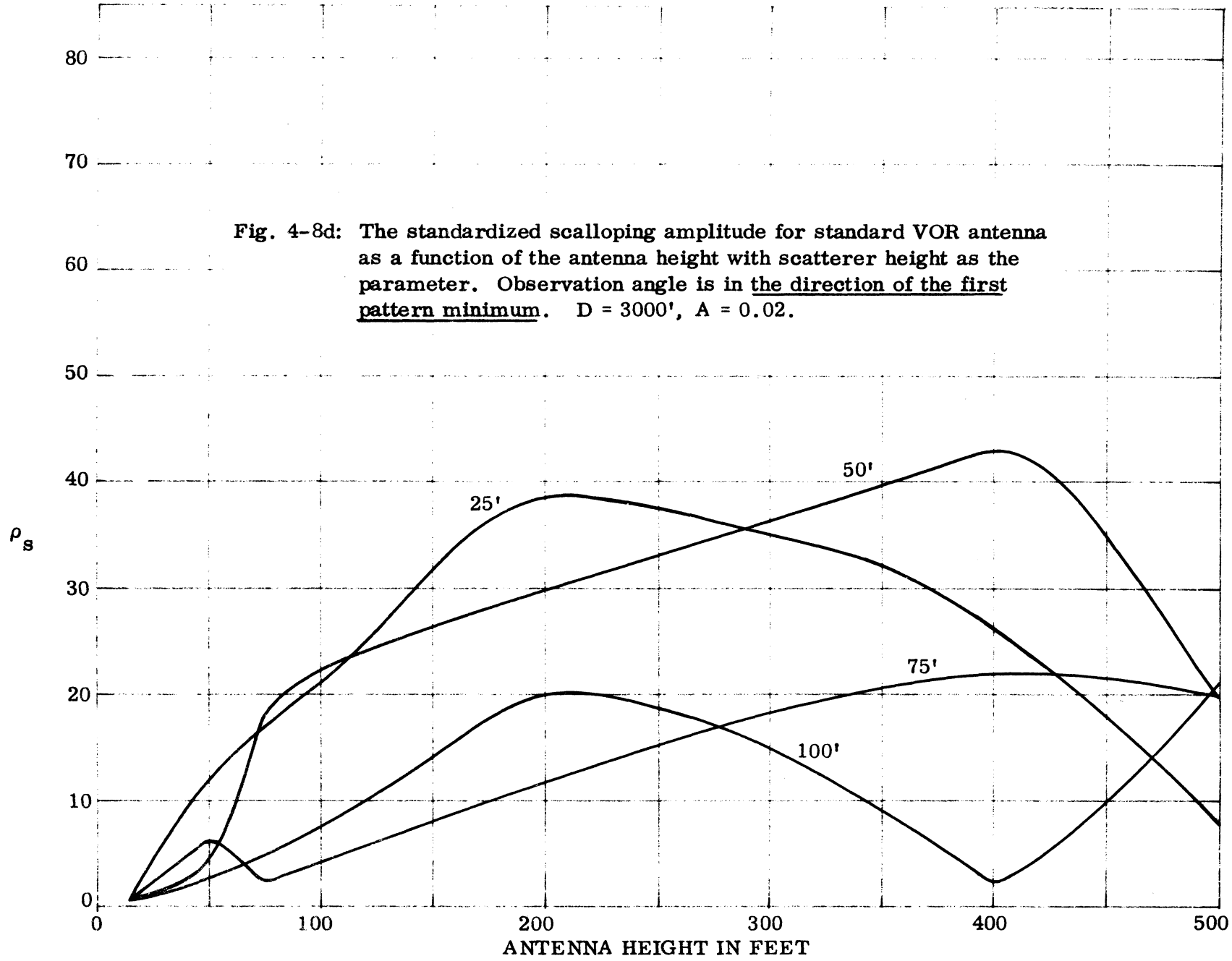

Fig. 4-8d: The standardized scalloping amplitude for standard VOR antenna as a function of the antenna height with scatterer height as the parameter. Observation angle is in the direction of the first pattern minimum. D = 3000', A = 0.02.

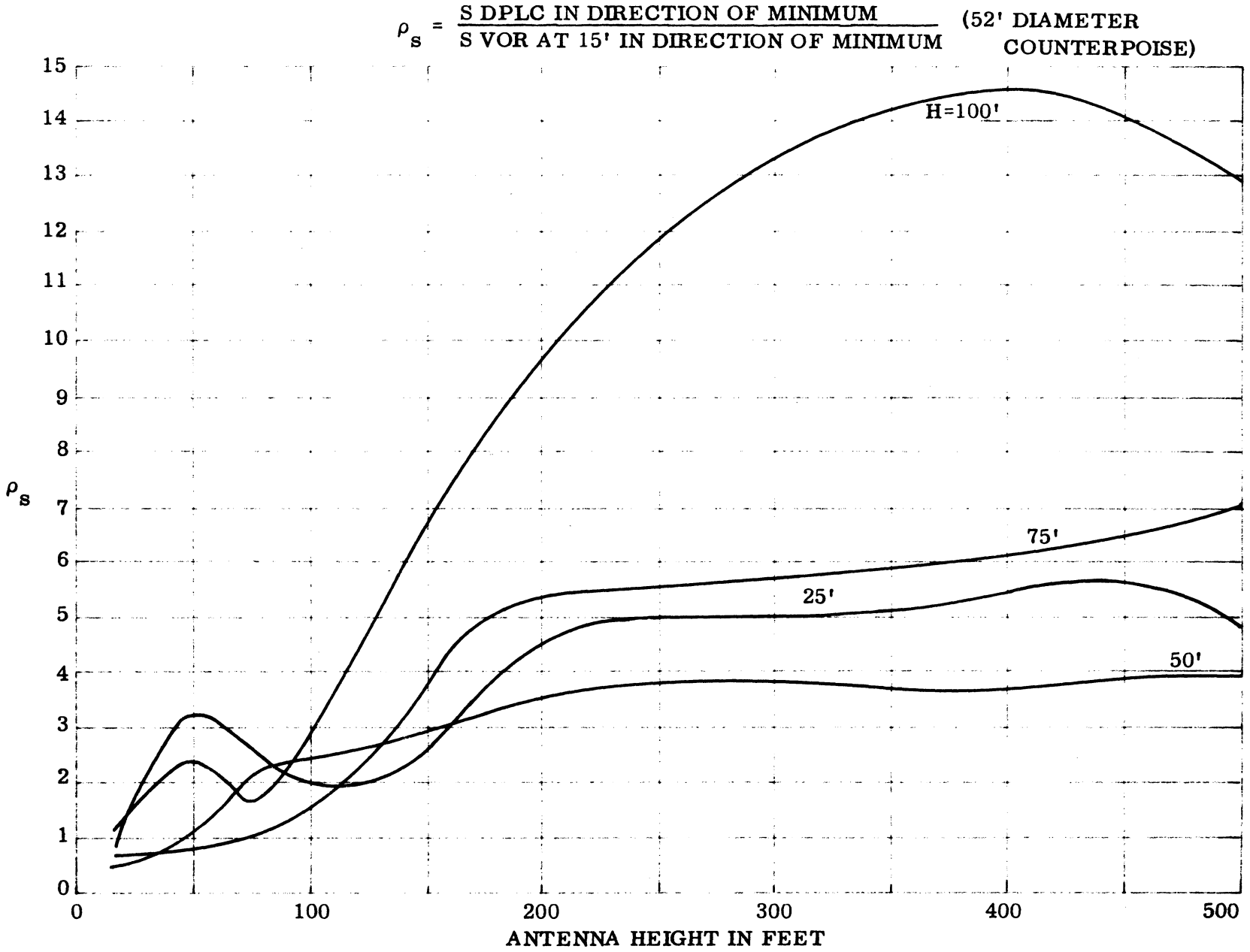

Fig. 4-9a: The standardized scalloping amplitude for a DPLC antenna as a function of the antenna height with scatterer height as the parameter. Observation angle is in the direction of the first pattern minimum. D = 500', A = 0.02.

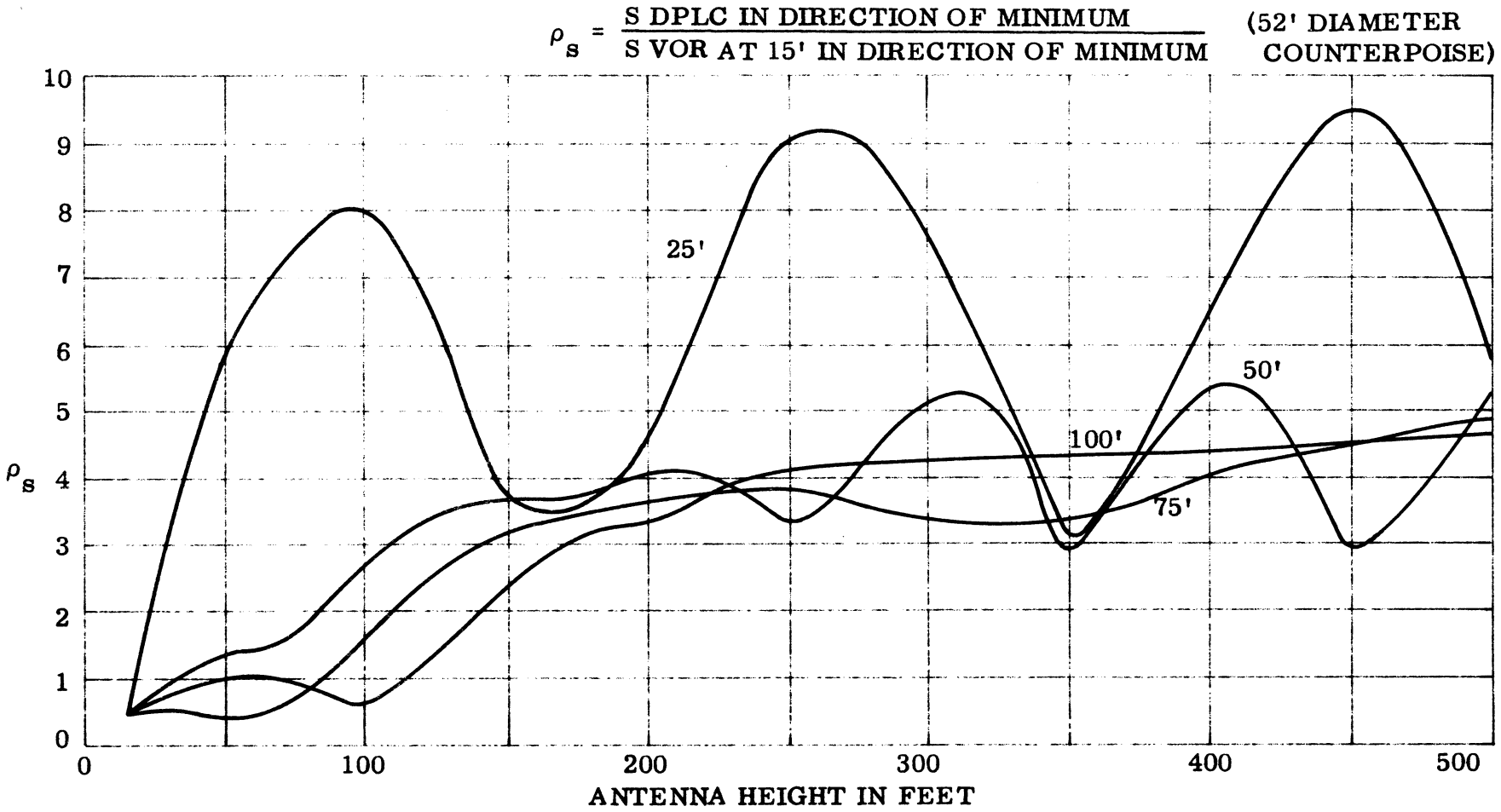

Fig. 4-9b: The standardized scalloping amplitude for DPLC antenna as a function of the antenna height with scatterer height as the parameter. Observation angle is in the direction of the first pattern minimum. D = 1000', A = 0.02.

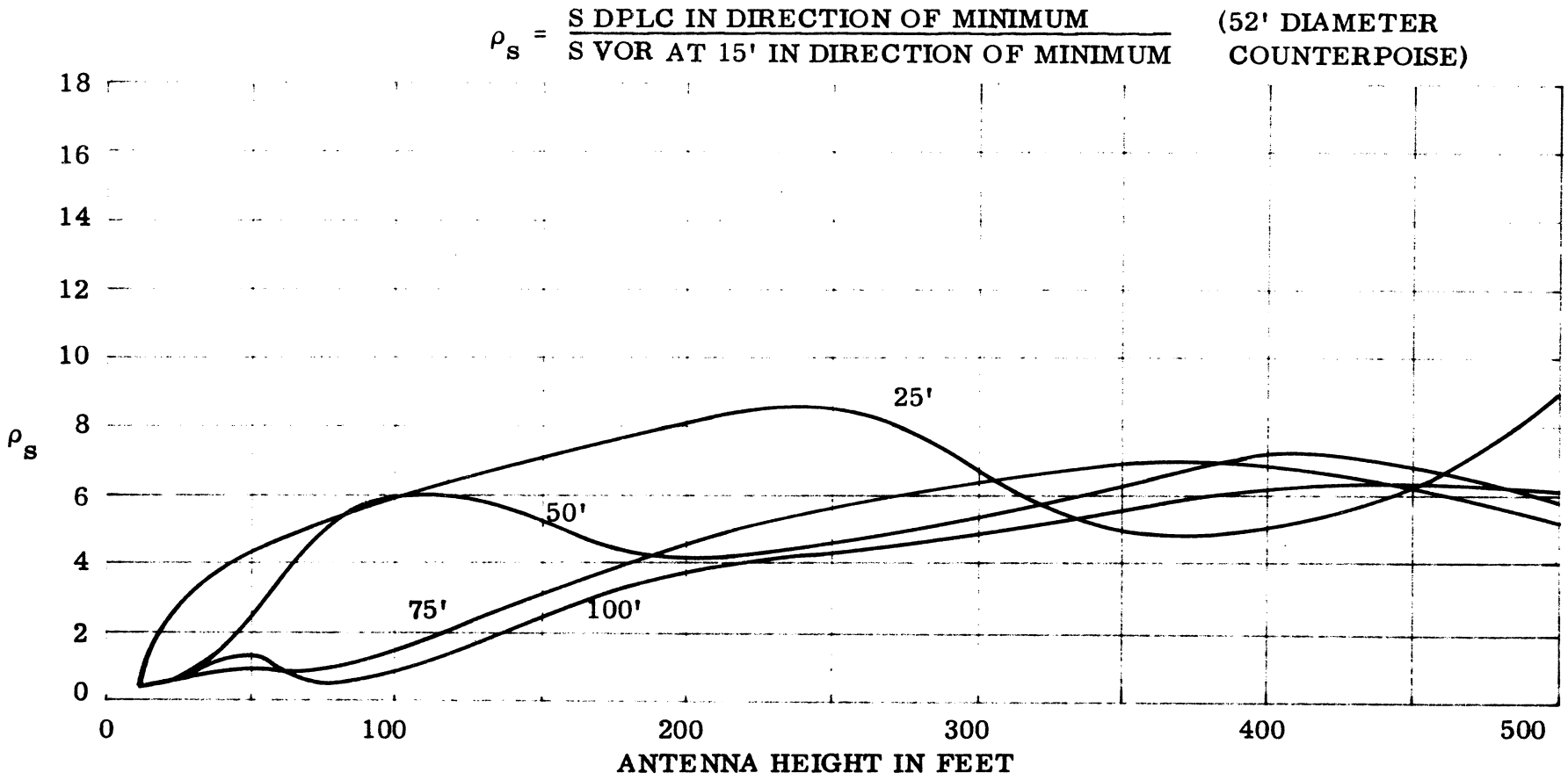

Fig. 4-9c: The standardized scalloping amplitude for DPLC antenna as a function of the antenna height with scatterer height as the parameter. Observation angle is in the direction of the first pattern minimum. D = 2000', A = 0.02.

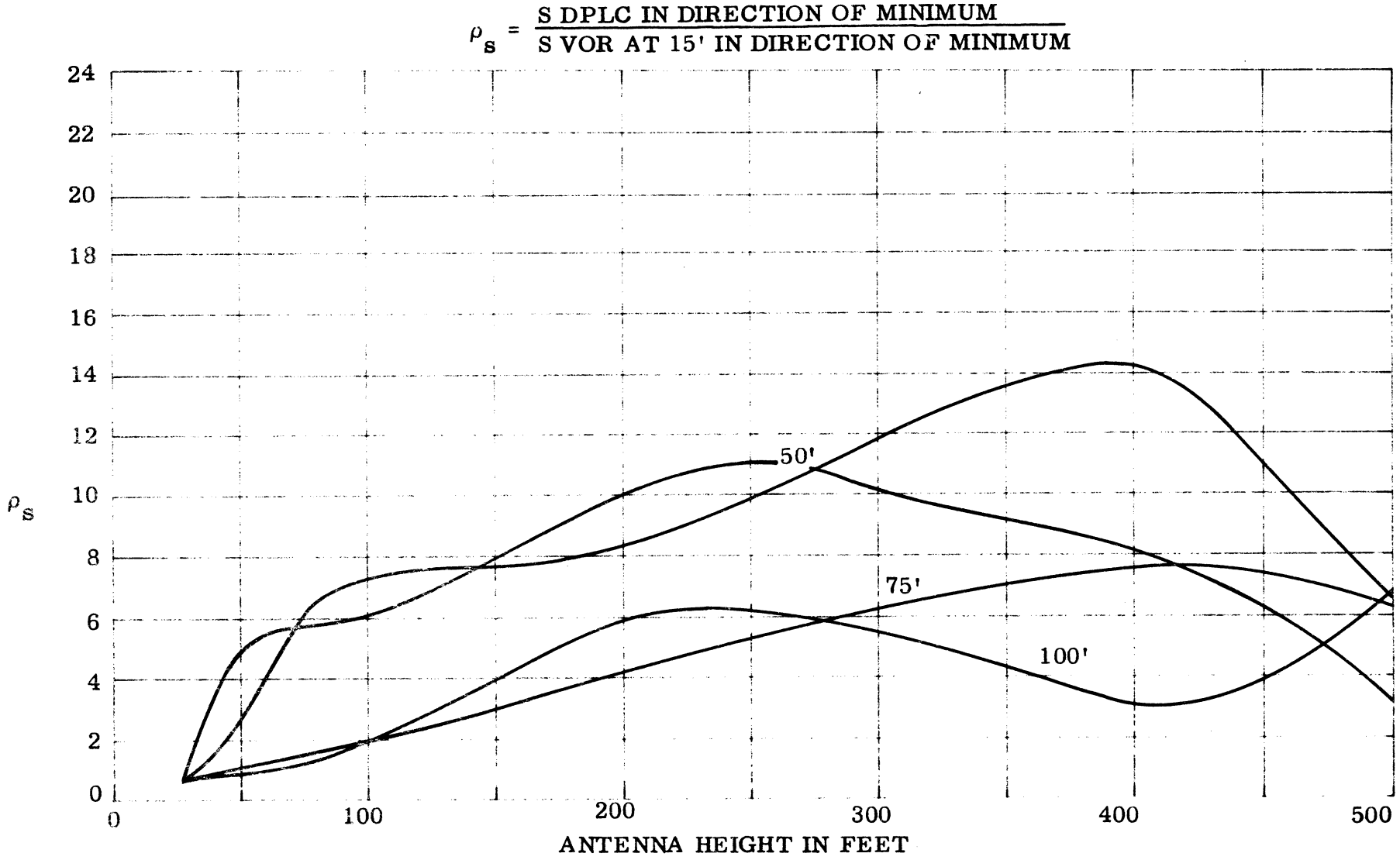

Fig. 4-9d: The standardized scalloping amplitude for DPLC antenna as a function of the antenna height with scatterer height as the parameter. Observation angle is in the direction of the first pattern minimum. D = 3000', A = 0.02.

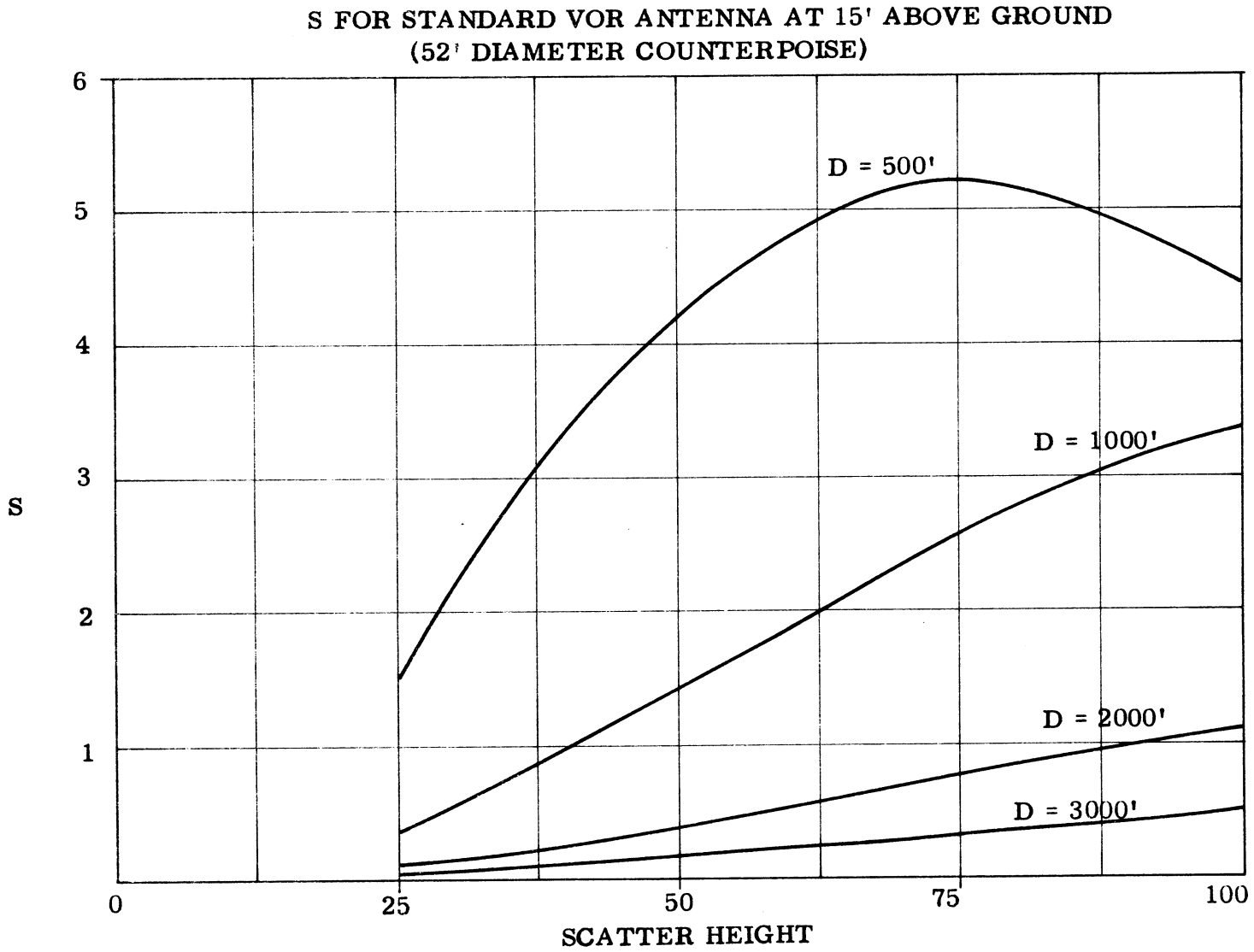

Fig. 4-10: The average scalloping amplitude S as a function of scatter height for a VOR antenna located 15' above ground with the scatterer distance as the parameter. Observation angle is in the direction of the first pattern minimum. A = 0.02.

Figures 4-11a through 4-11d show the standardized scalloping amplitude ρ_s as functions of the standard VOR antenna height above ground with the scatterer height as the parameter and for a variable distance D of the scatterer from the antenna. The observation angles in each case correspond to the lowest pattern maxima.

Corresponding results for the DPLC antenna are shown in Figs. 4-12a through 4-12d. Note that for H = 100' and D = 500' the scatterer is located approximately at the first minimum in the standard VOR pattern for Z_0 = 15'. This explains the large value of ρ_s ($\sim$ 2.6) at Z_0 = 15' for H = 100' in Fig. 4-12a. For other values of D the quantity

$$\frac{S_s^T(\theta_1)}{S_s^T(\theta)}$$

is approximately of the same order for both antennas for Z_0 = 15'. This explains why the curves 4-12b - 4-12d start from $\rho_s \sim 1$.

It is interesting to observe from Fig. 4-11 that raising the antenna beyond 15' at first reduces ρ_s and it assumes a minimum at a height of 50'. This should be compared with the results in the null direction where it is found that ρ_s increases with antenna height. No such general behavior is found with the DPLC antenna.

4.7 Scalloping Amplitude as a Function of D

In this section we discuss the variation of the scalloping amplitude as a function of distance D of the scatterer from the antenna. The scalloping amplitude given by Eq. (4.2) depends on D through the parameter A and θ_1. In general, the magnitude of the scattering coefficient varies inversely with the distance D. In order to bring out the dependence of S on D we define a modified scattering coefficient A' such that

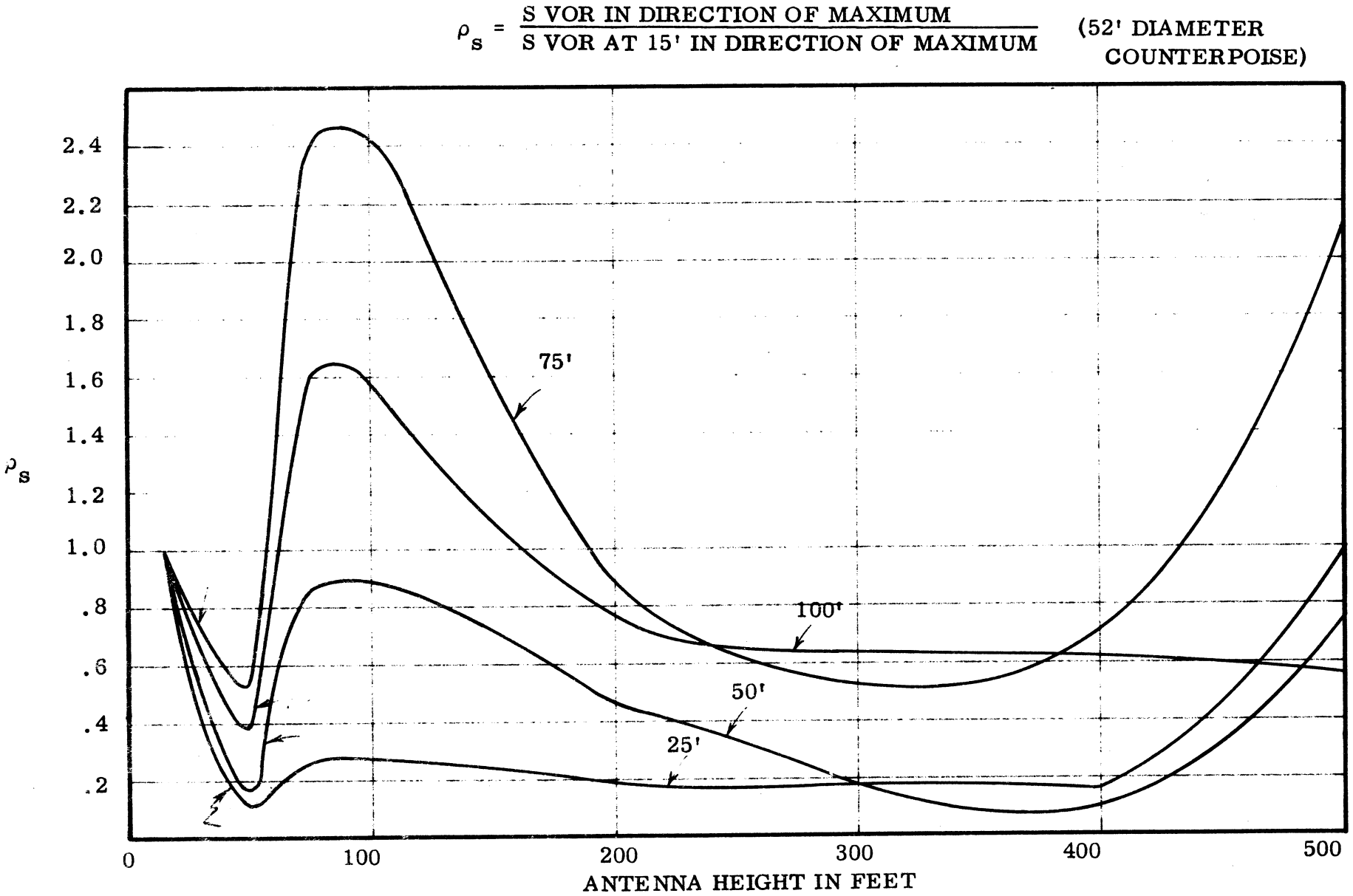

Fig. 4-11a: The standardized scalloping amplitude for standard VOR antenna as a function of the antenna height with scatterer height as the parameter. Observation angle is in the direction of the first pattern maximum. D = 500', A = 0.02.

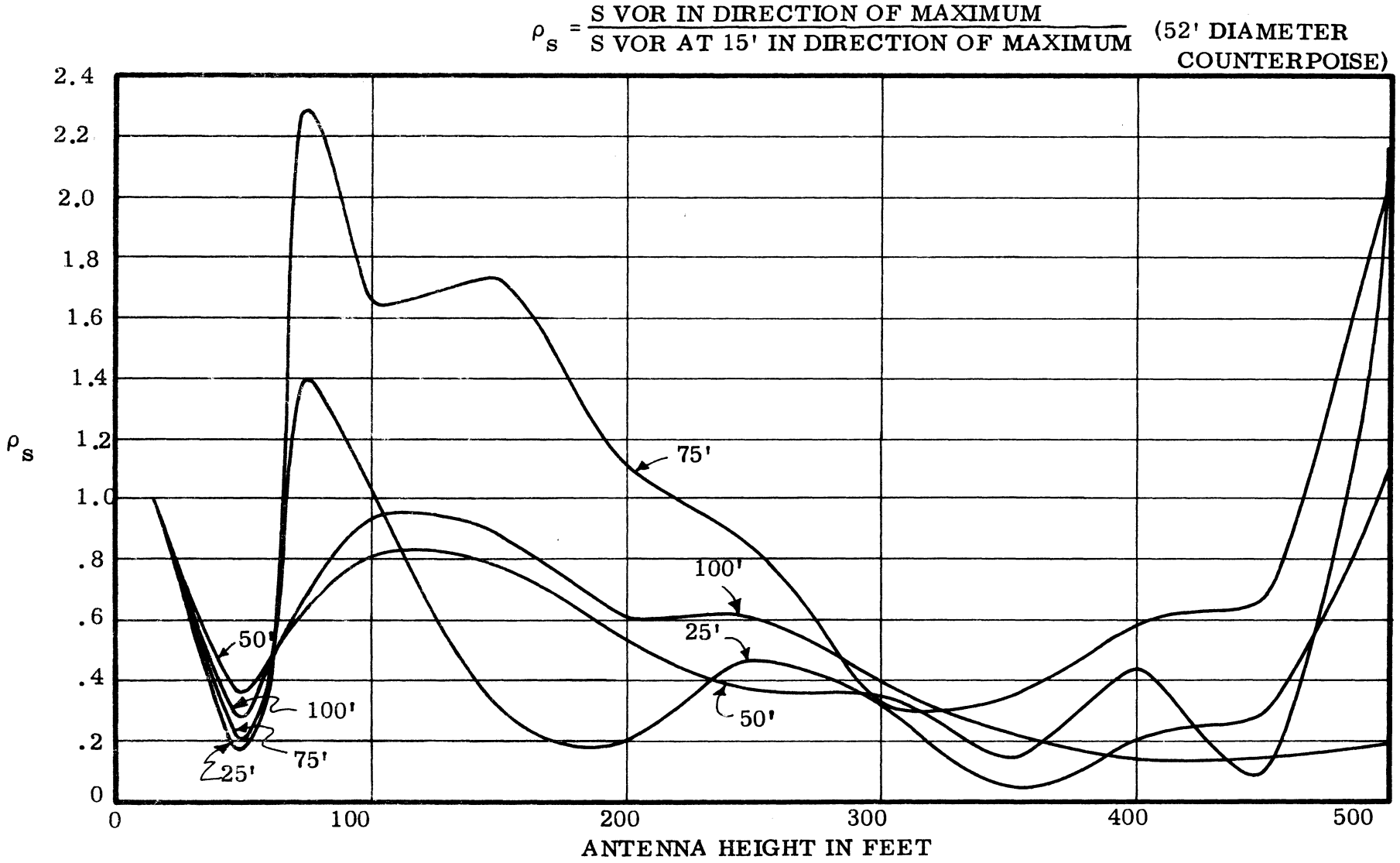

Fig. 4-11b: The standardized scalloping amplitude for standard VOR antenna as a function of the antenna height with scatterer height as the parameter. Observation angle is in the direction of the first pattern maximum. D = 1000', A = 0.02.

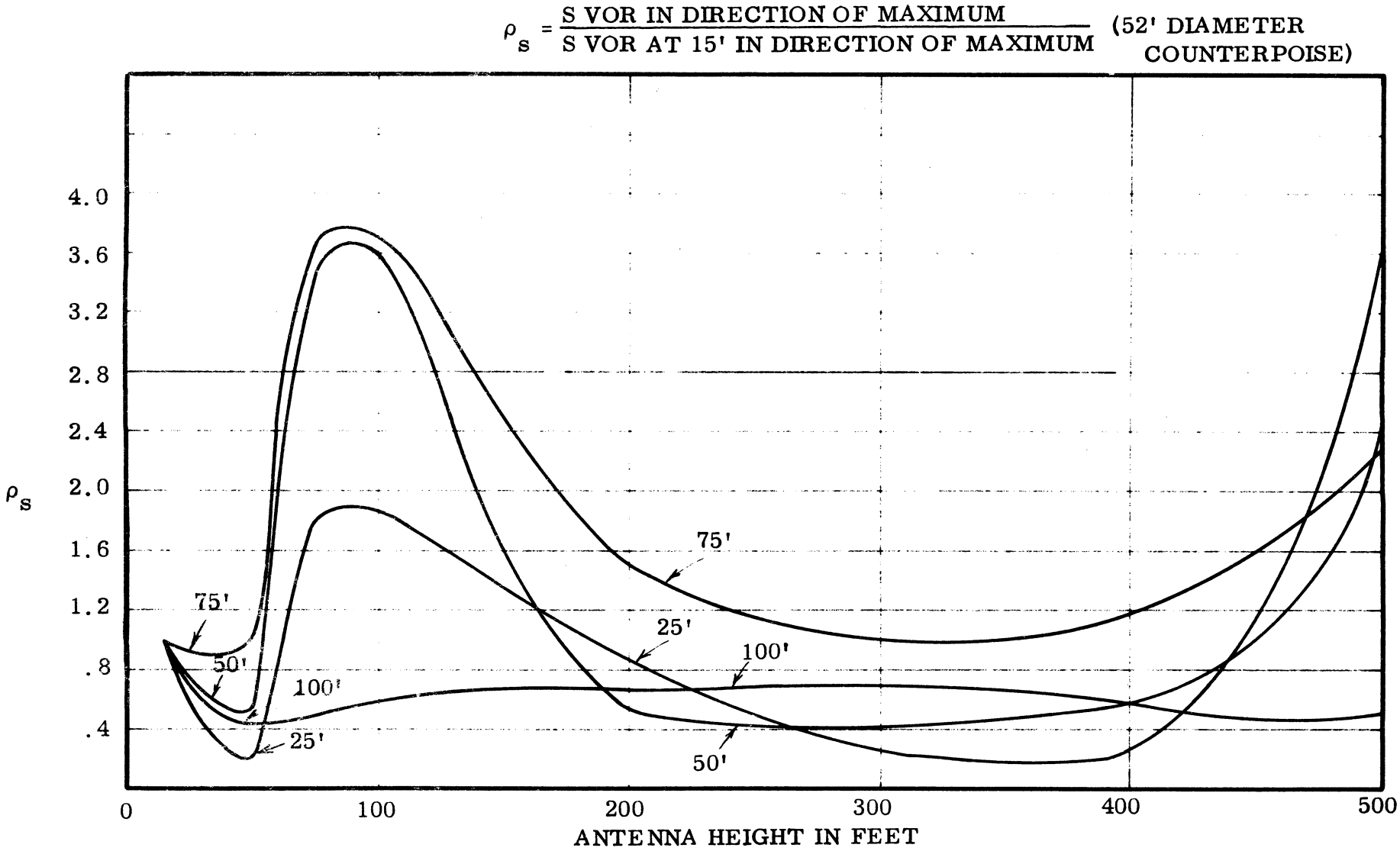

Fig. 4-11c: The standardized scalloping amplitudes for standard VOR antenna as a function of the antenna height with the scatterer height as the parameter. Observation angle is in the direction of the first pattern maximum. D = 2000', A = 0.02.

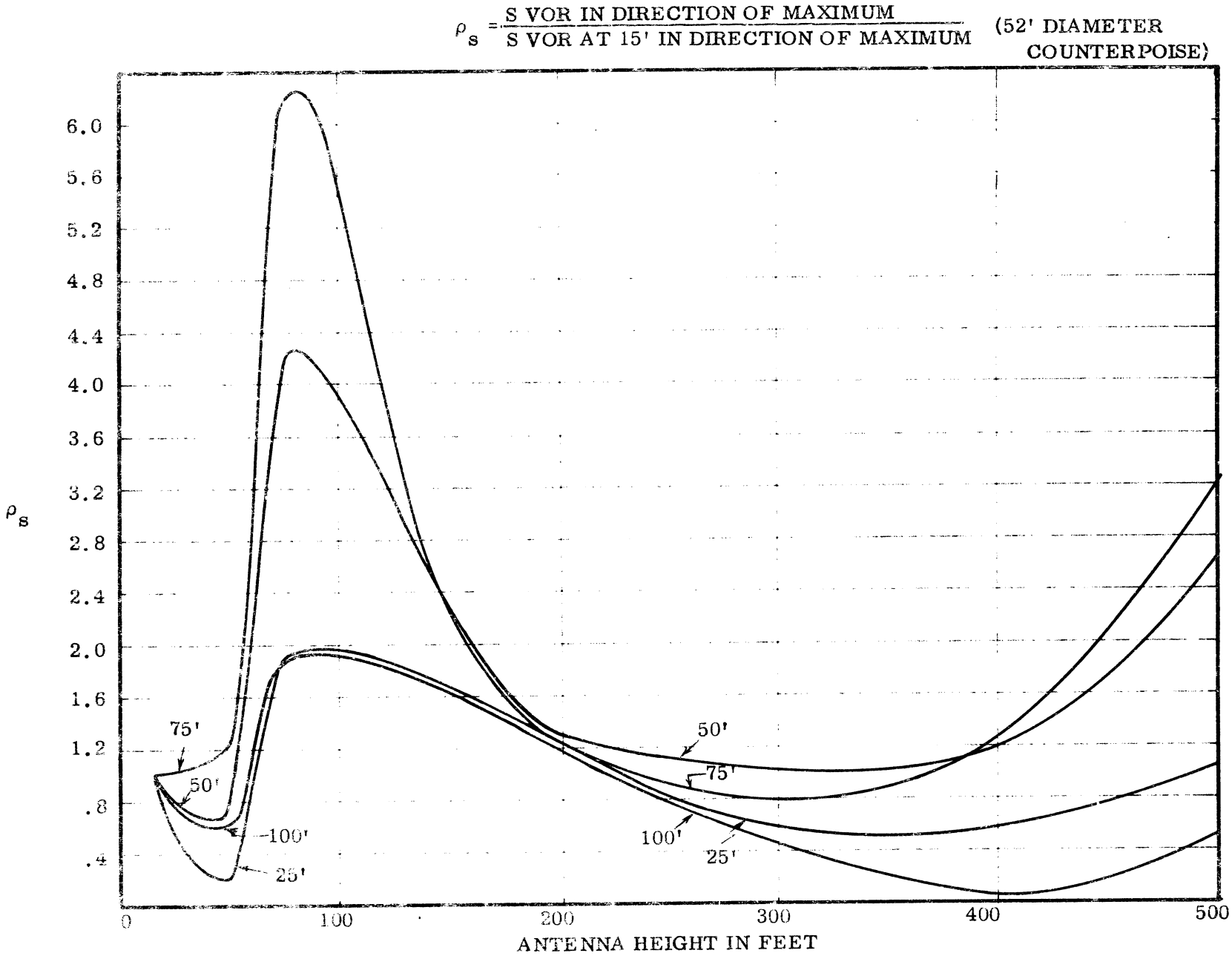

Fig. 4-11d: The standardized scalloping amplitude for standard VOR antenna as a function of the antenna height with scatterer height as the parameter. Observation angle is in the direction of the first pattern maximum. D = 3000', A = 0.02.

$$\rho_s = \frac{\text{S DPLC IN DIRECTION OF MAXIMUM}}{\text{S VOR AT 15' IN DIRECTION OF MAXIMUM}}$$ (52' DIAMETER COUNTERPOISE)

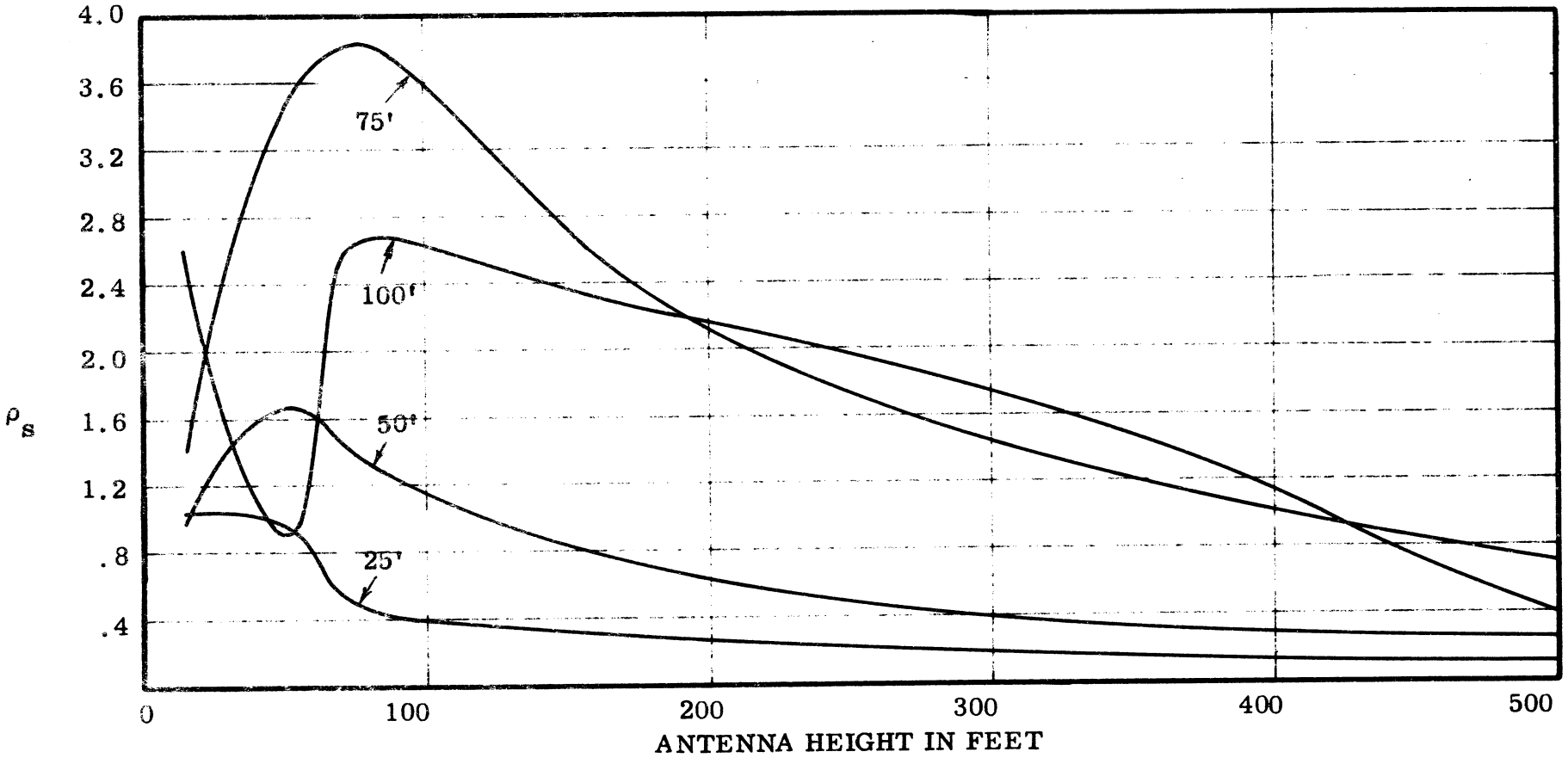

Fig. 4-12a: The standardized scalloping amplitude for DPLC antenna as a function of the antenna height with scatterer height as the parameter. Observation angle is in the direction of the first pattern maximum. D = 500', A = 0.02.

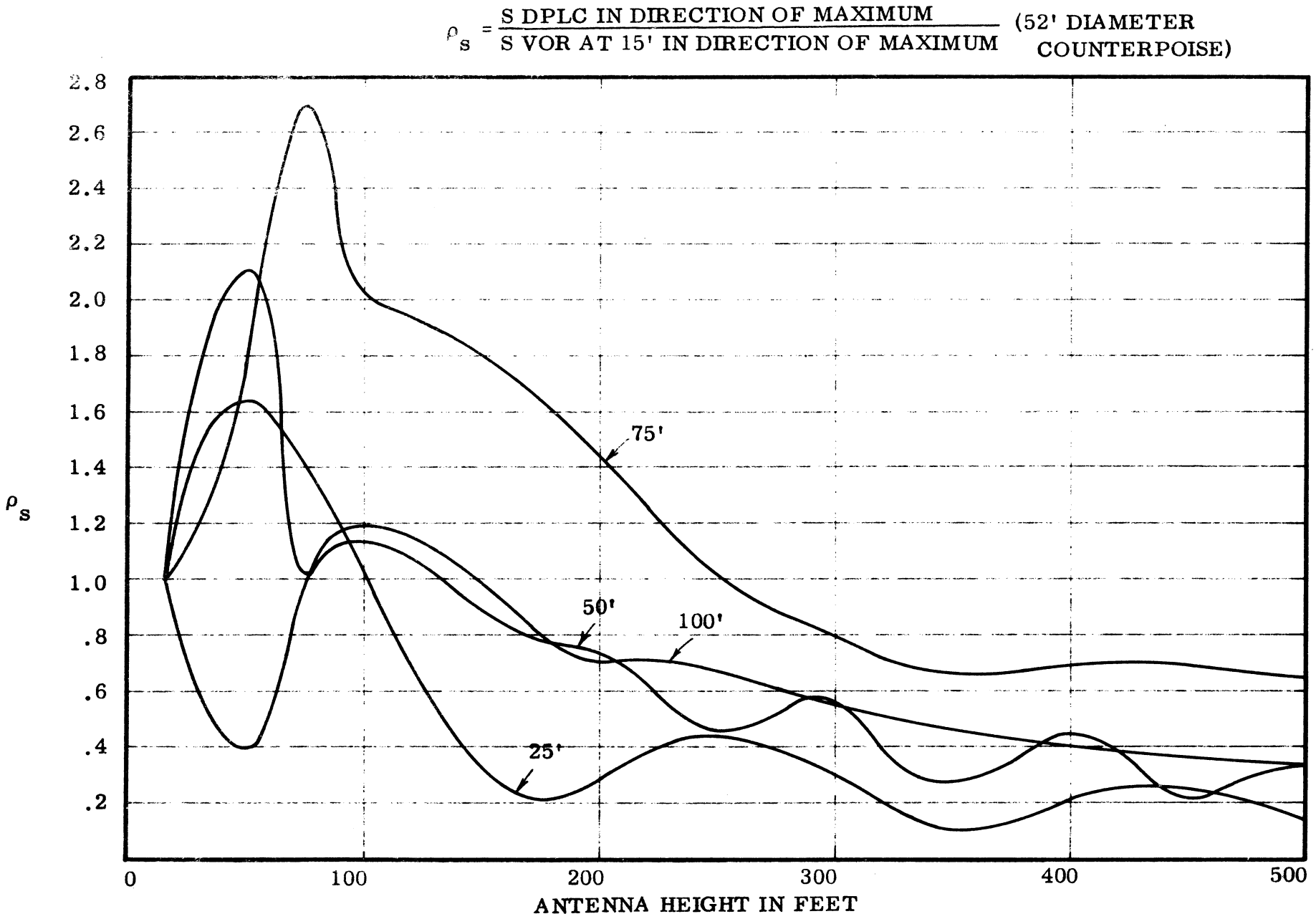

Fig. 4-12b: The standardized scalloping amplitude for DPLC antenna as a function of the antenna height with scatterer height as the parameter. Observation angle is in the direction of the first pattern maximum. D = 1000', A = 0.02.

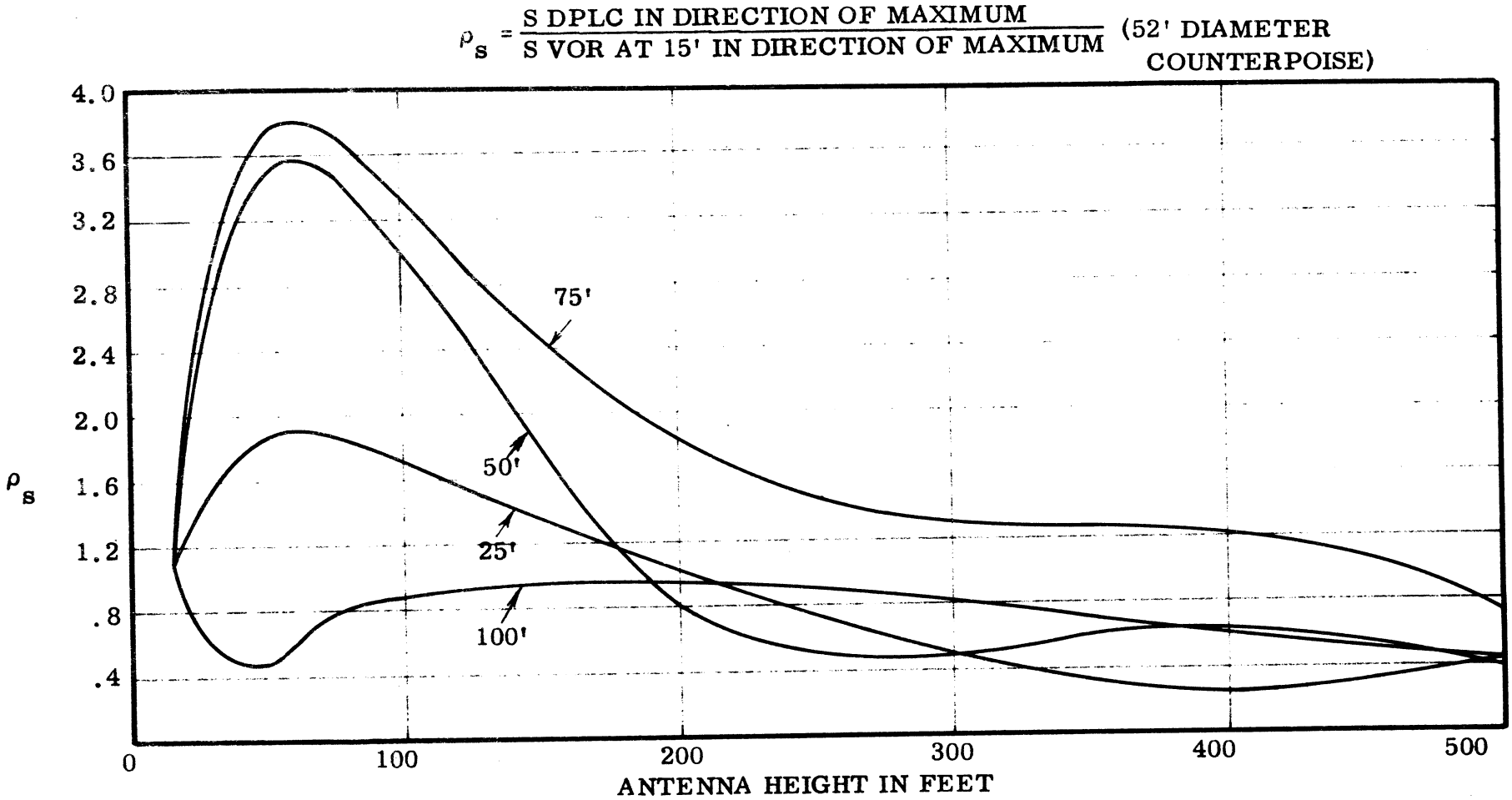

Fig. 4-12c: The standardized scalloping amplitude for DPLC antenna as a function of the antenna height with scatterer height as the parameter. Observation angle is in the direction of the first pattern maximum. D = 2000', A = 0.02.

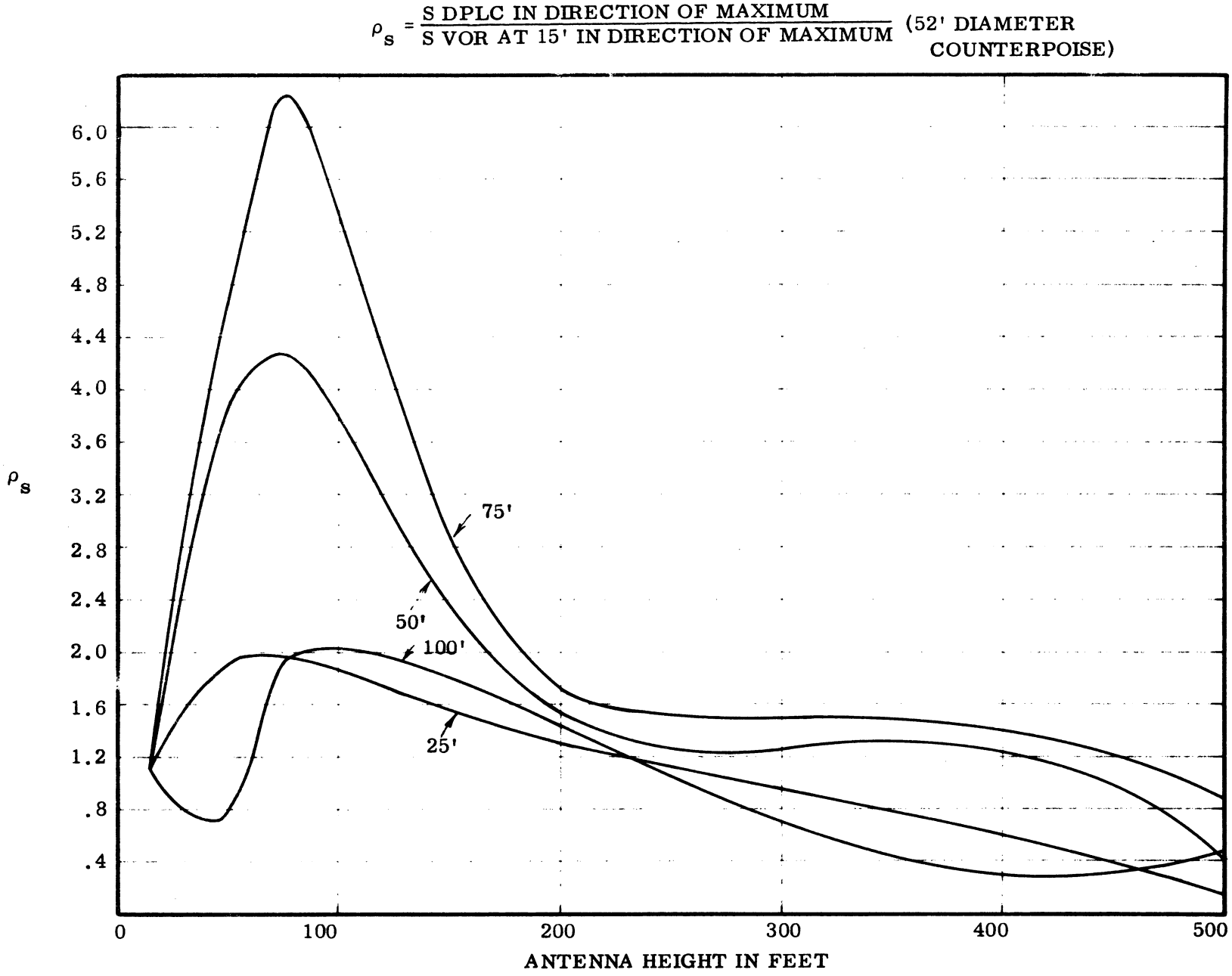

Fig. 4-12d: The standardized scalloping amplitude for DPLC antenna as a function of the antenna height with scatterer height as the parameter. Observation angle is in the direction of the first pattern maximum. D = 3000', A = 0.02.

$$A' = \frac{A \times 1000}{D} \quad , \tag{4.5}$$

where the distance D is expressed in feet. Note that A' is noramlized such that at D = 1000', A' = A. We shall assume that A=0.02, as before. With this modified definition of the scattering coefficient we calculate S_1 by using Eq. (4.2). The results obtained for the standard VOR antenna located 15' above ground are shown in Figure 4-13. The elevation of the flight path corresponds to the first minimum in the pattern of the antenna. In general, the scalloping amplitude decreases with increase of D. The cross-over points in some cases are attributed to the image effects on the scattered field at the observation point, i.e., due to the special combination of the values of H and θ.

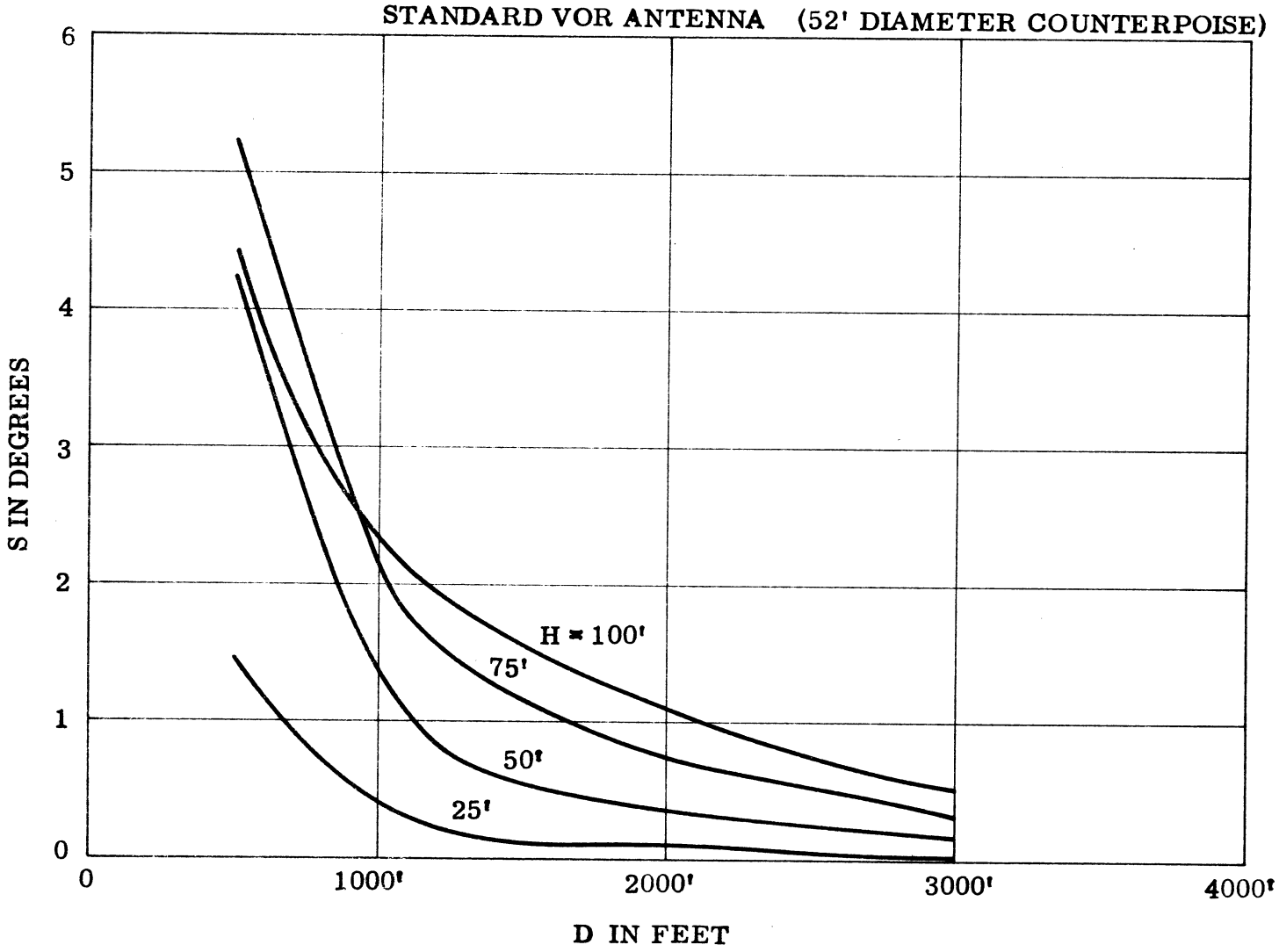

Fig. 4-13: Average maximum scalloping as a function of D with the scatterer height as the parameter. Observation angle is in the direction of the first pattern minimum. $Z_o = 15'$, VOR antenna.

V

SOME OBSERVATIONS AND CONCLUSIONS

5.1 Introduction

The results of an investigation of the radiation characteristics of standard VOR and large gradient VOR antennas located above a perfectly conducting ground have been given in Chapters II and III. The detailed scalloping results observed with a standard VOR system using these antennas and in the presence of some known scatterers have been given in Chapter IV. On the basis of these results we make the following general observations and comments which may be found useful in evaluating performance of a large gradient standard VOR system.

5.2 Some Observations

The important observations are as follows:

(i) For the same height of the antennas above ground the depths of all the minima in the vertical plane patterns of large gradient VOR antennas are found to be less than those of the standard VOR antenna patterns. In general, the reduction in the depths of the first few minima increases rapidly with height up to about 200' ($\sim$21 λ) and then it assumes a constant value. For minimum nearest to the horizon (first minimum) the maximum reduction is found to be about 10dB. The maximum reduction value decreases with decrease of the field gradient of the large gradient antenna.

(ii) The scalloping amplitude observed during an orbital flight is maximum in the direction of the first minimum in the vertical plane pattern of the antenna and it increases with increase of the depth of that minimum.

(iii) For a given antenna the maximum value of the scalloping amplitude decreases with increase of the field gradient associated with the antenna.

(iv) In general, it is found that for the same height of the antennas above ground the scalloping observed with a large gradient antenna is less than that obtained with a standard VOR antenna. The amount of improvement increases with increase of the field gradient of the former antenna.

As discussed in section 4.4, the Manheim flight test results indicate the DPLC antenna produces a scalloping error in the null which is about 0.17 times that produced by the standard VOR antenna.

(v) Notice that in Figure 3-15 the filling factor for the first minimum of the DPLC antenna pattern increases rapidly, at first, up to a height of about 50' ($\sim 5\lambda$) and then it saturates to a value of about 10dB. Note also that the depth of the first minimum in the pattern of the DPLC antenna located 50' above ground (Figure 3-2e) is about the same as the depth of the first minimum in the pattern of the standard VOR antenna located 15' above ground (Figure 3-1c). This would imply that compared with the standard VOR antenna located 15' above ground the DPLC antenna would produce less scalloping for heights up to about 50'. Beyond this height the DPLC antenna would produce scalloping larger than the standard VOR located at standard heights. This limiting value of the height, of course, will be increased if the field gradient associated with the DPLC is increased further.

5.3 Conclusions

If in a given terrain the antenna is required to be raised above ground beyond the height of 15', then the large gradient antenna will definitely produce less scalloping. The amount of improvement obtained will depend on the field gradient associated with the antenna. In such cases the use of the large gradient antenna is recommended.

For the large gradient antennas studied here it is found that for antenna heights up to 50', the scalloping produced by such antennas would be less than that produced by standard antennas located at standard heights above ground. For obtaining better results beyond the height of 50', antennas with larger field gradients should be considered.

In brief the results reported in the present Handbook show that a standard VOR antenna about 15' above ground is at an optimum height. Almost every example indicates that raising the standard VOR antenna increases the scalloping and worsens the null problem. The large gradient antenna must have sufficient field gradient to more than overcome these difficulties in order to make an improvement.

ACKNOWLEDGMENT

The author wishes to acknowledge the benefit of several helpful discussions with Mr. Sterling R. Anderson. He also akcnowledges the valuable counsel and suggestions by Professor Ralph E. Hiatt. The computer programming for the report has been prepared by Mr. Philip Chan.

VI

REFERENCES

Anderson, S.R., H.F.Keary and W.L.Wright (June 1953), "The Four-Loop VOR Antenna", T.D. Report No. 210, Civil Aeronautics Administration Technical Development and Evaluation Center, Indianapolis, Indiana.

Anderson, S. R. (1965), "VHF Omnirange Accuracy Improvements", IEEE Trans., AME-12 No. 1, pp. 26-35.

Federal Aviation Administration, Department of Transportation (1968), Handbook: VOR/VORTAC Siting Criteria, No. 6700.11, Systems Research and Development Service, Washington, D.C.

Hurley, H.C., S.R.Anderson and H.F. Keary (1951), "The Civil Aeronautics Administration VHF Omnirange", Proc. IRE, 39, No. 12, pp. 1506-1520.

Sengupta, D.L. and J.E.Ferris (1970), "On the Radiation Patterns of Parasitic Loop Counterpoise Antennas", IEEE Trans. AP-18, No. 1, pp. 34-41.

Sengupta, D.L. and J.E.Ferris (1972), "Investigation of Parasitic Loop Counterpoise Antennas and Their Application to VOR Systems", Report No. FAA-RD-72-32, Department of Transportation, FAA, Systems Research and Development Service, Washington, D.C. 20591.

Sengupta, D.L. (1971), "Theory of VOR Antenna Radiation Patterns", IEE Electronic Letters (London), Vol. 7, No. 15, pp. 418-420.

Sengupta, D.L. (1973), "Theory of Double Parasitic Loop Counterpoise Antenna Radiation Patterns", IEEE Trans., AP-21, No. 1, pp. 94-97.

Sengupta, D.L. and V.H.Weston (1969), "Investigation of the Parasitic Loop Counterpoise Antenna", IEEE Trans., AP-17, No. 2, pp. 180-191.

Sengupta, D.L. and P. Chan (1972a),"Application of the Large Gradient VOR Antenna," Interim Engineering Report No.1, No. 011218-1-T, The University of Michigan Radiation Laboratory, Ann Arbor, Michigan.

Sengupta, D.L. and P. Chan (1972b), "Application of the Large Gradient VOR Antenna," Interim Engineering Report No. 2, No. 011218-2-T, The University of Michigan Radiation Laboratory, Ann Arbor, Michigan.

Sengupta, D.L. and P. Chan (1973a), "Application of the Large Gradient VOR Antenna," Interim Engineering Report No. 3, No. 011218-3-T, The University of Michigan Radiation Laboratory, Ann Arbor, Michigan.

Sengupta, D.L. and P. Chan (1973b), "Course Scalloping Amplitudes in Standard VOR Bearing Indications," Interim Engineering Report No. 4, No. 011218-4-T, The University of Michigan Radiation Laboratory, Ann Arbor, MIch.

Winick, A. B. and D.M.Brandewie (1970), "VOR/DME System Improvements", Proc. IEEE, Vol. 58, No. 3, pp. 430-437.

APPENDIX A

THEORY OF VOR COURSE SCALLOPING AMPLITUDES IN BEARING INDICATIONS

A.1 Introduction

VOR course scalloping amplitudes in bearing indications, discussed in Chapter IV, have been obtained by using the simplified expression given by Eq. (4.2). In the present appendix a rigorous theory is developed for the course scalloping amplitudes observed in the bearing indications of an airborne standard VOR receiver in the presence of multipath signals. The VOR transmitting antenna pattern characteristics, the scattering properties of the multipath source and the effects of ground reflection are all built into the theory so that their combined effects on the scalloping may be quantitatively investigated. The analysis assumes that the VOR receiver characteristics are ideal.

In the absence of any multipath between the aircraft and the VOR transmitter, the accuracy of the bearing indications of the airborne VOR receiver are found to be satisfactory (FAA, 1968; Hurley et al, 1951). Whenever there exist multipaths between a VOR station and a flying aircraft, the multipath signals combine with the desired signal to produce various types of siting errors in the VOR bearing indications at the airborne receiver (FAA 1968; Anderson 1965). The sources of these multipaths may be nearby scattering objects like trees, buildings, water towers, etc., or even the terrain surrounding the station. In the present study we discuss the theory of those siting errors which appear as course scalloping in the VOR bearing indications.

General discussions of observed course scalloping amplitudes produced by different types of scattering objects are given in (FAA 1968; Anderson 1965). For idealized cases approximate theory of scalloping has been developed in (FAA 1968). However, because of the various basic approximations made, the existing theory is unable to explain satisfactorily many of the observed results.

A.2 VOR Radiated Signal

Although the VOR system operates above ground, it is instructive to study the signal radiated by a standard VOR antenna located in free space. Assuming the antenna to be located at the origin of a spherical coordinate system, the radiated signal at an observation point located at (r, θ, ϕ) may be written as follows:

$$\vec{E}' = \hat{e}_\phi K \cdot \frac{\exp[-i(\omega t - kr)]}{r} \left\{ S_c(\theta) \left[1 + m \cos(\omega_s t + m_f \sin \omega_m t) \right] + S_s(\theta) m \cos(\omega_m t - \phi) \right\} , \quad (1)$$

where

$\hat{e}_\phi$ is the unit vector in the ϕ-direction and gives the polarization of the radiated field which is horizontal in the present case,

K is a constant,

ω is the carier frequency in radians per second,

$k = \omega/c$ is the propagation constant in free space,

$S_c(\theta)$ is the free space carrier mode elevation plane far field complex pattern of the VOR transmitting antenna,

$S_s(\theta)$ is the free space side-band mode elevation plane far field complex pattern of the VOR transmitting antenna,

ω_s is the subcarrier frequency in radians per second,

ω_m is the modulation frequency in radians per second,

m is the amplitude modulation index,

m_f is the frequency modulation index.

In the ideal case [2] it is assumed that $S_c(\theta) \equiv S_s(\theta)$. Under this condition the detected signal at the reference phase channel output of the airborne receiver is proportional to $\cos\omega_m t$ and that at the variablephase channel output is proportional to $\cos(\omega_m t - \phi)$. The phase comparison of these two signals yields the desired bearing ϕ of the observation point. From the viewpoint of obtaining the azimuth information it is sufficient to consider the envelope of the following signal at the input of the VOR receiver:

$$E(P) = K \frac{\exp[-i(\omega t - kr)]}{r} \left[S_c(\theta) + S_s(\theta)\cos(\omega_m t - \phi)\right] , \qquad (2)$$

where the modulation index m of the space amplitude modulated wave is assumed to be included in $S_s(\theta)$.

As indicated in Eqs. (1) and (2), observe that in general the carrier and side-band signals are not in RF phase with each other. The implication of this phase relationship will be discussed later. Explicit expressions for the free space carrier and side-band mode complex patterns have been discussed elsewhere (Sengupta and Weston 1969; Sengupta 1971). In the present problem it is assumed that $S_c(\theta)$ and $S_s(\theta)$ are known. For later reference the two pattern functions are written as follows:

$$S_c(\theta) = \left|S_c(\theta)\right| \exp\left[i\alpha_c(\theta)\right] \quad , \tag{3}$$

$$S_s(\theta) = \left|S_s(\theta)\right| \exp\left[i\alpha_s(\theta)\right] \quad . \tag{4}$$

The VOR transmitting antennas are usually located 12 feet above ground [3]. As a result the elevation plane pattern expressions given by Eqs. (3) and (4) must be modified to take into account the effects of ground. For this purpose let us assume that the antenna is located at a height Z_0 above a perfectly conducting infinite planar earth (Fig. 4-1.) The full scale test results (Sengupta and Ferris 1972) of standard VOR antennas justify the assumption of perfect conductivity of ground at VOR frequencies. Under this condition the field at the observation point $P(r, \theta, \phi)$ is given by the following:

$$E^i(P) = K \frac{\exp\left[-i(\omega t - kr)\right]}{r} \left[S_c^T(\theta) + S_s^T(\theta) \cos(\omega_m t - \phi)\right] \quad , \tag{5}$$

where $S_c^T(\theta)$ and $S_s^T(\theta)$ are the modified carrier and side-band mode patterns and are given by:

$$S_c^T(\theta) = \left|S_c^T(\theta)\right| \exp\left[i\alpha_c^T(\theta)\right]$$

$$= S_c(\theta) \exp(-ikZ_0 \cos\theta) - S_c(\pi - \theta) \exp(ikZ_0 \cos\theta) \quad , \tag{6}$$

$$S_s^T(\theta) = \left|S_s^T(\theta)\right| \exp\left[i\alpha_c^T(\theta)\right]$$

$$= S_s(\theta) \exp(-ikZ_0 \cos\theta) - S_s(\pi - \theta) \exp(ikZ_0 \cos\theta) \tag{7}$$

The validity of Eqs. (6) and (7) is discussed in (Sengupta and Ferris 1972).

A.3 Multipath Signal at P

Let the VOR station, the scattering object producing the multipath signal and a stationary aircraft be located above a perfectly conducting earth as in Fig. 4-1. The aircraft location P is assumed to be in the far zone of the VOR antenna. The direct signal received at P is given by Eq. (5). To obtain the multipath signal at P we assume that the scattering object S is located sufficiently far from the VOR station so that $kd_1 \gg 1$. Under this condition the usual geometrical optics approximation may be used to obtain the field $E^i(S)$ incident at S from the VOR antenna. The field $E^i(S)$ incident at the scattering object consists of the direct and reflected waves originating from the VOR antenna and reaching the scatterer. It can be shown that $E^i(S)$ is given by

$$E^i(S) = K \exp(-i\omega t)\left\{ \frac{\exp\left[ikd_1\left(1-\frac{Z_0}{d_1}\cos\theta_1\right)\right]}{d_1\left(1-\frac{Z_0}{d_1}\cos\theta_1\right)} f(\theta_1', \phi_1) - \frac{\exp\left[ikd_1\left(1+\frac{Z_0}{d_1}\cos\theta_1\right)\right]}{d_1\left(1+\frac{Z_0}{d_1}\cos\theta_1\right)} f(\pi-\theta_1'', \phi_1)\right\}, \quad (8)$$

where

$$f(\theta,\phi) = S_c(\theta) + S_s(\theta)\cos(\omega_m t - \phi), \quad (9)$$

$$\left.\begin{aligned} \sin\theta_1' &\simeq \frac{\sin\theta_1}{1-\frac{Z_0}{d_1}\cos\theta_1} \\ \sin\theta_1'' &\simeq \frac{\sin\theta_1}{1+\frac{Z_0}{d_1}\cos\theta_1} \end{aligned}\right\} \quad \text{for } \frac{Z_0}{d_1} \ll 1. \quad (10)$$

The multipath signal at P will be that portion of the incident field given by Eq. (8) which is scattered by the object in the direction of P. It is assumed that the scattering object does not produce any depolarization of the field. For a finite object the scattered field at P will appear as a spherical wave originating from S. The multipath signal at P may thus be written as

$$\bar{E}^{s}(P) = \frac{\exp(ikr_1)}{r_1} A(d_1, \theta_1, \phi_1; \theta, \phi) \exp\left[i\delta(d_1, \theta_1, \phi_1; \theta, \phi)\right] \quad , \tag{11}$$

where

r_1 is the distance between the scattering object and the observation point P (Fig. 4-1),

$A(d_1, \theta_1, \phi_1; \theta, \phi)\, e^{i\delta}$ may be identified with the scattering function appropriate for the scatterer. By definition A and δ are real quantities.

The dependence of the incident and scattering angles and the location of the scattering object are explicitly written in the definitions of A and δ to emphasize the fact that in many cases of practical interest the scattered fields from an object depend on these parameters. In the present case it can be shown that:

$$A(d_1, \theta_1, \phi_1; \theta, \phi) = \left[\frac{\sigma(\theta_1, \phi_1; \theta, \phi)}{4\pi d_1^2}\right]^{1/2} \quad , \tag{12}$$

where $\sigma(\theta_1, \phi_1; \theta, \phi)$ is the generalized definition of the bistatic scattering cross section of the multipath object. From now on for simplicity we shall represent the scattering function of the object by $Ae^{i\delta}$.

The effects of the perfectly conducting ground must be taken into account to obtain the scattered field at P. It can be shown that the total multipath signal at P is given by

$$E^s(P) = K \frac{\exp[-i(\omega t - kr)]}{r} \left[\frac{\exp(-ikZ_0 \cos\theta_1)}{1 - \frac{Z_0}{d_1}\cos\theta_1} f(\theta_1', \phi_1) \right.$$

$$\left. - \frac{\exp(ikZ_0 \cos\theta_1)}{1 + \frac{Z_0}{d_1}\cos\theta_1} f(\pi - \theta_1'', \phi_1) \right] A$$

$$\times \left(\exp\left\{ i \left[kd_1(1 - \cos\gamma) + \delta \right] \right\} - \exp\left\{ i \left[kd_1(1 - \cos\gamma') + \delta \right] \right\} \right) , \qquad (13)$$

where

$$\left. \begin{aligned} \cos\gamma &= \sin\theta \sin\theta_1 \cos(\phi - \phi_1) + \cos\theta \cos\theta_1 \\ \cos\gamma' &= \sin\theta \sin\theta_1 \cos(\phi - \phi_1) - \cos\theta \cos\theta_1 \end{aligned} \right\} \qquad (14)$$

After some algebraic manipulations, Eq. (13) may be rearranged in the following form:

$$E^s(P) = K \frac{\exp[-i(\omega t - kr)]}{r} 2A \sin(kH \cos\theta) e^{i\xi}$$

$$\times \left[\frac{\exp(-ikZ_0 \cos\theta_1)}{1 - \frac{Z_0}{d_1}\cos\theta_1} f(\theta_1', \phi_1) - \frac{\exp(ikZ_0 \cos\theta_1)}{1 + \frac{Z_0}{d_1}\cos\theta_1} f(\pi - \theta_1'', \phi_1) \right] \qquad (15)$$

where

$$\xi = kd_1\left[1 - \sin\theta \sin\theta_1 \cos(\phi - \phi_1)\right] + \delta - \pi/2$$

$$d_1 \cos\theta_1 = H \quad ,$$

where H is the height of the scatterer above ground (Fig. 1).

If it is assumed that the scatterer is located in the far zone of the VOR antenna, then $\theta_1' \simeq \theta_1'' \simeq \theta_1$ and because of the assumption $Z_0/d_1 \ll 1$ we can neglect the terms $Z_0/d_1 \cos\theta_1$ in the denominators of the terms within the parentheses of Eq. (13). Under these conditions Eq. (13) simplifies to:

$$E^S(P) = K \frac{\exp\left[-i(\omega t - kr)\right]}{r} \; 2A \exp(i\xi) \sin(kH\cos\theta)\left[S_c^T(\theta_1) + S_s^T(\theta_1)\cos(\omega_m t - \phi_1)\right] \quad . \tag{16}$$

We shall use the simplified expression given by Eq. (16) for the multipath signal at P. For better accuracy, Eq. (15) should be used for the multipath signal at P if the scattering object is located in the radiating near field zone of the VOR transmitting antenna.

A.4 Total Field at the Observation Point and the Bearing Error

The total field of interest for detection by the variable phase channel of the airborne VOR receiver at P is obtained by adding Eqs. (5) and (16). After some algebraic manipulations we write the total field in the following form:

$$E^T(P) = E^i(P) + E^S(P)$$

$$= K \frac{\exp\left\{-i\left[\omega t - kr - \alpha_c^T(\theta) - \xi\right]\right\}}{r} \left|S_c^T(\theta)\right| (f_c + f_s) \quad , \tag{17}$$

where

$$f_c^2 = 1+4A^2\left|\frac{S_c^T(\theta_1)}{S_c^T(\theta)}\right|^2 \sin^2(kH\cos\theta)$$

$$+4A\left|\frac{S_c^T(\theta_1)}{S_c^T(\theta)}\right| \sin(kH\cos\theta)\cos\left[\xi+\alpha_c^T(\theta_1)-\alpha_c^T(\theta)\right] \quad , \tag{18}$$

$$\tan\zeta = \frac{2A\left|\frac{S_c^T(\theta_1)}{S_c^T(\theta)}\right| \sin(kH\cos\theta)\sin\left[\xi+\alpha_c^T(\theta_1)-\alpha_c^T(\theta)\right]}{1+2A\left|\frac{S_c^T(\theta_1)}{S_c^T(\theta)}\right| \sin(kH\cos\theta)\cos\left[\xi+\alpha_c^T(\theta_1)-\alpha_c^T(\theta)\right]} \quad , \tag{19}$$

$$f_s = \frac{S_s^T(\theta)}{S_c^T(\theta)}\exp(-i\zeta)\cos(\omega_m t-\phi)+2A\left|\frac{S_s^T(\theta_1)}{S_c(\theta)}\right| \sin(kH\cos\theta)\exp\left[i(\xi-\zeta)\right]\cos(\omega_m t-\phi_1) \; . \tag{20}$$

In Eq. (17) the term involving f_c may be identified with the combined carrier signal at P and it contains no azimuth information. Similarly the term involving f_s may be identified with the combined side-band signal at P which contains the azimuth information of the aircraft and the scattering object. The detector output at the variable phase channel of the ideal VOR receiver at P is proportional to the real part of f_s. If we write f = real part of f_s, then it can be shown that

$$f = \left|\frac{S_s^T(\theta)}{S_s^T(\theta)}\right| \cos\left[\alpha_s^T(\theta)-\alpha_c^T(\theta)-\zeta\right]\cos(\omega_m t-\phi)$$

$$+2A\left|\frac{S_s^T(\theta_1)}{S_c^T(\theta)}\right| \sin(kH\cos\theta)\cos\left[\alpha_s^T(\theta_1)-\alpha_c^T(\theta)+\xi-\zeta\right]\cos(\omega_m t-\phi_1) \tag{21}$$

For interpreting the results in a better way we write f in the following manner:

$$f = N\cos(\omega_m t - \phi + \alpha) \quad . \tag{22}$$

From Eqs. (21) and (22) it can be shown that

$$N^2 = \left|\frac{S_s^T(\theta)}{S_c^T(\theta)}\right|^2 \cos^2\left[\alpha_s^T(\theta) - \alpha_c^T(\theta) - \zeta\right]$$

$$+4A^2\sin^2(kH\cos\theta)\left|\frac{S_s^T(\theta_1)}{S_c^T(\theta)}\right|^2 \cos^2\left[\alpha_s^T(\theta_1) - \alpha_c^T(\theta) + \xi - \zeta\right]$$

$$+4A\left|\frac{S_s^T(\theta)}{S_c^T(\theta)}\right|\left|\frac{S_s^T(\theta_1)}{S_c^T(\theta)}\right| \sin(kH\cos\theta)\cos\left[\alpha_s^T(\theta) - \alpha_c^\theta(\theta) - \zeta\right] \quad , \tag{23}$$

$$\tan\alpha = \frac{2A\left|\frac{S_s^T(\theta_1)}{S_c^T(\theta)}\right| \sin(kH\cos\theta)\cos\left[\alpha_s^T(\theta_1) - \alpha_c^T(\theta) + \xi - \zeta\right]\sin(\phi - \phi_1)}{\left|\frac{S_s^T(\theta)}{S_c^T(\theta)}\right| \cos\left[\alpha_s^T(\theta) - \alpha_c^T(\theta) - \zeta\right]}$$

$$+2A\left|\frac{S_s^T(\theta_1)}{S_c^T(\theta)}\right| \sin(kH\cos\theta)\cos\left[\alpha_s^T(\theta_1) - \alpha_c^T(\theta) + \xi - \zeta\right]\cos(\phi - \phi_1) \quad . \tag{24}$$

Note that in the absence of multipath signal A = 0 and Eq. (22) simplifies to

$$f = \left|\frac{S_s^T(\theta)}{S_c^T(\theta)}\right| \cos\left[\alpha_s^T(\theta) - \alpha_c^T(\theta)\right]\cos(\omega_m t - \phi) \quad . \tag{25}$$

Eq. (25) indicates that the phase of the detected signal gives the true bearing of the aircraft. However, the amplitude of the detected signal depends strongly on the RF phase relationship between the side-band and carrier signals assuming $\left|S_s^T(\theta)/S_c^T(\theta)\right|$ is slowly varying. For maximum detection efficiency the carrier and side-band signals should remain in RF phase, i.e., $\alpha_s^T(\theta) = \alpha_c^T(\theta)$ for all θ.

The bearing indication of the airborne VOR receiver is given by the phase of Eq. (22). Let us write the bearing indication of the receiver as:

$$B = \phi + \Delta\phi \quad , \tag{26}$$

where $\Delta\phi$ is the error introduced due to the existence of multipath signal. On comparing Eqs. (26) and (22) we obtain the following expression for the bearing error $\Delta\phi$:

$$\Delta\phi = -\alpha = -\tan^{-1}\left\{\frac{2A\left|S_s^T(\theta_1)\right| \sin(kH\cos\theta)\cos\left[\alpha_a^T(\theta_1) - \alpha_c^T(\theta) + \xi - \zeta\right] \sin(\phi - \phi_1)}{S_s^T(\theta)\cos\left[\alpha_s^T(\theta) - \alpha_c^T(\theta) - \zeta\right] + 2A\left|S_s^T(\theta_1)\right| \sin(kH\cos\theta)\cos\left[\alpha_s^T(\theta_1) - \alpha_c^T(\theta) + \xi - \zeta\right]\cos(\phi - \phi_1)}\right\}, \tag{27}$$

where

$$\xi = kd_1\left[1 - \sin\theta\sin\theta_1\cos(\phi - \phi_1)\right] + \delta - \pi/2 \tag{28}$$

$$\zeta = \tan^{-1}\left\{\frac{2A\left|\frac{S_c^T(\theta_1)}{S_c^T(\theta)}\right| \sin(kH\cos\theta)\sin\left[\xi + \alpha_c^T(\theta_1) - \alpha_c^T(\theta)\right]}{1 + 2A\left|\frac{S_c^T(\theta_1)}{S_c^T(\theta)}\right| \sin(kH\cos\theta)\cos\left[\xi + \alpha_c^T(\theta_1) - \alpha_c^T(\theta)\right]}\right\} . \tag{29}$$

A.5 Course Scalloping Amplitude

In the presence of multipath signal the bearing error in the VOR indications of a stationary aircraft receiver is given by Eq. (27). As the aircraft flies $\Delta\phi$ will change due to the variations of the parameters θ and ϕ of the aircraft. For a radial flight with respect to the VOR station θ is variable and ϕ is constant. Whereas for an orbital flight at constant altitude θ is constant and ϕ is variable. In both cases $\Delta\phi$ changes with θ and ϕ.

Before investigating the nature of the variation of $\Delta\phi$, it is instructive to study the variation of the parameters ξ and ζ with the motion of the aircraft. If we make the physically reasonable assumption that $A\left|S_c^T(\theta_1)/S_c^T(\theta)\right| \ll 1$, then Eq. (29) indicates that ζ is a small quantity, i.e., $\zeta \ll 1$, and the effects of its variation with the aircraft motion on the final results would be negligible. The parameter ξ given by eq. (28) may be a large quantity ($kd_1 \gg 1$) and its variation with ϕ is also large. As a result, the terms involving ξ in Eq. (27) will oscillate between +1 and -1 as the aircraft moves. As a result of this, the variation of $\Delta\phi$ with the aircraft motion will be a slow variation with ϕ (or θ as the case may be) mounted on top of a rapidly oscillatory variation determined mainly by the parameter ξ. It is clear that $\Delta\phi$ fluctuates between positive and negative values with the motion of the aircraft. The amplitudes of these positive and negative swings of the bearing error $\Delta\phi$ are termed the course scalloping amplitudes. We now write the bearing indications of the airborne VOR receiver as:

$$B = \phi - S_{1,2} \quad , \tag{30}$$

where

S_1 is the value of $\Delta\phi$ evaluated from Eq. (27) when

$$\cos\left[\alpha_s^T(\theta_1) - \alpha_c^T(\theta) + \xi - \zeta\right] = 1$$

S_2 is the value of $\Delta\phi$ evaluated from Eq. (27) when

$$\cos\left[\alpha_s^T(\theta_1) - \alpha_c^T(\theta) + \xi - \zeta\right] = -1 \ .$$

The course scalloping amplitudes S_1 and S_2 give the two bounds of the scalloping errors as the aircraft moves. Notice that S_1 and S_2 are of opposite signs and in general $|S_1| \neq |S_2|$.

By definition,

$$S_1 = \Delta\phi \text{ evaluated at } \xi = \xi_{01},\ \zeta = \zeta_{01} \tag{31}$$

where

$$\alpha_s^T(\theta_1) - \alpha_c^T(\theta) + \xi_{01} - \zeta_{01} = 2n\pi \ , \qquad n \text{ is an integer} \tag{32}$$

$$\tan\zeta_{01} = \frac{2A\left|\dfrac{S_c^T(\theta_1)}{S_c^T(\theta)}\right| \sin(kH\cos\theta)\sin\left[\xi_{01} + \alpha_c^T(\theta_1) - \alpha_c^T(\theta)\right]}{1 + 2A\left|\dfrac{S_c^T(\theta_1)}{S_c^T(\theta)}\right| \sin(kH\cos\theta)\cos\left[\xi_{01} + \alpha_c^T(\theta_1) - \alpha_c^T(\theta)\right]} \tag{33}$$

Eqs. (32) and (33) can be solved for ζ_{01} and we obtain

$$\zeta_{01} = -\sin^{-1}\left\{A\left|\frac{S_c^T(\theta_1)}{S_c^T(\theta)}\right| \sin(kH\cos\theta)\sin^{-1}\left[\alpha_s^T(\theta_1) - \alpha_c^T(\theta)\right]\right\} \tag{34}$$

After using Eqs. (27), (31) - (34) the following is obtained:

$$S_1 = -\tan^{-1} \frac{2A\left|S_s^T(\theta_1)\right|\sin(kH\cos\theta)\sin(\phi-\phi_1)}{\left|S_s^T(\theta)\right|\cos\left[\alpha_s^T(\theta)-\alpha_c^T(\theta)-\zeta_{01}\right]+2A\left|S_s^T(\theta_1)\right|\sin(kH\cos\theta)\cos(\phi-\phi_1)} \tag{35}$$

Following a similar method, S_2 is obtained as:

$$S_2 = \tan^{-1} \frac{A\left|S_s^T(\theta_1)\right|\sin(kH\cos\theta)\cos(\phi-\phi_1)}{\left|S_s^T(\theta)\right|\cos\left[\alpha_s^T(\theta)-\alpha_c^T(\theta)\ -\zeta_{02}\right]-2A\left|S_s^T(\theta_1)\right|\sin(kH\cos\theta)\cos(\phi-\phi_1)} \tag{36}$$

where

$$\zeta_{02} = \sin^{-1}\left\{2A\left|\frac{S_c^T(\theta_1)}{S_c^T(\theta)}\right|\sin(kH\cos\theta)\sin\left[\alpha_s^T(\theta_1)-\alpha_c^T(\theta_1)\right]\right\} . \tag{37}$$

If $\alpha_s^T(\theta) = \alpha_c^T(\theta)$, $\zeta_{01} = \zeta_{02} = 0$ and the two scalloping amplitudes can be written as

$$S_{\frac{1}{2}} = \mp\tan^{-1}\left[\frac{2A\left|\frac{S_s^T(\theta_1)}{S_s^T(\theta)}\right|\sin(kH\cos\theta)\sin(\phi-\phi_1)}{1\pm 2A\left|\frac{S_s^T(\theta_1)}{S_s^T(\theta)}\right|\sin(kH\cos\theta)\cos(\phi-\phi_1)}\right] . \tag{38}$$

Eq. (38) is the same as Eq. (4.2) given in Chapter IV.

In an idealized case when it is assumed that the system operates in free space (i.e., the ground effects are neglected), it can be shown that the corresponding free space scalloping expressions are given by:

$$S^F_{\frac{1}{2}} = \mp\tan^{-1}\frac{A\left|S_s(\theta_1)\right|\sin(\phi-\phi_1)}{\left|S_s(\theta)\right|\cos\left[\alpha_s(\theta)-\alpha_c(\theta)-\zeta'_{01}\right]\pm A\left|S_s(\theta_1)\right|\cos(\phi-\phi_1)} \tag{39}$$

where

$$\zeta'_{01}{}_{2} = \mp \sin^{-1}\left\{A\left|\frac{S_c(\theta_1)}{S_c(\theta)}\right| \sin\left[\alpha_s(\theta_1) - \alpha_c(\theta_1)\right]\right\} . \tag{40}$$

Approximate free space course scalloping amplitude expressions are given in the VOR Handbook (FAA 1968). Let us discuss in the light of the present theory the expressions given in the VOR Handbook. The physical arrangement of the VOR station, the multipath source and the position of the aircraft considered imply in our notation

$\theta = \theta_1 = \pi/2$, i.e., the observation point and the multipath source are located at the same elevation angles.

A is a constant.

$\delta = 0$.

The system operates in free space. Under these conditions, Eq. (39) yields

$$S^F_{1\,2} = \mp \tan^{-1}\left\{\frac{A\sin(\phi - \phi_1)}{\cos\left[\alpha_s(\pi/2) - \alpha_c(\pi/2)\right] \pm \sin^{-1}\left[A\sin\,\alpha_s(\pi/2) - \alpha_c(\pi/2)\right] \pm A\cos(\phi - \phi_1)}\right\} \tag{41}$$

If it is now assumed that $\alpha_s(\pi/2) = \alpha_c(\pi/2)$, we obtain the following from Eq. (41):

$$S^F_{1\,2} = \mp \tan^{-1}\left[\frac{A\sin(\phi - \phi_1)}{1 \pm A\cos(\phi - \phi_1)}\right] . \tag{42}$$

Under the assumption $A \ll 1$, Eq. (42) reduces the Eq. (4.1) given in [2]. Because of the various fundamental approximations made in obtaining Eq. (42), its application to explain the scalloping amplitudes would be highly restricted. For example, Eq. (42) indicates that the scalloping is independent of the elevation plane patterns of the VOR antenna.

A.6 RF Phase Relationship Between Carrier and Side-Band Signals

It was mentioned earlier that the rf phase relationship between the received side-band and carrier signals plays an important role in the detection efficiency of the VOR receiver at the aircraft. From the scalloping expressions developed in the previous sections it is also found that the same phase relationship has considerable effects on the observed course scalloping amplitudes. For an antenna located in free space this phase difference may be represented by $\alpha_s(\theta) - \alpha_c(\theta)$ where $\alpha_s(\theta)$ and $\alpha_c(\theta)$ are the phase angles of the side-band and carrier complex patterns respectively, as defined by Eqs. (A.3) and (A.4). For an antenna located above infinite planar ground the phase difference is represented by $\alpha_s^T(\theta) - \alpha_c^T(\theta)$ where $\alpha_s^T(\theta)$ and $\alpha_c^T(\theta)$ are as defined by Eqs. (A.6) and (A.7).

The results discussed in the previous sections indicate that in general if $\alpha_c(\theta) = \alpha_s(\theta)$ or $\left[\alpha_c^T(\theta) = \alpha_s^T(\theta)\right]$ for all θ, then the detection efficiency is maximum and also the observed course scalloping would be minimum. It is therefore important to study the variation of the rf phase difference between the two signals as a function of θ for a given antenna. Complete expressions

for the carrier and side-band mode complex patterns of various standard VOR antennas have been given in the references quoted earlier. Here we discuss only the variations of the phases of the complex patterns as functions of θ.

Figure A-1 shows the variations of $\alpha_c(\theta)$, $\alpha_s(\theta)$ and $\alpha_s(\theta)-\alpha_c(\theta)$ as functions of θ for a standard VOR antenna located in free space. The corresponding results for a standard VOR antenna located 15' above an infinite planar ground are shown in Fig. A-2. For the standard VOR antenna it is found that the phase difference is almost constant for all θ in both cases. For the parasitic antenna case the phase difference is found to be reasonably constant in the range $55^{o} \leq \theta \leq 95^{o}$ for the free space case; the phase difference fluctuates with an average value near 100^{o} for $50^{o} \leq \theta \leq 85^{o}$ for the same antenna located above ground.

On the basis of the results given here it can be concluded that it is sufficient to adjust the rf phase between the carrier and side-band signals radiated by a standard VOR antenna at a certain convenient angle (say, at the monitor).

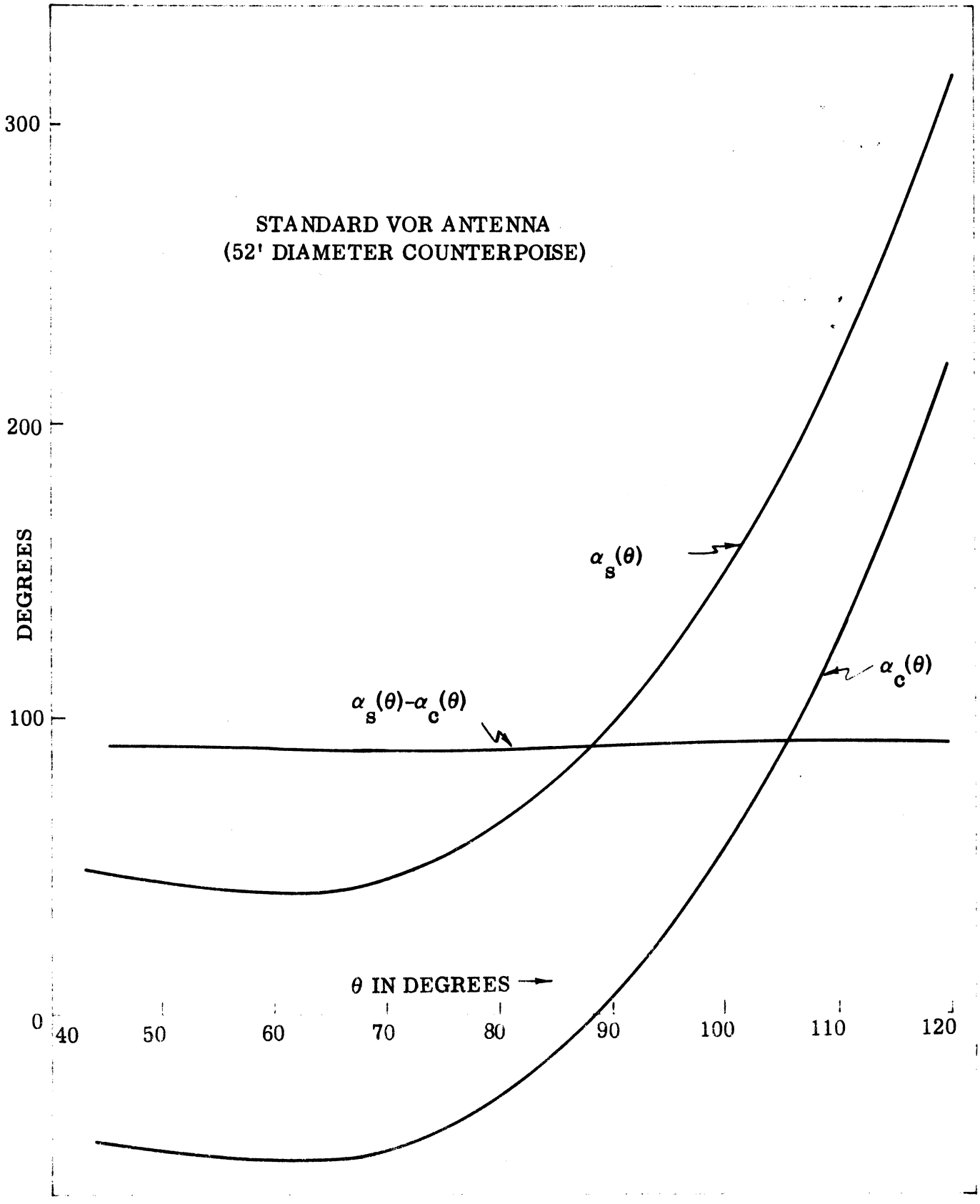

Fig. A-1: $\alpha_c(\theta)$, $\alpha_s(\theta)$ and $\alpha_s(\theta)-\alpha_c(\theta)$ as functions of θ for a standard VOR antenna in free space. kA_o=18.0859, kd=0.9276, kh=2.7755, f=109 MHz.

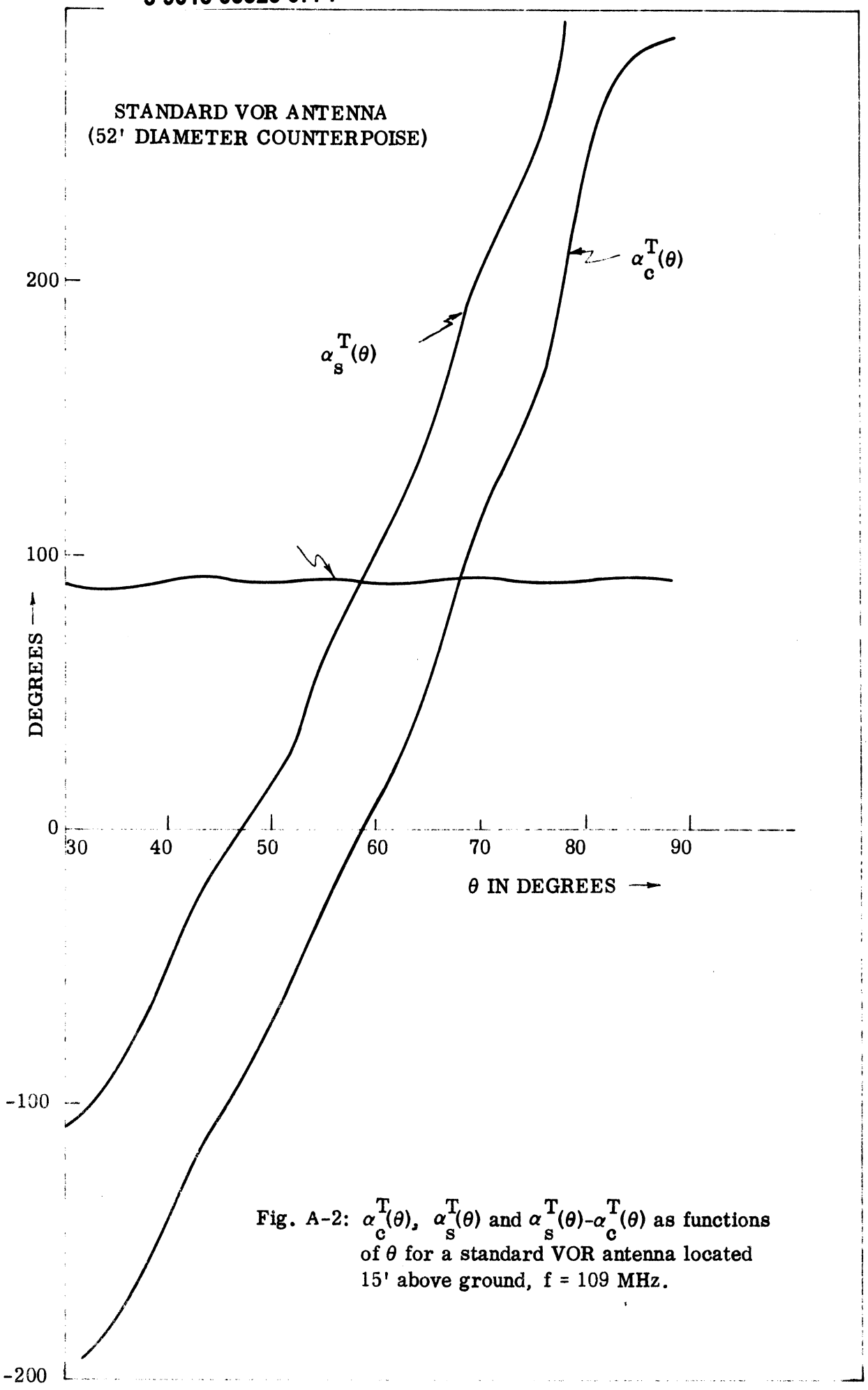

Fig. A-2: $\alpha_c^T(\theta)$, $\alpha_s^T(\theta)$ and $\alpha_s^T(\theta)-\alpha_c^T(\theta)$ as functions of θ for a standard VOR antenna located 15' above ground, f = 109 MHz.